165
5/14/81
M.E.
(2)
DR-2822
Received - 165
Bins - 111
NTIS - 25

DOE/OR/05035-T2

MASTER

DOSHI EZEKH

ADVANCED INDUSTRIAL GAS TURBINE TECHNOLOGY READINESS DEMONSTRATION PROGRAM

Phase II Final Report, Compressor Rig Fabrication, Assembly and Test

By
Jeffrey K. Schweitzer
James D. Smith

March 1981

Work Performed Under Contract No. AC05-76OR05035

Pratt & Whitney Aircraft Group
Government Products Division
United Technologies Corporation
West Palm Beach, Florida

U. S. DEPARTMENT OF ENERGY

DISCLAIMER

This report was prepared as an account of work sponsored by an agency of the United States Government. Neither the United States Government nor any agency Thereof, nor any of their employees, makes any warranty, express or implied, or assumes any legal liability or responsibility for the accuracy, completeness, or usefulness of any information, apparatus, product, or process disclosed, or represents that its use would not infringe privately owned rights. Reference herein to any specific commercial product, process, or service by trade name, trademark, manufacturer, or otherwise does not necessarily constitute or imply its endorsement, recommendation, or favoring by the United States Government or any agency thereof. The views and opinions of authors expressed herein do not necessarily state or reflect those of the United States Government or any agency thereof.

DISCLAIMER

Portions of this document may be illegible in electronic image products. Images are produced from the best available original document.

DISCLAIMER

"This book was prepared as an account of work sponsored by an agency of the United States Government. Neither the United States Government nor any agency thereof, nor any of their employees, makes any warranty, express or implied, or assumes any legal liability or responsibility for the accuracy, completeness, or usefulness of any information, apparatus, product, or process disclosed, or represents that its use would not infringe privately owned rights. Reference herein to any specific commercial product, process, or service by trade name, trademark, manufacturer, or otherwise, does not necessarily constitute or imply its endorsement, recommendation, or favoring by the United States Government or any agency thereof. The views and opinions of authors expressed herein do not necessarily state or reflect those of the United States Government or any agency thereof."

This report has been reproduced directly from the best available copy.

Available from the National Technical Information Service, U. S. Department of Commerce, Springfield, Virginia 22161.

Price: Printed Copy A06
Microfiche A01

DOE/OR/05035-T2
Distribution Category UC-93

ADVANCED INDUSTRIAL GAS TURBINE TECHNOLOGY READINESS DEMONSTRATION PROGRAM

PHASE II FINAL REPORT

COMPRESSOR RIG FABRICATION, ASSEMBLY AND TEST

Jeffrey K. Schweitzer
James D. Smith

Pratt & Whitney Aircraft Group
Government Products Division
United Technologies Corporation
P.O. Box 2691
West Palm Beach, Florida 33402

For the
U.S. Department of Energy
Office of Coal Utilization
Washington, D.C. 20545
Under Contract No. DE-AC05-760R05035

THIS PAGE

WAS INTENTIONALLY

LEFT BLANK

ABSTRACT

This report presents the results of a component technology demonstration program to fabricate, assemble and test an advanced axial/centrifugal compressor. This work was conducted as part of a Department of Energy sponsored program to demonstrate the utilization of advanced aircraft gas turbine cooling and high pressure compressor technology to improve the performance and reliability of future industrial gas turbines. Specific objectives of the compressor component testing were to demonstrate 18:1 pressure ratio on a single spool at 90% polytropic efficiency with 80% fewer airfoils as compared to current industrial gas turbine compressors.

The compressor design configuration utilizes low aspect ratio/highly-loaded axial compressor blading combined with a centrifugal backend stage to achieve the 18:1 design pressure ratio in only 7 stages and 281 axial compressor airfoils. Initial testing of the compressor test rig was conducted with a vaneless centrifugal stage diffuser to allow documentation of the axial compressor performance. Peak design speed axial compressor performance demonstrated was 91.8% polytropic efficiency at 6.5:1 pressure ratio. Subsequent documentation of the combined axial/centrifugal performance with a centrifugal stage pipe diffuser resulted in the demonstration of 91.5% polytropic efficiency and 14% stall margin at the 18:1 overall compressor design pressure ratio. The demonstrated performance not only exceeded the contract performance goals, but also represents the highest known demonstrated compressor performance in this pressure ratio and flow class. The performance demonstrated is particularly significant in that it was accomplished at airfoil loading levels approximately 15% higher than that of current production engine compressor designs. The test results provide conclusive verification of the advanced low aspect ratio axial compressor and centrifugal stage technologies utilized.

FOREWORD

This report was prepared by the Pratt & Whitney Aircraft Group, Government Products Division of United Technologies Corporation to present the results of a program to fabricate, assemble, and test an advanced 18:1 pressure ratio axial/centrifugal compressor. This work was conducted under Phase II, Tasks II and III of U. S. Department of Energy Contract DE-AC05-76ORO5035, Advanced Industrial Gas Turbine Technology Readiness Demonstration Program. John W. Fairbanks, Heat Engines Branch of the DOE Office of Coal Utilization, was the project manager. The P&WA program manager was Jeffrey K. Schweitzer.

The authors would like to additionally acknowledge the much appreciated efforts of the following persons who made significant contributions to the success of the program: E. T. Singleton, axial compressor aerodynamic design; J. D. Walter, rig mechanical design; and G. C. Nicholson, compressor rig fabrication and assembly.

TABLE OF CONTENTS

LIST OF ILLUSTRATIONS

ILLUSTRATIONS (Continued)

ILLUSTRATIONS (Continued)

LIST OF TABLES

LIST OF SYMBOLS

AR	Aspect ratio
b	Chord length (in.)
C_L	Seal clearance (in.)
C'_N	Impeller blade-to-blade loading
C'_O	Impeller hub-to-shroud loading
C_x	Axial velocity (ft/sec)
D_f	Diffusion factor
E	Multiple of rotor frequency
LER	Airfoil leading edge radius (in.)
M_n	Mach number
N	Rotor Speed (rpm)
P	Static pressure (psia)
P_T, P_O	Total pressure (psia)
PR	Pressure ratio
r	Radius (in.)
R	Temperature recovery ratio
T,T_T	Total temperature (°R)
U	Rotor wheel velocity (ft/sec)
w	Relative velocty (ft/sec)
W	Flowrate (lb_m/sec)
β^*	Metal angle (degrees)
γ	Ratio of specific heats
δ	Ratio of P_T to standard sea level pressure of 14.696 psia
η	Efficiency
θ	Ratio of T_T to standard sea level temperature of 518.688°R
τ	Airfoil circumferential spacing (in.)

LIST OF SYMBOLS (Continued)

Subscripts

ad	Adiabatic
D	Downstream side
env	Pipe diffuser envelope
le	Leading edge
max	Maximum
min	Minimum
P	Polytropic
tan	Diffuser pipe centerline tangency radius
tip	Impeller tip
U	Upstream side
1	Inlet plenum instrumentation station
2	Axial compressor discharge instrumentation station
3	Diffuser exit instrumentation station

SECTION I
INTRODUCTION

A concerted national effort is currently in progress to conserve energy and increase utilization of our abundant domestic energy resources. A major part of this effort is aimed at the development of more efficient stationary power systems that can use coal or coal-derived fuels. Gas turbines, which comprise a significant portion of this category of power systems, are being used in increasingly large numbers in electric power generation and in numerous pumping and mechanical drive applications. Substantial improvements in efficiency are currently feasible through the use of advanced thermodynamic cycles and improved component efficiencies, especially when the gas turbine is used in conjunction with a waste heat recovery system in either a combined cycle or cogeneration system.

In January 1976 a contract was awarded by the Energy Research and Development Administration (reorganized in October 1977 into the Department of Energy) to Pratt & Whitney Aircraft/Government Products Division (P&WA/GPD) to investigate the utilization of advanced aircraft gas turbine component technology to provide a near-term energy saving potential in stationary power system applications. Goals were to significantly improve industrial gas turbine performance and durability, and to accomplish this with the capability of operating with a wide range of fuels including the heavier low-grade petroleum fuels and minimally processed coal-derived liquid fuels. Additional emphasis was placed on reducing the number of parts to improve reliability and lower initial cost to enhance commercialization.

In Phase I of this program, the latest aircraft turbine cooling and high pressure compressor technology was applied in the definition of a conceptual advanced industrial gas turbine in the 15,000 shp/10 MW class (figure I-1) capable of meeting the above goals. The design approach, as discussed in Reference 1, included:

- Designing to higher cycle pressure ratio (18:1) and combustor exit temperature (2500°F) for increased cycle efficiency and specific power.
- Incorporating a single-spool axial/centrifugal compressor reflecting the latest aerodynamic technology to attain a polytropic efficiency goal of 90% with minimum number of stages.
- Utilizing wafer turbine cooling techniques to minimize cooling air requirements at the elevated combustor exit temperature and yet maintain a 20,000 hr/10,000 cycle hot section life.
- Incorporating an externally-mounted can-type combustor designed for low emissions and maintenance ease.

Heat transfer cascade test data obtained in Phase II of the contract for the first stage turbine wafer airfoil cooling designs exceeded design goals (1500°F maximum metal temperature at 2500°F CET) and demonstrated cooling effectiveness levels higher than any current production industrial or aircraft engine airfoils (Reference 2). Additionally, the high cooling effectiveness levels demonstrated were attained with essentially all-convectively cooled designs, eliminating leading edge showerhead holes or the extensive use of film-cooling holes both of which are susceptible to plugging in a low-grade industrial fuel environment.

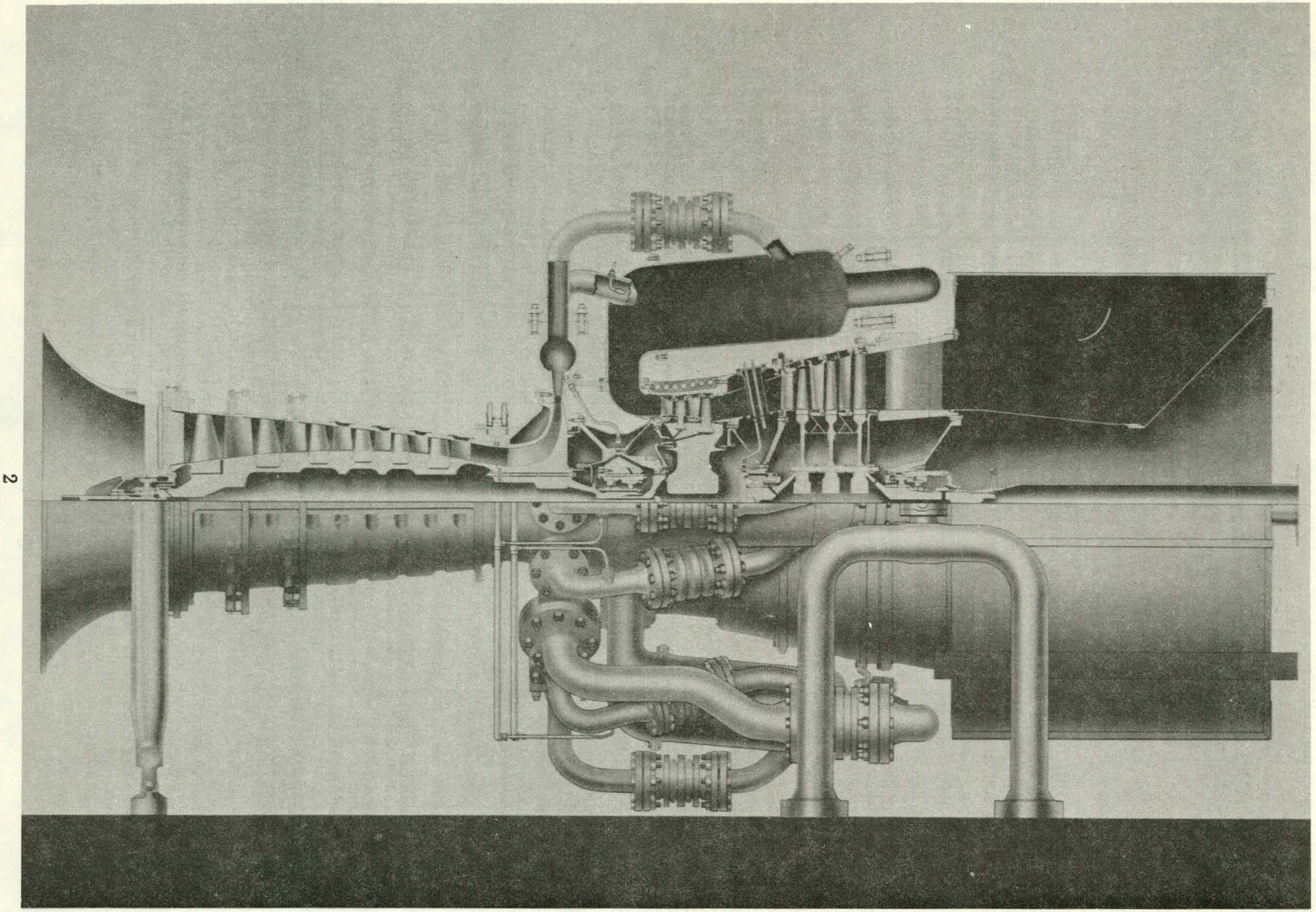

Figure I-1. Advanced Technology 10 MW Industrial Gas Turbine

The compressor configuration combines advanced low aspect ratio (long chord) axial compressor blading aerodynamics with a centrifugal backend stage. The inherent benefits of low aspect ratio blading have been investigated by P&WA and others in recent years, beginning with single-stage rig test programs (References 3 and 4) and proceeding through full-scale multi-stage rig development programs. The test results have consistently demonstrated the capability of low aspect ratio blading to achieve increased efficiency and stability at high axial compressor loading levels. The low aspect ratio/high loading combination additionally results in fewer required stages and fewer airfoils per stage for a given overall compressor pressure ratio. The large geometry low aspect ratio blades also provide improved durability and increased performance retention.

Significant advances have also been made in the past decade in centrifugal compressor technology such that performance approaching that of axial compressors can be obtained especially in low flow, low pressure ratio applications. This makes the centrifugal compressor stage attractive for use as a backend stage, where a single rugged centrifugal stage can replace a number of smaller axial stages. The utilization of the centrifugal compressor stage thus can result in a further reduction in the number of required stages where frontal area is not a critical constraint (such as in stationary gas turbines). The combination of the centrifugal stage with low aspect ratio axial compressor aerodynamics in this particular configuration allows the achievement of 18:1 pressure ratio on a single spool with high efficiency and 80% fewer parts as compared to current industrial gas turbine compressors.

The detail aerodynamic and mechanical designs of a full scale axial/centrifugal compressor test rig was completed under Phase I of Contract DE-AC05-76ORO5035 and is presented in Reference 1. This report presents a description of the compressor rig fabrication and demonstration testing conducted under Phase II. A brief summary of the compressor design is presented for convenience in Section II. Details of the compressor rig fabrication and assembly are presented in Section III. The test equipment and facilities utilized are described in Section IV and the test procedures are outlined in Section V. Section VI presents the test results. Concluding remarks are found in Section VII.

THIS PAGE

WAS INTENTIONALLY

LEFT BLANK

SECTION II
DESIGN SUMMARY

Objectives of the compressor design were to obtain 18:1 pressure ratio at 90% polytropic efficiency with an 80% reduction in the number of parts relative to current industrial gas turbine compressors. The specific approach taken to fulfill these objectives was to combine low aspect ratio/highly-loaded axial compressor blading with a centrifugal backend stage on a single spool. A comprehensive parametric study was conducted to optimze the selection of the primary compressor variables. The study results indicated that the peak compressor performance potential could be attained with a six-stage axial/single-stage centrifugal compressor configuration with a 6.67/2.7 pressure ratio split. An inlet airflow rate of 70 lbm/sec was selected to be compatible with an advanced industrial gas turbine application in the 15,000 shp/10 MW class. A schematic of the final compressor flowpath is presented in figure II-1. Details of the component parametric studies and compressor rig aerodynamic and mechanical design can be found in Reference 1. A brief summary of the design is included in the following paragraphs.

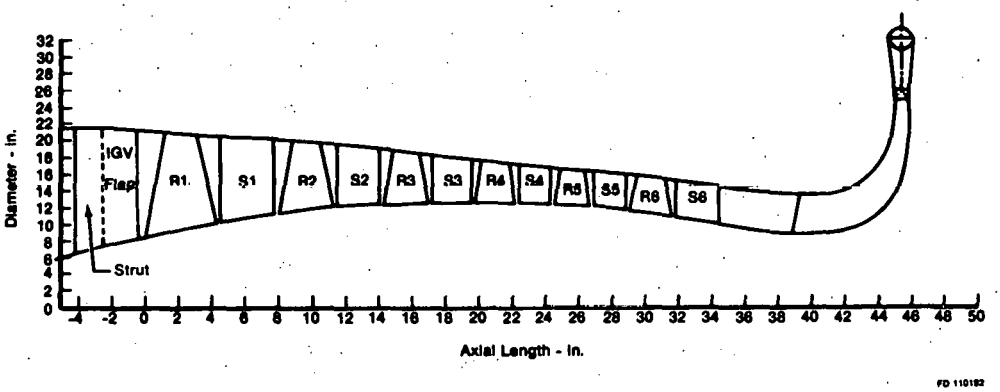

Figure II-1. Axial/Centrifugal Compressor Flowpath

A. AXIAL COMPRESSOR AERODYNAMIC DESIGN

The objective of the axial compressor aerodynamic design was to exploit to the maximum extent possible, without jeopardizing near-term applicability, the potential of low aspect ratio blading to achieve high aerodynamic loading levels with high efficiency and good stability. An aggressive loading limit was therefore set, figure II-2, which although providing an approximate 15% increase in loading levels over current production engine compressors, represented a logical next step advancement in the state-of-the-art relative to previous multistage compressor development test rig programs. The low hub/tip ratio, bulged ID flowpath (figure II-1) evolved as the flowpath which provided the best efficiency/loading trade while maintaining a low loss transition to the centrifugal stage.

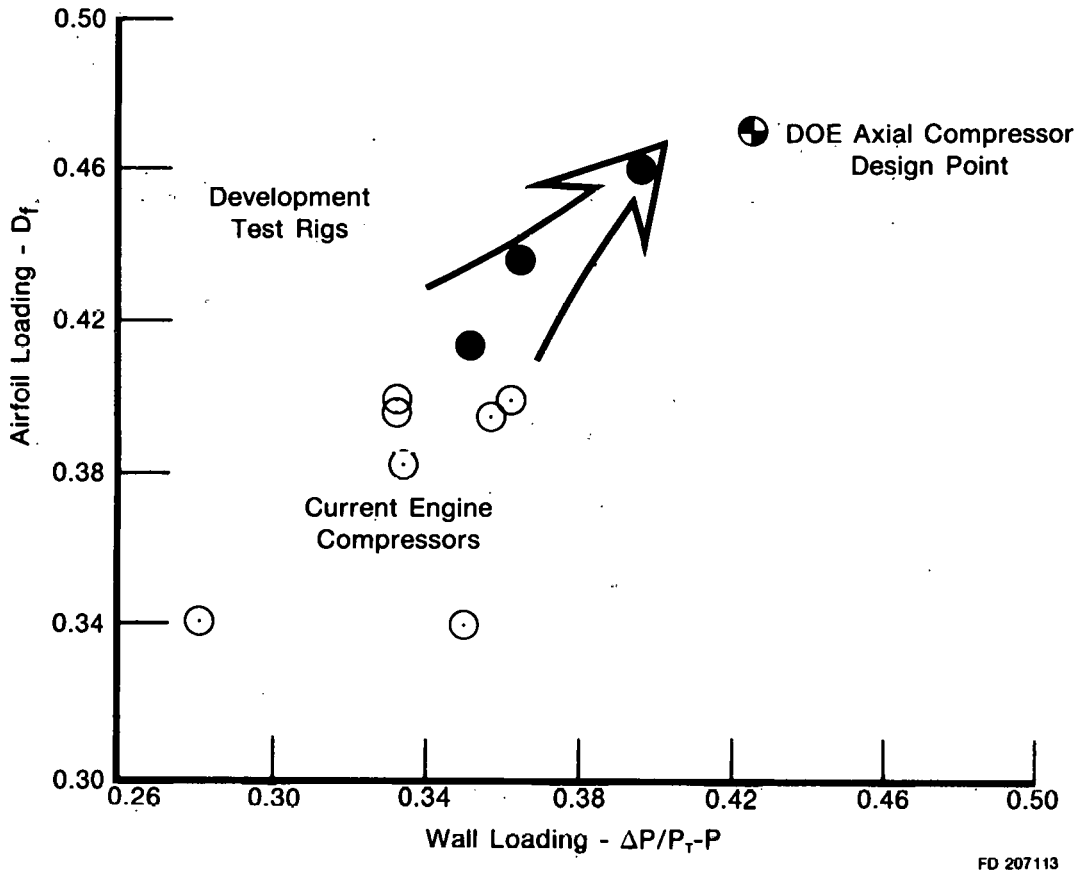

Figure II-2. Axial Compressor Loading Comparison

A summary of the axial compressor design meanline parameters is preseted in table II-1. The compressor design average aspect ratio is 1.038; average D-factor is 0.471. Distributions by blade row of aspect ratio, gap-to-chord ratio, and loadings are shown in figures II-3 and II-4.

The selection of airfoil blading geometry for each blade row was made on the basis of optimizing airfoil performance for the particular Mach number regime for that row. The airfoil series selection for each blade row, along with the number of airfoils in each row, are given in table II-2. A multiple circular arc airfoil was chosen for rotors one and two since their inlet relative Mach numbers are supersonic in the tip region. Incidence for the supersonic portions of the airfoils was set at approximately 1.2 degrees to the A′ station, a point on the suction surface halfway between the leading edge and the first captured Mach wave emanation point. The incidence selection was based on a LER/τ correlation presented in Reference 5. The incidence of the subsonic portions of the blades was selected to provide minimum loss based on cascade data for circular arc airfoils. Deviation was determined by a modified Carter's rule plus an experience factor. The remainder of the axial compressor airfoil metal geometries were determined based on cascade correlations. Incidence was selected to provide minimum loss at the design point. Complete definition of the metal geometry for all the axial compressor airfoils is contained in Appendix A of Reference 1.

Table II-1. Axial Compressor Meanline Design Summary

Corrected Speed, rpm	15,000
Corrected Flow, lbm/sec	70
Pressure Ratio	6.67:1
Number of Stages	6
Number of Airfoils (not including IGV's)	281
First Rotor Tip Speed, ft/sec	1376
First Rotor Hub/Tip Ratio	0.4
First Rotor Specific Flow, lbm/sec/ft^2	35
Exit Hub/Tip Ratio	0.708
Exit Mach Number	0.385
Average Rotor Exit Cx/U	0.53
Average Stage Reaction	0.64
Rotor Average Aspect Ratio	1.058
Stator Average Aspect Ratio	1.017
Compressor Average Aspect Ratio	1.038
Rotor Average Solidity	1.439
Stator Average Solidity	1.345
Compressor Average Solidity	1.390
Rotor Average D-Factor	0.478
Stator Average D-Factor	0.464
Compressor Average D-Factor	0.471
Rotor Average $\Delta P/P_T$-P	0.444
Stator Average $\Delta P/P_T$-P	0.408
Compressor Average $\Delta P/P_T$-P	0.426

Table II-2. Axial Compressor Airfoil Series Selection

Blade Row	*No. Airfoils*	*Airfoil Series*
IGV	13	63
R1	18	MCA
S1	20	CA
R2	21	MCA
S2	22	CA
R3	25	CA
S3	24	65/CA
R4	27	CA
S4	26	65/CA
R5	27	65/CA
S5	26	65/CA
R6	25	65/CA
S6	20	400

MCA — Multiple circular arc

CA — Circular arc

65/CA — 65 series thickness distribution superimposed on a circular arc meanline.

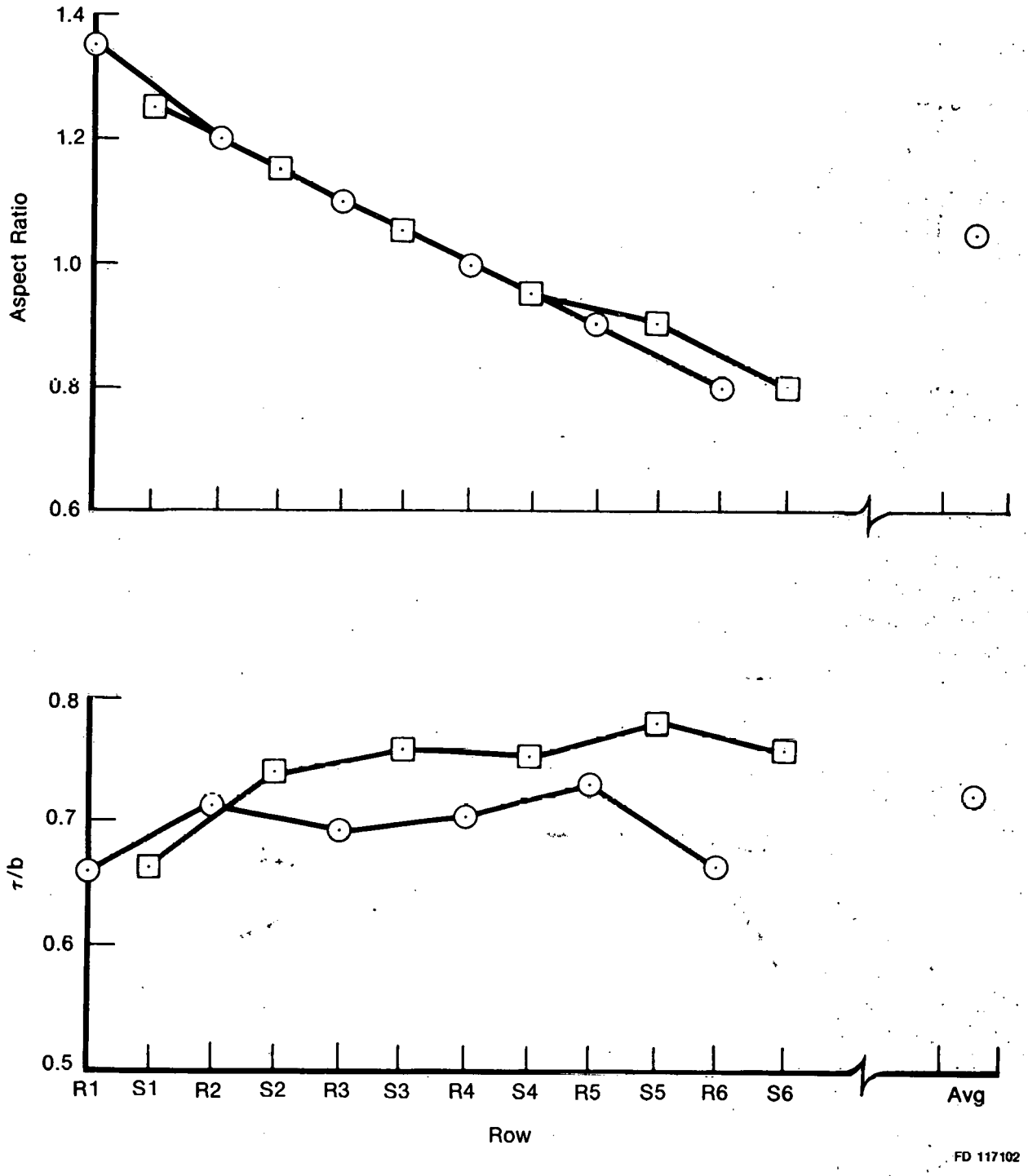

Figure II-3. Axial Compressor Blade Row Aspect Ratio and Gap/Chord Distributions

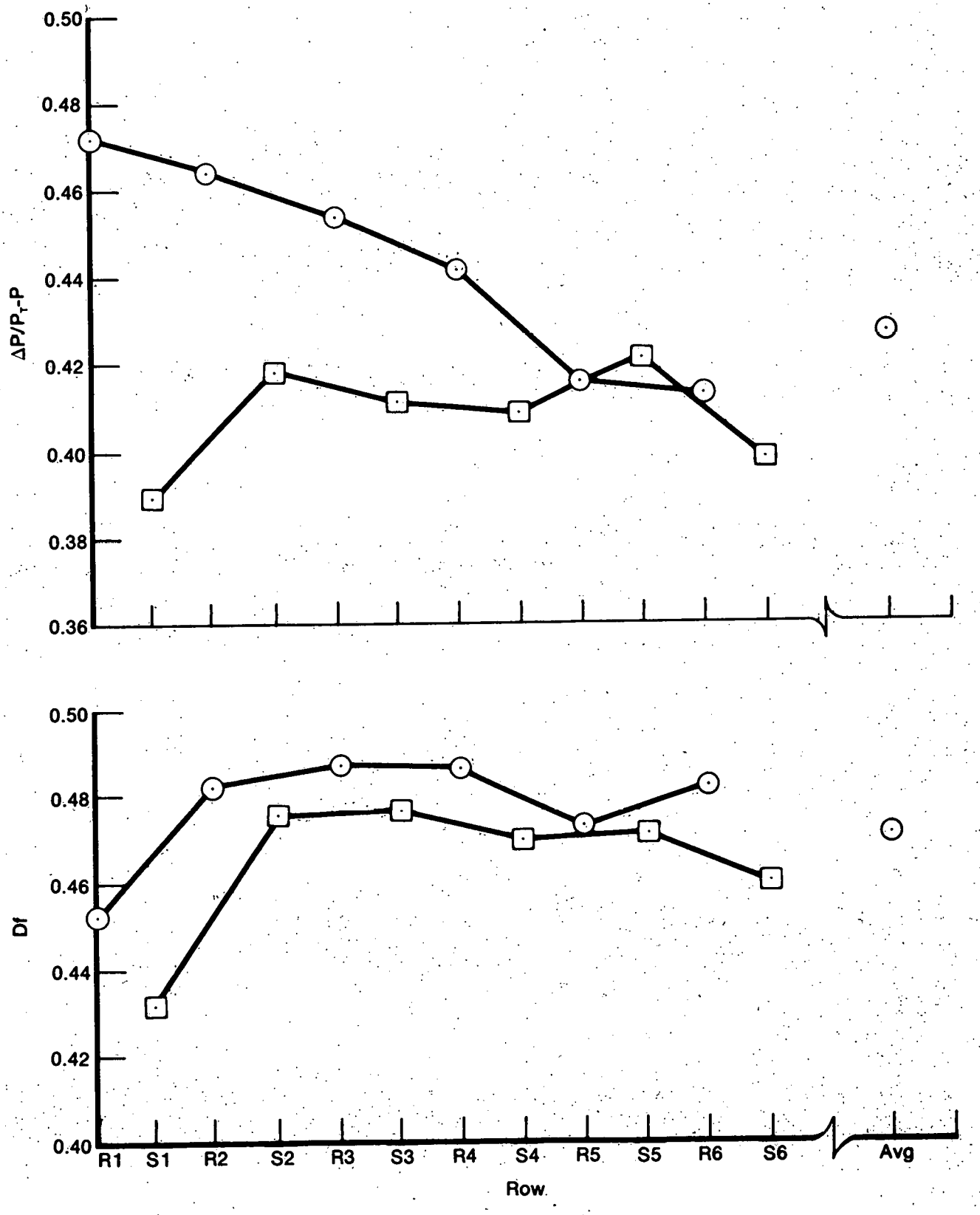

Figure II-4. Axial Compressor Blade Row Meanline Loading Distributions

The predicted design point distributions of stage pressure ratio, inlet corrected speed, inlet corrected flow, and adiabatic efficiency are presented in table II-3. The resultant predicted overall axial compressor performance was 89.0% adiabatic efficiency (91.5% polytropic efficiency) at a pressure ratio f 6.67:1 and 24.5% surge margin.

Table II-3. Predicted Axial Compressor Design Point Performance

Row	$N/\sqrt{\theta}$	$W\sqrt{\theta}$	*PR*	$\eta_{A.D}$~%
IGV - Rotor 1	15,000	70.0	1.55	91.0
Stator 1 - Rotor 2	14,006	48.2	1.48	91.1
Stator 2 - Rotor 3	13,173	34.6	1.41	91.8
Stator 3 - Rotor 4	12,500	25.9	1.35	91.8
Stator 4 - Rotor 5	11,940	20.1	1.29	91.6
Stator 5 - Rotor 6	11,492	16.2	1.19	90.2
Overall	15,000	70.0	6.67	89.0

The variable vane schedule for the inlet guide vane, stator 1, and stator 2 (figure II-5) was selected for the initial testing to provide an adequate off-design efficiency/surge margin characteristic based on meanline predictions and prior highly loaded P&WA compressor experience. Additional vane travel capability for all the axial compressor stages was included to allow for performance optimization as required. The vane travels selected, table II-4, were kept at the expected minimum necessary in order to limit vane trailing edge end gaps.

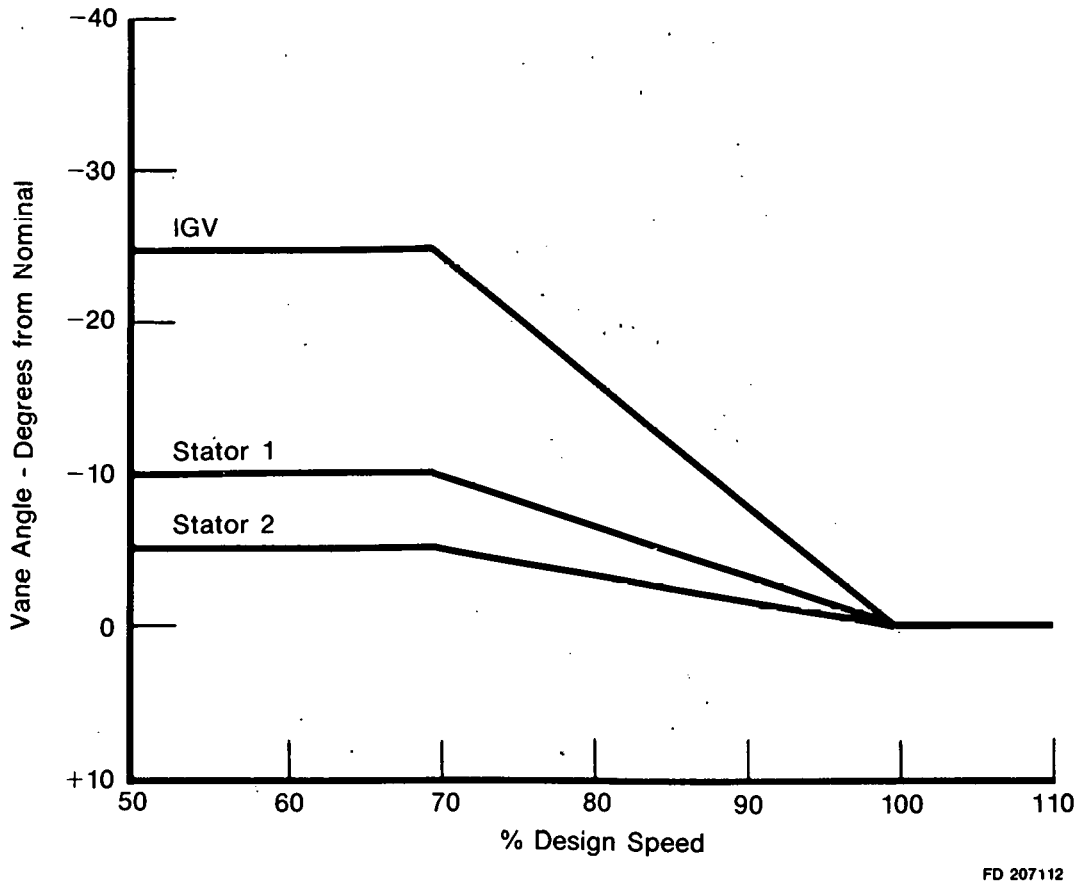

Figure II-5. Variable Vane Schedule

Table II-4. Axial Compressor Vane Travel Capability

Vane	Meanline Nominal Angle - Deg.	Travel Angle - Deg.
IGV	82.0	+10, −40
S1	63.7	+ 5, −15
S2	60.9	+ 5, −10
S3	60.9	±5
S4	60.8	±5
S5	59.9	±5
S6	62.6	±10

B. CENTRIFUGAL STAGE AERODYNAMIC DESIGN

A summary of the centrifugal stage aerodynamic design is presented in table II-5. The stage is comprised of a 25 deg back-swept impeller and a 2:1 area ratio conical pipe diffuser designed to produce 2.7:1 pressure ratio (total-to-total) at an inlet corrected flow of 14.1 lbm/sec. Performance goals were to achieve 85.8% adiabatic efficiency at a minimum of 10% surge margin.

Table II-5. Centrifugal Stage Design Summary

Stage	
Corrected Speed, rpm	11,182
Corrected Flow, lbm/sec	14.1
Specific Speed	64
Pressure Ratio (T-T)	2.7
Adiabatic Efficiency, %	85.8
Minimum Surge Margin, %	10
Impeller	
Prewhirl, degrees	20
Backsweep, degrees	25
Inlet Hub/Tip Ratio	0.66
No. Blades (Full/Splitter)	18/18
Pressure Ratio	2.82
Adiabatic Efficiency, %	90
Inlet Tip Relative Mach No.	0.60
Max Blade-to-Blade Loading (C'n)	0.64
Max Hub-to-Shroud Loading (C'o)	0.57
Diffusion (Wmax/Wmin)	1.57
Exit Tip Speed, ft/sec	1634
Exit Air Angle, degrees	17
Exit Mach No.	0.88
Aerodynamic Slip Factor	0.922
Diffuser	
Number of Pipes	26
Area Ratio	2:1
Cone Angle, degrees	3-5
Leading Edge Mach No.	0.83
Exit Mach No.	0.35
Tangency Radius Ratio	1.006
Leading Edge Radius Ratio	1.062
Bisector Angle, degrees	17.2
Total Pressure Loss, %	4.2

1. Impeller

The impeller meridional flowpath profile and blade metal angle distribution are shown in figures II-6 and II-7. The impeller has 18 full blades with one set of splitter blades. The combination of a maximum blade metal angle of 84 degrees with 36 exit blades provided the highest efficiency potential while still maintaining maximum blade-to-blade loading within demonstrated limits for previous P&WA impeller designs. The splitter blade leading edges were located at 37.5% of the full blade passage length to help stabilize the flow during the last part of the impeller diffusion and to maintain blade-to-blade loading at a moderate level in the knee region. The resulting impeller loading and relative velocity distributions are presented in figures II-8 and II-9. The mean impeller diffusion ratio (w_{max}/w_{min}) is 1.57; maximum hub-to-shroud and blade-to-blade loadings are 0.57 and 0.64, respectively.

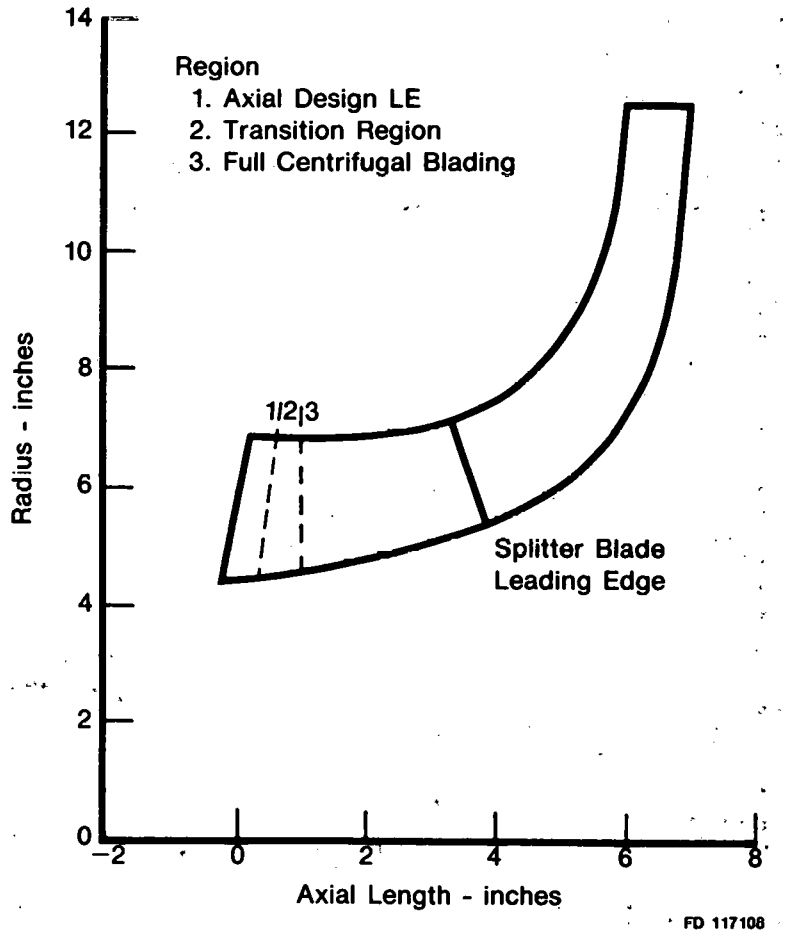

Figure II-6. Impeller Meridional Profile

The inducer region of the impeller was modified slightly to accommodate the leading edge geometry of a 400-series axial compressor airfoil. Incidence was set to obtain minimum loss based on axial compressor cascade data. The axially-defined leading edge geometry was then transitioned into the conventional impeller blading as indicated in figure II-6. The splitter blade leading edges were defined by superimposing a 400-series airfoil thickness distribution on the local impeller metal angle.

The impeller design pressure ratio was 2.82:1 at a goal adiabatic efficiency of 90%.

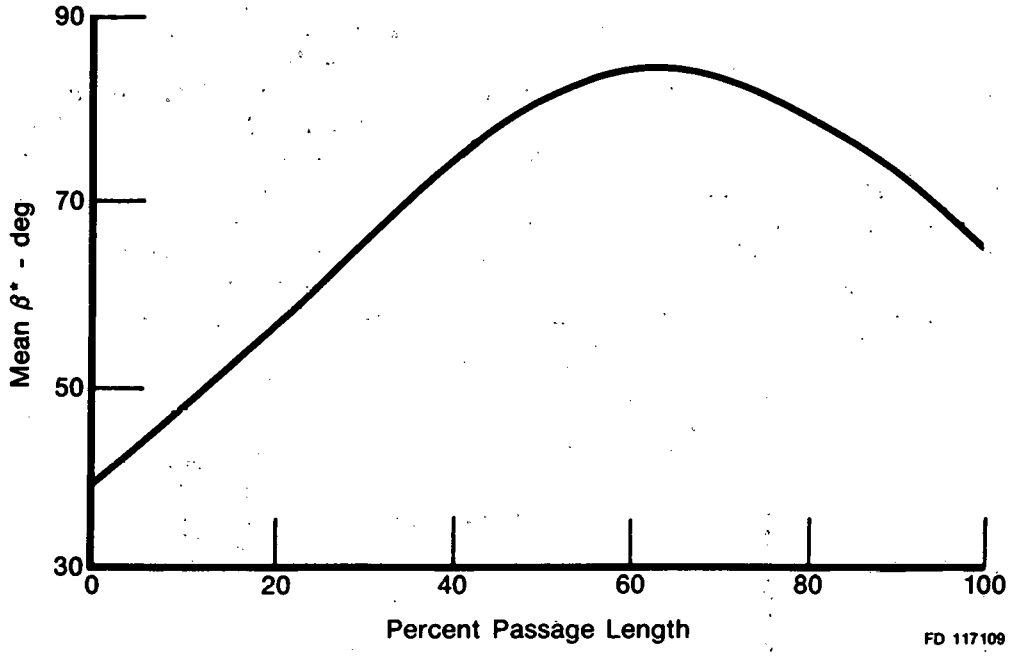

Figure II-7. Impeller Mean Blade Metal, Angle Distribution

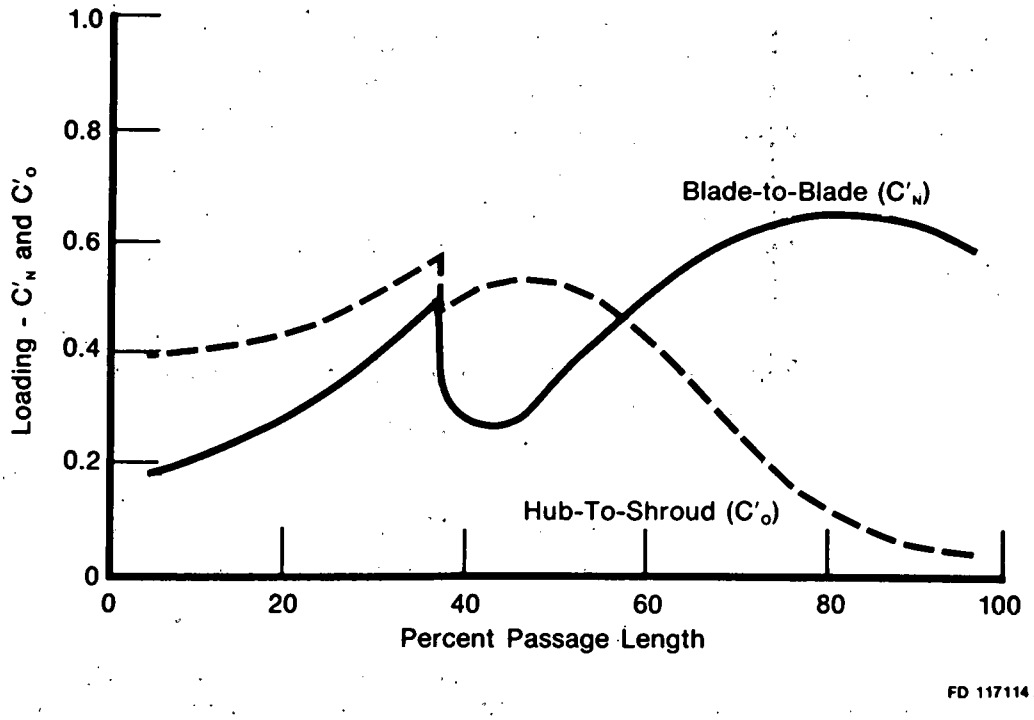

Figure II-8. Impeller Hub-to-Shroud and Blade-to-Blade Loading Distributions

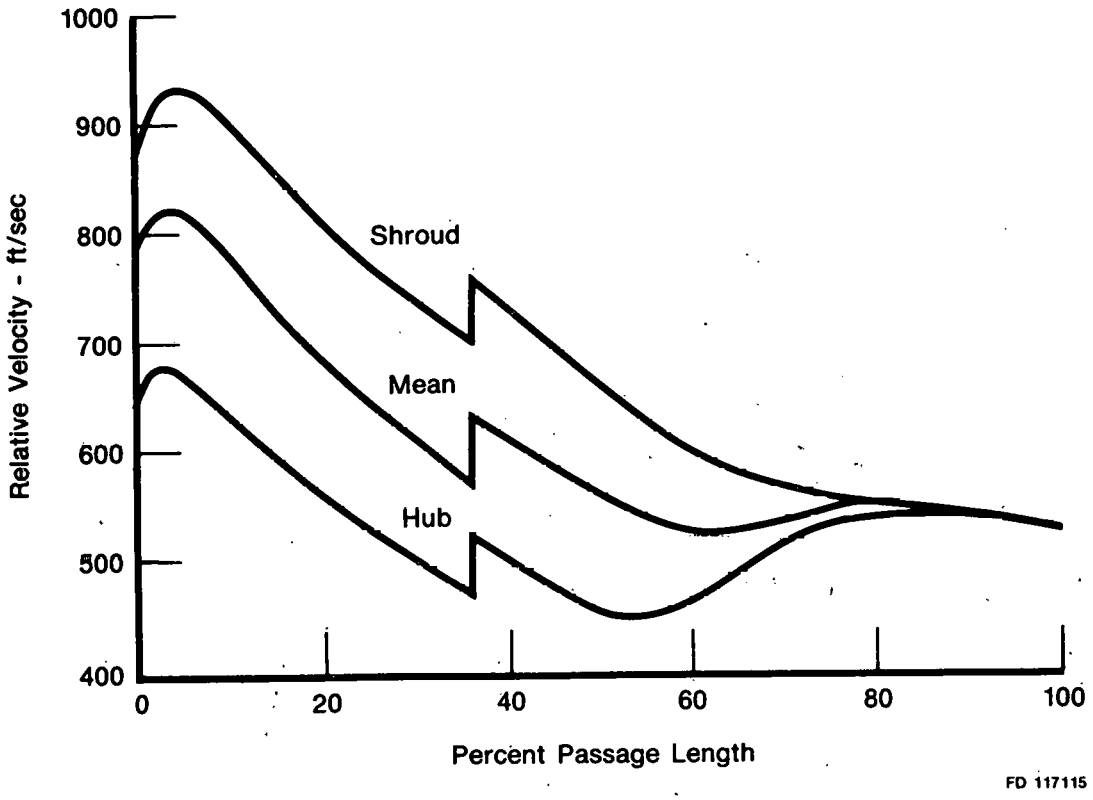

Figure II-9. Impeller Hub-to-Shroud Velocity Distribution

2. Diffuser

A schematic of the conical pipe diffuser is presented in figure II-10. The diffuser passages consist of a 3 deg cone angle segment to a 1.2:1 area ratio followed by a 5 deg cone angle segment to 2:1 area ratio. A constant diameter throat length of 0.100 inch was included to reduce the sensitivity of the throat area to manufacturing deviations and leading edge wear. The pipe centerline tangency radius was located as close as possible to the impeller tip (allowing for impeller radial growth and a small chamfer at the diffuser entrance) to keep vaneless space losses at a minimum. The design diffuser total pressure loss ($\Delta P_T/P_T$) was 4.2% at a leading edge Mach number of 0.83.

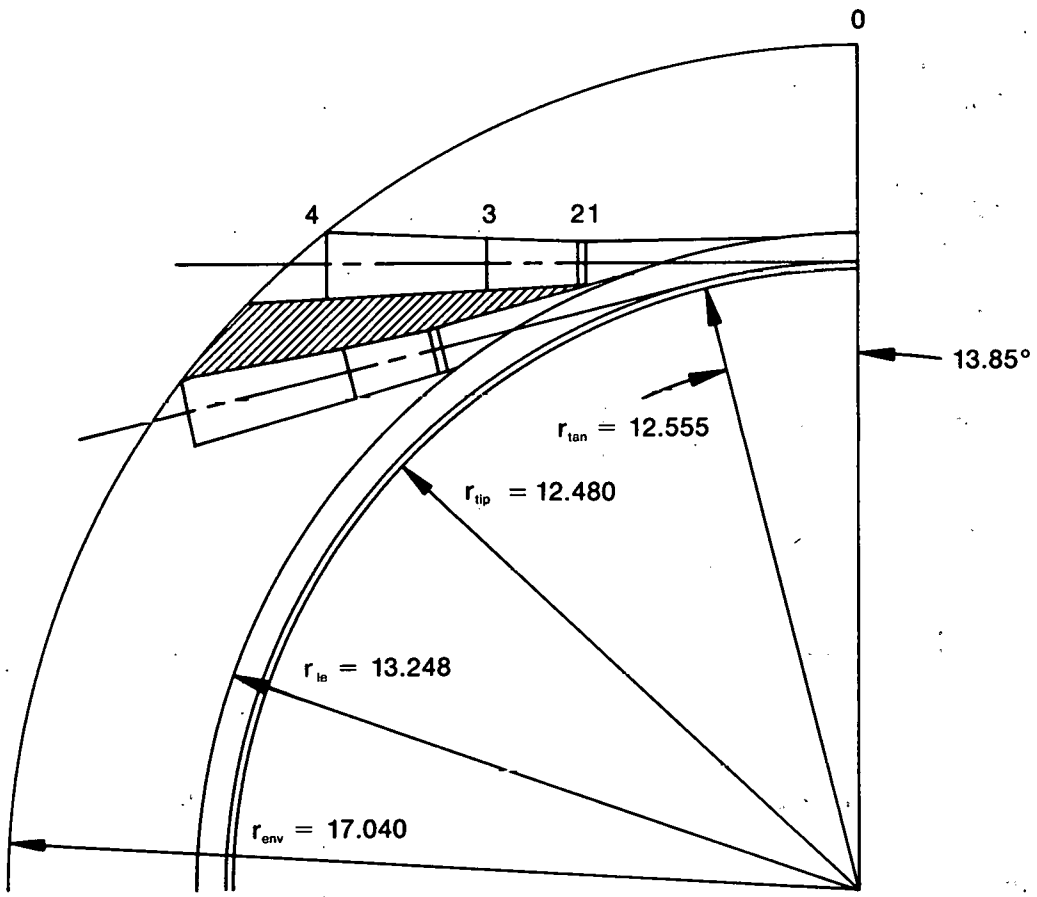

Cone Angles		Area Ratio		Pipe Diameter	
1-2	0 deg	1-2	1.0	1	0.950
2-3	3 deg	3-2	1.2	2	0.950
3-4	5 deg	4-2	2.0	3	1.041
				4	1.344

FD 117119

Figure II-10. 26-Pipe Conical Diffuser

C. COMPRESSOR RIG MECHANICAL DESIGN

A cross-section of the axial/centrifugal compressor test rig is shown in figure II-11. The major rig components were designed to be consistent with industrial engine design criteria and meet an industrial engine life goal of 20,000 hrs/10,000 cycles where practical. The rig is configured to provide sufficient flexibility to allow onstand performance optimization capability and minimize the required amount of test time. Specific features incorporated include:

- Variable, flapped inlet guide vanes
- Variable, cantilevered stators on all stages
- Split stator case
- Active impeller tip-to-shroud clearance control and measurement
- 30% interstage bleed capabiity
- Rotor axial thrust load measurement and control
- Centrifugal impeller backface buffer seal
- Capability to change diffusers on the test stand without dismounting the rig
- Oil damped roller bearings on both ends of rotor

The design philosophy, material selection, and structural analysis of the compressor rig components is detailed in Reference 1. A summary of the major hardware items is included below.

1. Rotor Assembly

The low aspect ratio axial compressor blades are mounted in a single-piece drum rotor made of Inconel 718. Blades for stages two through six are loaded circumferentially into annular grooves in the disk through loading slots provided on diametrically opposite sides of the rotor. Blade locks on the side of each loading slot secure the final blade inserted. The first stage blade attachment is a conventional axial blade lug configuration in order to obtain sufficient lug shear area at the relatively small first stage bore diameter. An abrasive coating consisting of a mixture of 97% aluminum oxide and 3% titanium dioxide is applied to the drum rotor flowpath between blades to provide stator tip rub protection. The drum rotor is designed to operate up to 17,250 rpm (110% design speed, 100°F inlet) and still have 20% burst margin. Titanium 6Al-4V was selected for the axial compressor blading for its light weight, corrosion resistance, and good fracture toughness.

The Inconel 718 centrifugal impeller is attached to the axial compressor drum rotor by means of a Curvic® coupling and 12 tiebolts. The impeller also is designed to maintain 20% burst margin up to 17,250 rpm. Maximum predicted blade stress is 103,000 psi at a 5-in. radius near the blade/disk fillet and the maximum disk/fillet stress is 108,000 psi at the impeller tip.

2. Axial Compressor Cases

The axial compressor cases consist of an inlet bellmouth, inlet strut case, and split stator case assembly. The bellmouth is designed to match with the rig ID nose cone to provide an area distribution consistent with that for a standard long ASME flow nozzle. The bellmouth construction is an aluminum sand casting with a minimum wall thickness of 3/8 inch. An annular ring seal surface is provided to match up with the test facility plenum pneumatic seal.

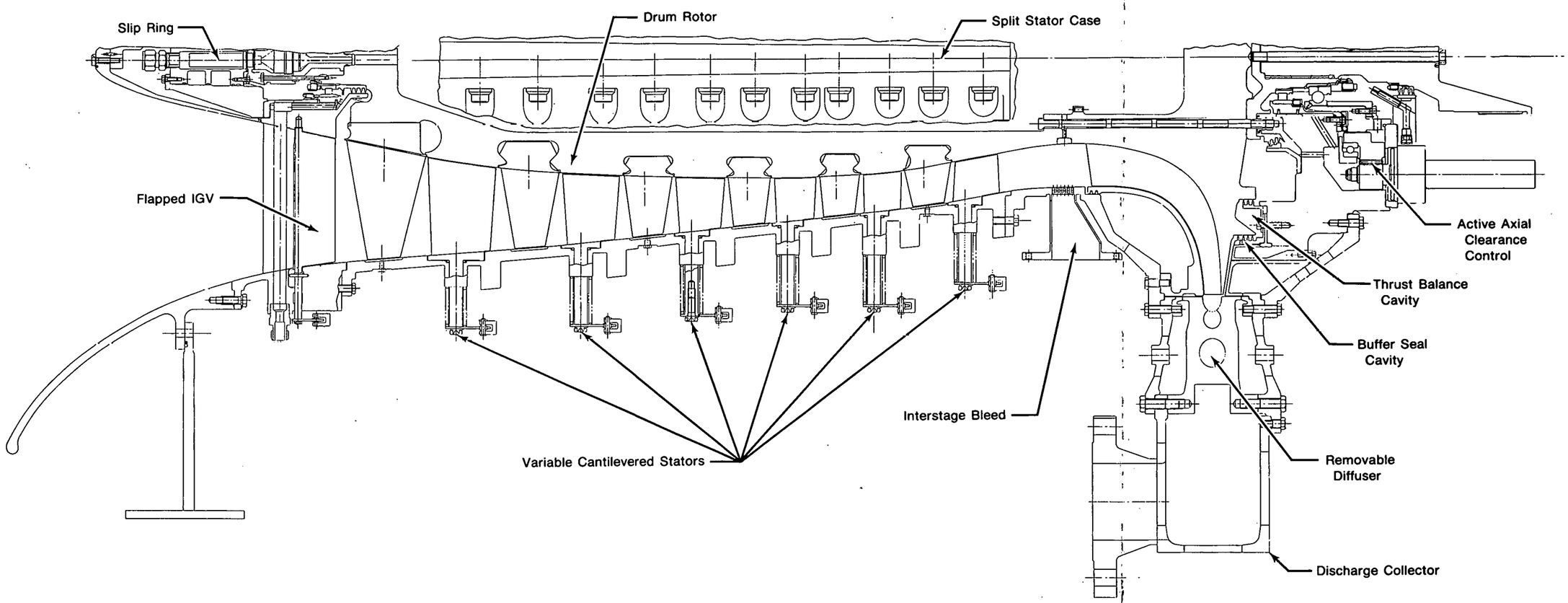

Figure II-11. Axial/Centrifugal Compressor Rig Cross Section

THIS PAGE

WAS INTENTIONALLY

LEFT BLANK

The inlet strut case, which was originally designed as an integral aluminum precision casting, was fabricated for the rig application from AISI 300 series stainless steel. Primary reasons for the material change included time and cost considerations associated with developing a casting for a single piece application and potential insufficient structural margins related to the low tensile and fatigue properties of aluminum. All of the front bearing compartment and slip ring services, including instrumentation routing, are provided through the thirteen inlet struts. Flapped inlet guide vanes are mounted immediately adjacent to each strut and are hydraulically driven through a sync ring to provide the desired rig inlet air angle.

The six stages of cantilevered stators are mounted in two horizontally-split case halves. All six stages are variable with the first two stages hydraulically operated and the remainder driven by electric motors. The case halves were machined from a single Wisco 625 centrifugal casting. Again, this method of fabrication was chosen due to the large development effort which would have been required for a precision casting of this size and complexity.

All of the axial compressor stators were cast out of Inconel 718. The center of gravity of each stator was located as close as possible to the support trunnion centerline to minimize trunnion surge bending stresses. To minimize endwall leakage losses the leading edges of the stators, where the maximum pressure differentials occur, are entirely supported by the button with the airfoil trailing edge cantilevered off the back of the button. A nominal 0.016 in. thick abradable coating of ekonol-aluminum was applied to the stator airfoil tips to work in conjunction with the drum rotor abrasive coating to provide rub protection. A silicone rubber rub strip material was included in the case OD flowpath wall over each rotor blade tip region for rotor rub protection.

3. Centrifugal Compressor Cases

The centrifugal compressor cases consist of the impeller shroud and its support structure, the diffuser case, exhaust collector manifold, and the rear support that ties to the bearing comparment. Material availability dictated the extensive use of AISI 410 stainless steel for this hardware in the rig although the majority of the comparable engine hardware would be fabricated (or cast) from Inconel 718.

The impeller shroud is bolted to its outer support case at the impeller exit with the inlet end of the shroud allowed free axial movement. With this configuration, deflection and thermal gradients in the structure do not impose strains on the shroud which could force it into the impeller. Piston rings are used to seal the shroud inlet. The shroud has a 0.003-0.005 in. thick silver coating to minimize the effects of a minor rub should one occur. The impeller-to-shroud axial clearance is adjustable with an active clearance control system. Provisions are made to monitor this clearance with a laser clearance probe at the impeller tip.

An interstage compressor bleed capability of up to 30% of the inlet flow rate is provided just forward of the impeller shroud for starting and off-design compressor matching. The bleed consists of 1632 1/8-in. diameter holes separated into four quadrants. Each quadrant has a separate manifold which connects to the facility ducting. A control valve and orifice in the test facility are used to regulate and measure the bleed flowrate.

The compressor rig hardware was designed to be compatible with two diffuser configurations: 1) a vaneless diffuser for use during the axial compressor performance documentation portion of the test program, and 2) a conical pipe diffuser for use during the overall compressor performance documentation testing. Capability was provided to change diffuser configurations on the test stand without dismounting the rig. Flow from the diffuser is discharged into an annular collector which has six exhaust flanges connected to the facility discharge ductwork.

The impeller backface region is segmented into three primary cavities by multi-element labyrinth seals. The pressures in these cavities are independently regulated to respectively prevent the flow of oil out of the rear bearing compartment, provide the proper rotor axial thrust load, and regulate the impeller tip backface leakage flow.

4. Bearing Compartments

A roller bearing is provided for the front end rotor support; the rear bearing compartment employs a dual bearing configuration in which a roller bearing carries all the radial load and a ball bearing carries all the thrust load. All three bearings are under-race cooled with holes provided through the inner race to direct oil to the cage riding surfaces and rolling elements. Hydraulically-damped bearing hairsprings are utilized for both roller bearings. Springrates were selected to achieve a 20% rotor critical speed margin. Radial clearance between the ball bearing outer race and its carrier prevents the ball bearing from seeing any radial loads, thus increasing ball bearing life. Predicted life for all the bearings exceeds 20,000 hours.

The ball bearing retainer can be moved axially to adjust the position of the compressor rotor relative to the cases and provide active control of the impeller-to-shroud tip clearance. The bearing retainer is threaded on the OD where it mates with a ring gear threaded on its ID. The ring gear is in turn driven by two gear motors. Actuation of the motors rotates the ring gear, advances its thread and thus moves the bearing and carrier fore and aft with the rotor. Thrust loads are transferred through the ring gear to a static ball bearing and into a bearing carrier supported on three axially-mounted load cells. The active clearance control device is designed failsafe; i.e., if the drive motors, gers or threads fail, the bearing carrier will still limit the forward motion of the rotor shaft.

Labyrinth seals at the rear of both bearing compartments are center-fed with high pressure air to prevent oil leakage out of the compartments.

SECTION III
COMPRESSOR RIG FABRICATION AND ASSEMBLY

A. HARDWARE FABRICATION

The materials and fabrication techniques utilized for each of the compressor rig major components are summarized in table III-1. Where practical from a cost and schedule standpoint, the materials and fabrication techniques were selected to be representative of those that would be used for production engine hardware. A brief discussion of each of the major rig hardware items is included below.

Table III-1. Compressor Hardware Fabrication Summary

Component	*Material*	*Fabrication Technique*
Drum Rotor	Forged PWA 1010 Nickel Alloy	Fully Machined
Rotor Blades	Forged Bar AMS 4928 Titanium Alloy	Individually, fully machined; hand ground to final contour; hand polished
Stator Vanes	Cast PWA 649 Nickel Alloy (Inco 718)	Fully machined case interface (spindles and buttons); flow path surfaces hand polished.
Impeller	Forged PWA 1010 Nickel Alloy	Fully machined; machine ground to final contour.
Inlet Case	Forged AISI 321 SST	Partially machined welded assembly
Axial Compressor Case	Centrifugally Cast Wisco 625	Fully machined
Interstage Bleed Manifold	Centrifugally Cast AISI 410 SST	Fully machined welded assembly
Impeller Shroud	Centrifugally Cast AISI 410 SST	Fully machined
Diffuser, Pipe	Centrifugally Cast AISI 410 SST	Fully machined
Collector	Forged AMS 5613 SST Plate	Partially machined welded assembly
Rear Bearing Support	AISI 4340 Steel	Fully machined
Vaneless Diffuser	Forged AMS 5613 SST Plate	Fully machined
Seal Support	Forged AMS 5613 SST Plate	Fully machined
Front Support, Collector	Forged AMS 5613 SST Plate	Fully machined
Rear Support, Collector	Centrifugally Cast AISI 410 SST	Fully machined, welded Assembly
Support	Centrifugally Cast AISI 410 SST	Fully machined

1. Axial Compressor Drum Rotor

The axial compressor drum rotor was machined from a single PWA 1010 nickel alloy (Inconel 718) forging through a series of six major steps as outlined in figure III-1. The forging was first rough machined and reference surfaces provided on both the front hub and rear face. The final flowpath, blade attachments, and rotor details were then machined. A photograph of the drum rotor at this stage is shown in figure III-2. The drum rotor fabrication was completed with machining of the curvic coupling and installation of an abrasive coating over the cantilevered stator tip locations.

2. Axial Compressor Airfoils

All the axial compressor blades were machined from wrought AMS 4928 titanium alloy (6-4) bar stock and hand ground and polished to obtain the desired final airfoil contour and surface finish. An anti-galling coating was applied to the attachment surfaces. Rubber seals were applied with a RTV compound to the under side of the blade platforms to minimize leakage into the attachment cavities. A photograph of a completed set of axial compressor airfoils is shown in figure III-3.

The axial compressor stator vanes were individually cast out of PWA 649 nickel alloy (Inconel 718). The vane airfoil surfaces were cast to final shape with light hand polishing the only subsequent operation performed. Excess casting stock was provided on the vane support buttons and spindles and these final surfaces were machined. Figure III-4 shows the vanes in the as-cast condition; a set of the completed vanes are shown in figure III-5.

A summary of the final airfoil surface finishes for both blades and vanes is presented in table III-2.

3. Centrifugal Impeller

The centrifugal impeller was machined from a solid PWA 1010 nickel alloy forging. A numerical tape-controlled three axis milling machine was used for the flowpath and blading contour machining. During rough machining of the impeller blading, a broken cutter damaged two adjacent airfoil surfaces. A weld repair and re-heat-treatment procedure was satisfactorily completed prior to continuation of the impeller machining. A photograph of the centrifugal impeller at the completion of the flowpath and blading contour machining is shown in figure III-6. Fabrication of the impeller was completed with machining of the curvic coupling.

4. Inlet Strut Case

The inlet strut case, figure III-7, was fabricated out of AISI 300 series stainless steel. The inner and outer case rings and the 13 struts were individually machined, and then welded into a single assembly. After heat-treatment, the critical case internal details and adjoining hardware mating surfaces were machined. Provisions were included for strut leading edge and bearing compartment instrumentation installation and routing. The inlet guide vane flaps were machined from wrought PWA 1009 nickel alloy (Inconel 718) bar stock.

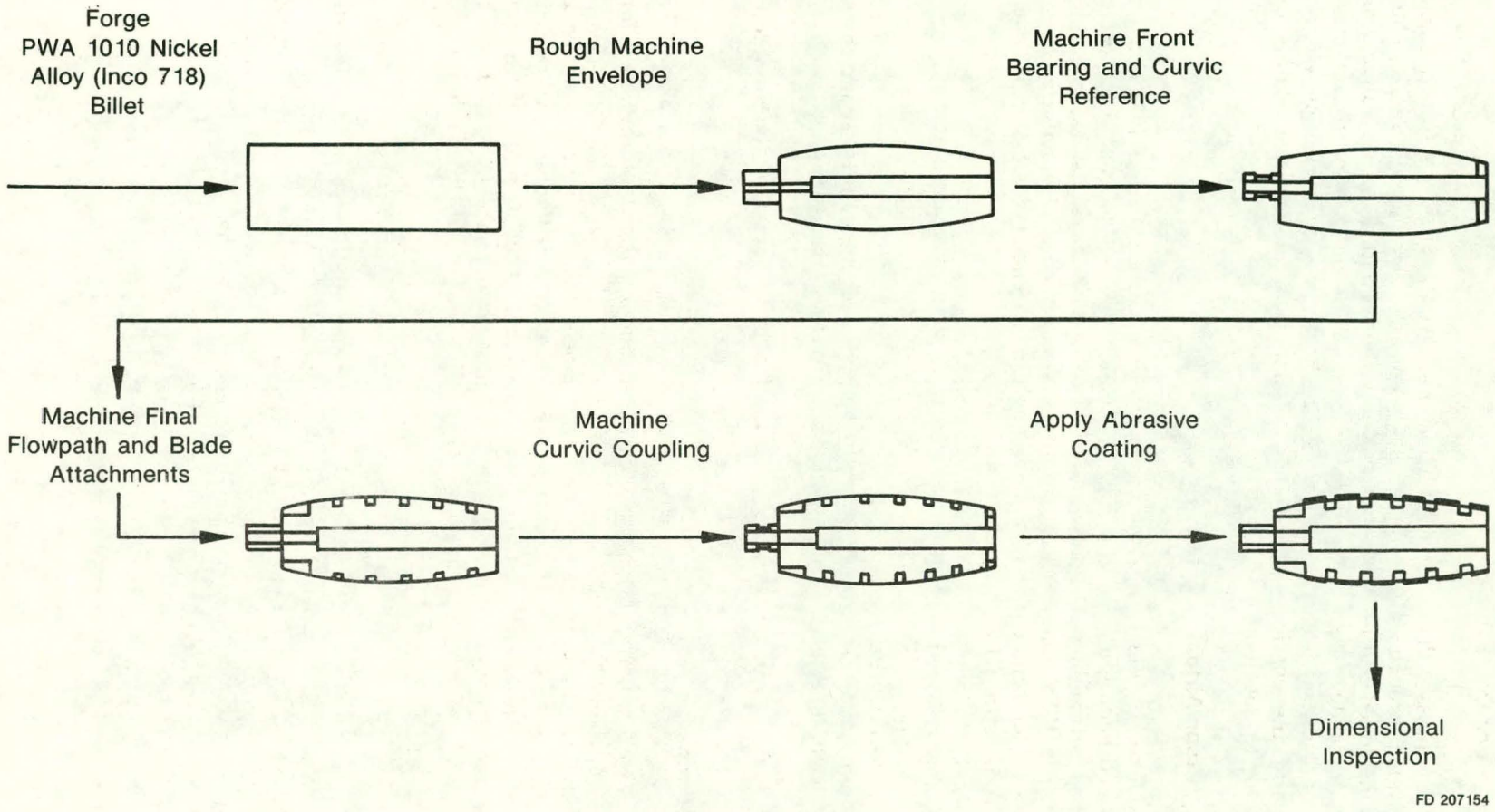

Figure III-1. Axial Compressor Drum Rotor Fabrication Procedure

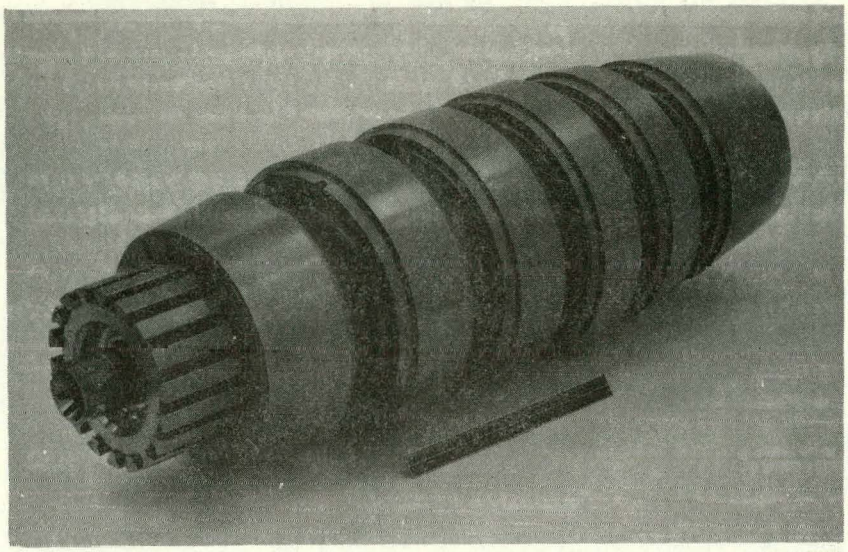

FE 173765
FD 207155

Figure III-2. Semi-Finished Axial Compressor Drum Rotor

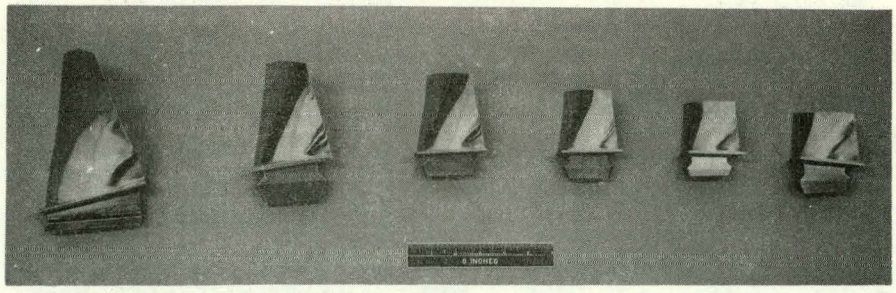

FE 195939

Figure III-3. Axial Compressor Rotor Blades

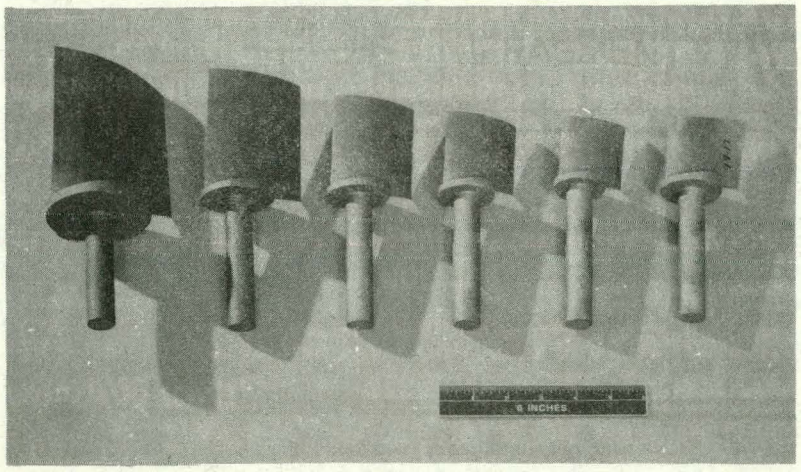

FE 173736

Figure III-4. Axial Compressor Variable Vanes in the As-Cast Condition

Table III-2. Airfoil Surface Finish Summary

		Average Surface Finish (Microns)		
		Prior	*After Polish*	
Stage	*Row*	*to Polish*	*Radial*	*Axial*
1	Rotor	20	12	10-12
	Stator	76-49	24	16
2	Rotor	20	8-10	10-12
	Stator	76-94	28	16
3	Rotor	20	8-10	14-16
	Stator	76-94	20	20
4	Rotor	20	12	18
	Stator	76-94	24	16
5	Rotor	20	10-12	20
	Stator	76-94	20	32
6	Rotor	20	10	8
	Stator	76-94	24	32

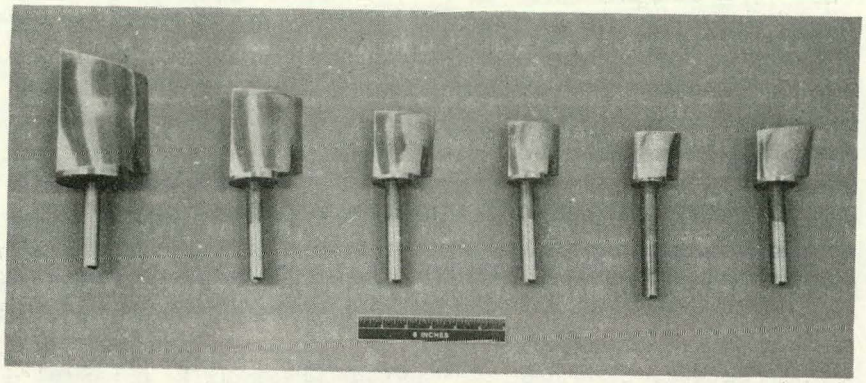

FE 195940

Figure III-5. Completed Axial Compressor Variable Vanes

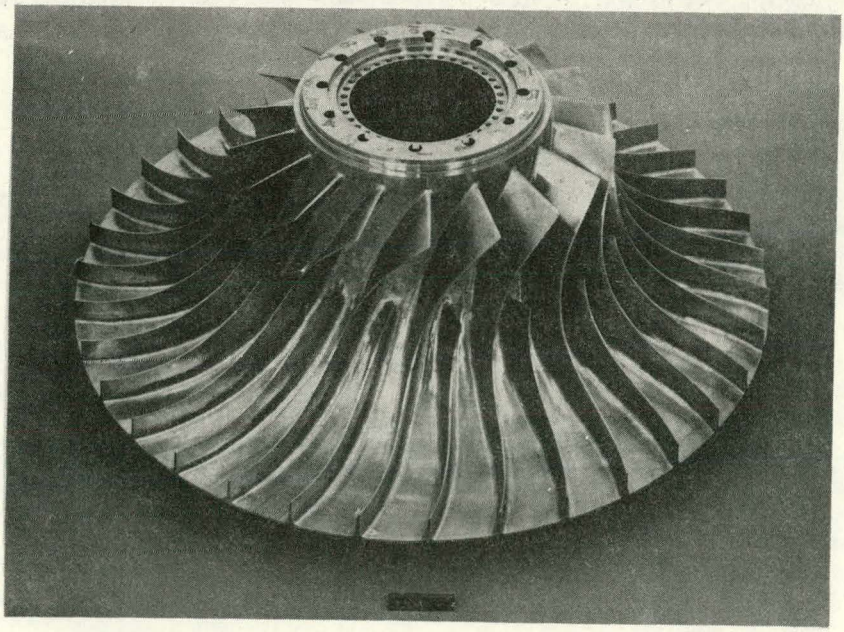

FE 177208

Figure III-6. Centrifugal Impeller

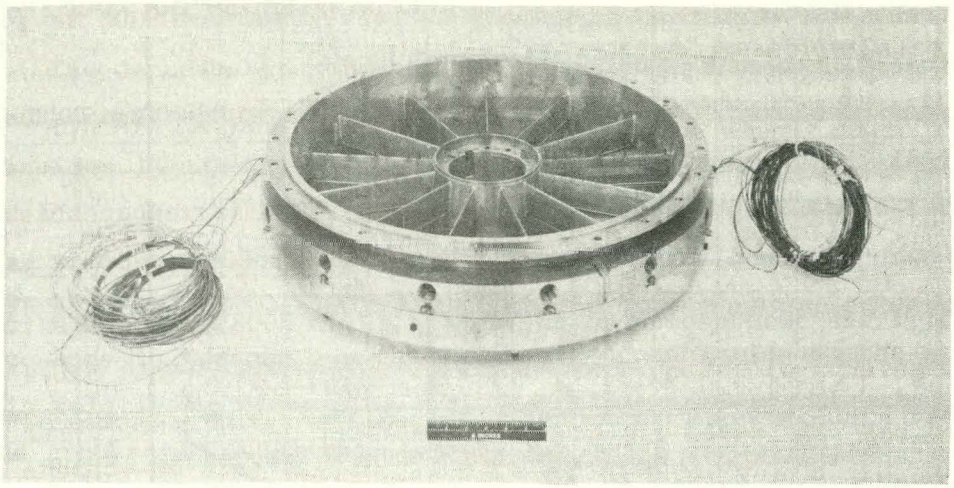

FE 182849
FD 207160

Figure III-7. Inlet Strut Case With IGV Flaps

5. Axial Compressor Stator Case

The axial compressor stator case was machined from a single centrifugally-cast Wisco 625 nickel alloy (similar to Inconel 625) conical shell. The fabrication process is outlined in figure III-8. After rough envelope machining, the cast conical shell was separated horizontally in halves and the exterior surfaces rough machined. The case was then heat-treated and machining of the exterior surfaces completed. Machining of the flowpath surfaces was conducted after all exterior surfaces were completed. The two case halves were first bolted together to the specfied torque, fixtured to a lathe, and the flowpath turned to the desired contour. Recesses were provided over the blade tip locations for subsequent installation of a PWA 407 silicone rubber abradable rub strip material. Excess rub strip material was initially installed and the surface later hand-blended to provide a smooth flowpath contour with the adjacent case surfaces. A complete dimensional check of all case critical surfaces, including the flowpath contour, was made at the completion of all fabrication operations.

6. Centrifugal Compressor Cases

The centrifugal compressor cases include the interstage bleed manifold housing, impeller shroud, diffuser, and discharge collector. All these hardware items except the collector were fabricated out of centrifugally cast AISI 410 stainless steel rings. The rig discharge collector was fabricated as a welded assembly from wrought AISI 410 stainless steel plate stock.

The interstage bleed manifold housing, figure III-9, was fabricated as a welded assembly. The majority of the exterior surface machining, bleed hole drilling, etc., was completed on the constituent detail items prior to welding. The welded assembly was then heat-treated and all close-tolerance machining completed. The impeller shroud housing was machined to final contour and a 0.003 to 0.005 inch thick silver plating applied to the flowpath surface. The pipe diffuser passages consist of a series of simple conical drillings which intersect to form the diffuser entrance flowpath geometry as shown in figure III-10.

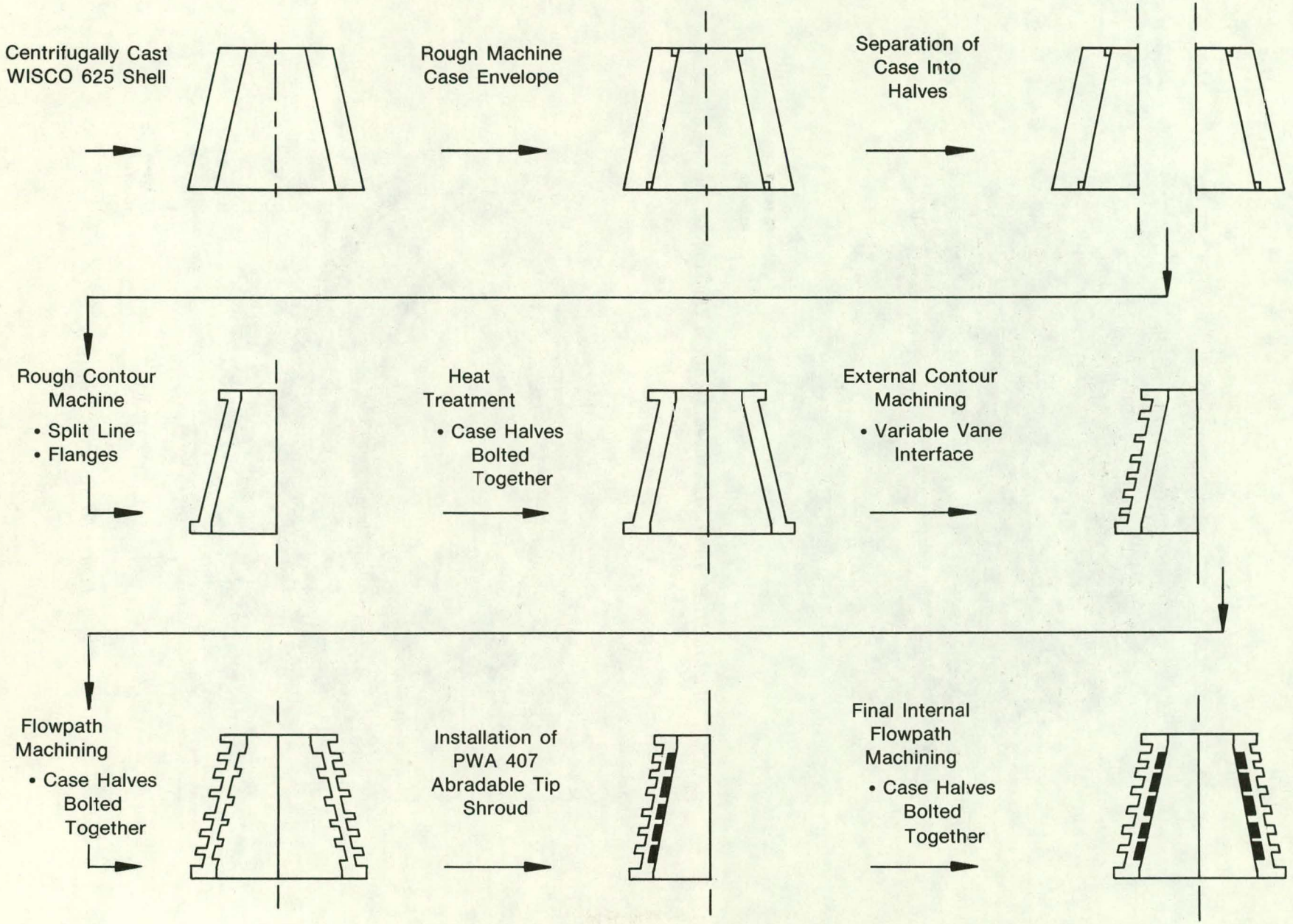

Figure III-8. Axial Compressor Split Case Fabrication Procedure

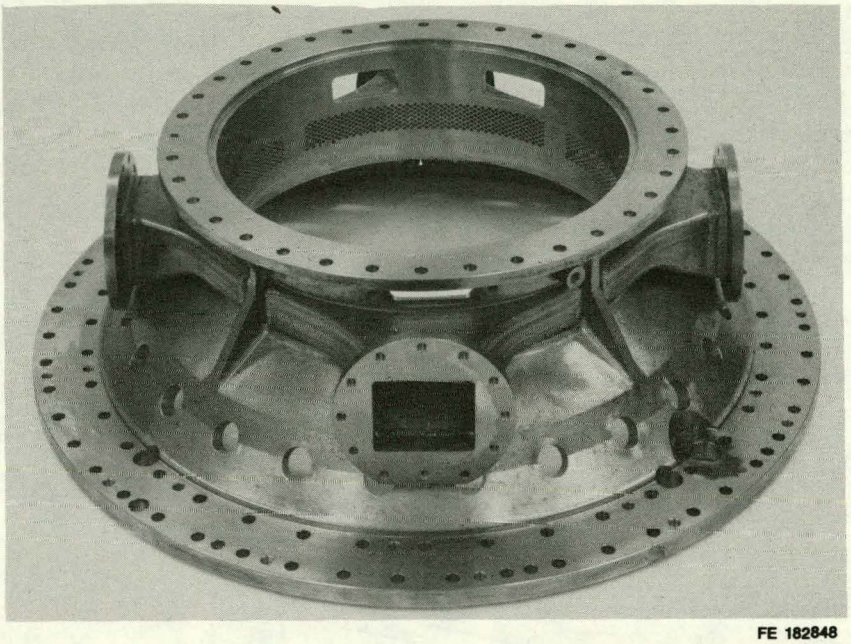

FE 182848
FD 207162

Figure III-9. Interstage Bleed Manifold Housing

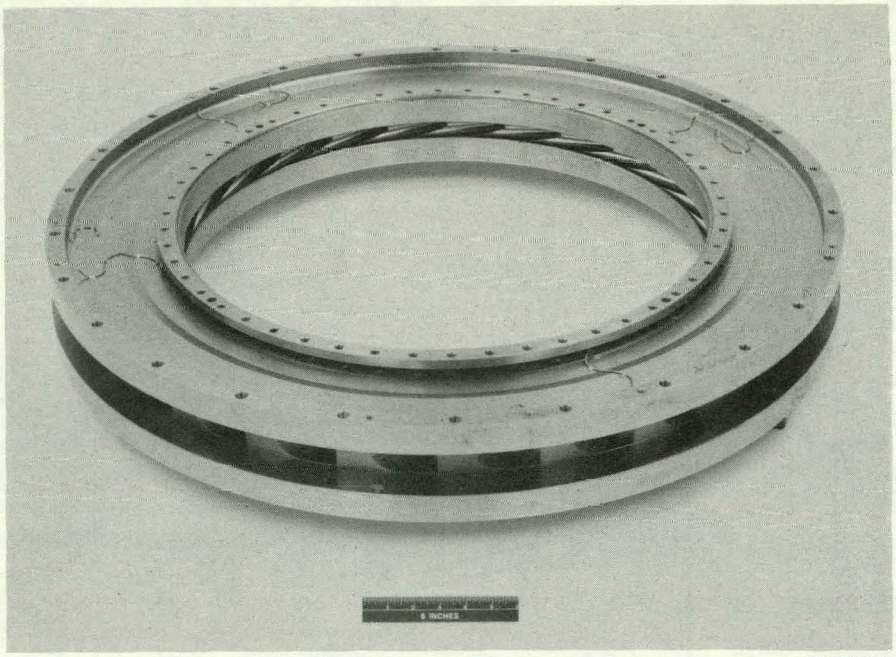

FE 182850
FD 207163

Figure III-10. Pipe Diffuser

B. COMPRESSOR RIG ASSEMBLY

The compressor test rig assembly effort was conducted in four phases: rotor assembly, axial compressor stator case assembly, major subassemblies, and final test article assembly. A roadmap of the compressor rig assembly sequence is presented in figure III-11. In addition, assembly support was required at test to change the vaneless and pipe diffusers. Each phase of the assembly effort and the diffuser replacement procedure are discussed in the following paragraphs.

1. Rotor Assembly

The rotor assembly for the compressor test rig consisted of a six-stage axial compressor drum rotor and a single-stage centrifugal impeller. The drum rotor and impeller were attached with longitudinal bolts through a curvic coupling. To ensure acceptable operating rotor dynamics while maintaining a clean aerodynamic configuration, a six-step process was utilized to assemble the rotor:

- Hardware inspection
- Component detail balance
- Initial rotor assembly and balance
- Blade tip grind
- Rotor strain gage installation
- Final rotor assembly and check balance

The initial step in the assembly process was to complete a detailed dimensional inspection of all rotor hardware including the drum rotor, impeller, blades, blade locks, and bearing hardware. Particular attention was directed toward critical fits, clearances, and aerodynamic surfaces. Airfoil contours were verified by tracing selected blade surfaces and comparing these tracings to the design airfoil profiles. In general, the blades were found to be within nominal manufacturing tolerances. Based upon the inspection results and the measured vibrational characteristics of each blade (Section IV-C), a set of blades for each stage was selected for use in the compressor test rig.

Detail dynamic balancing of the centrifugal impeller was accomplished by a combination of material removal and subsequent addition of small balance weights in the impeller front and rear balance planes. Final residual unbalance in both the impeller front and rear planes was 0.025 oz-in.

Detail balancing of the drum rotor was performed utilizing the balanced impeller as an arbor to support the rear of the drum rotor as shown in figure III-12. This procedure was adopted to minimize tooling costs. The drum rotor was balanced to within the sensitivity limit of the balance machine (approximately .06 oz-in.) utilizing this procedure. Since the compressor rig assembly sequence required that the axial compressor drum rotor and centrifugal impeller be disassembled after final balancing, a series of rotor disassembly/reassembly cycles were undertaken at this point to determine the repeatability of the balance. The variation in the balance was approximately 0.47 oz-in. even with strict adherence to the rotor assembly and tie-bolt torquing procedures. A review of the rotor dynamics analysis indicated that favorable rotor characteristics could be maintained up to an unbalance of approximately 0.5 oz-in., hence the balance repeatability achieved was acceptable, although larger than desired.

THIS PAGE

WAS INTENTIONALLY

LEFT BLANK

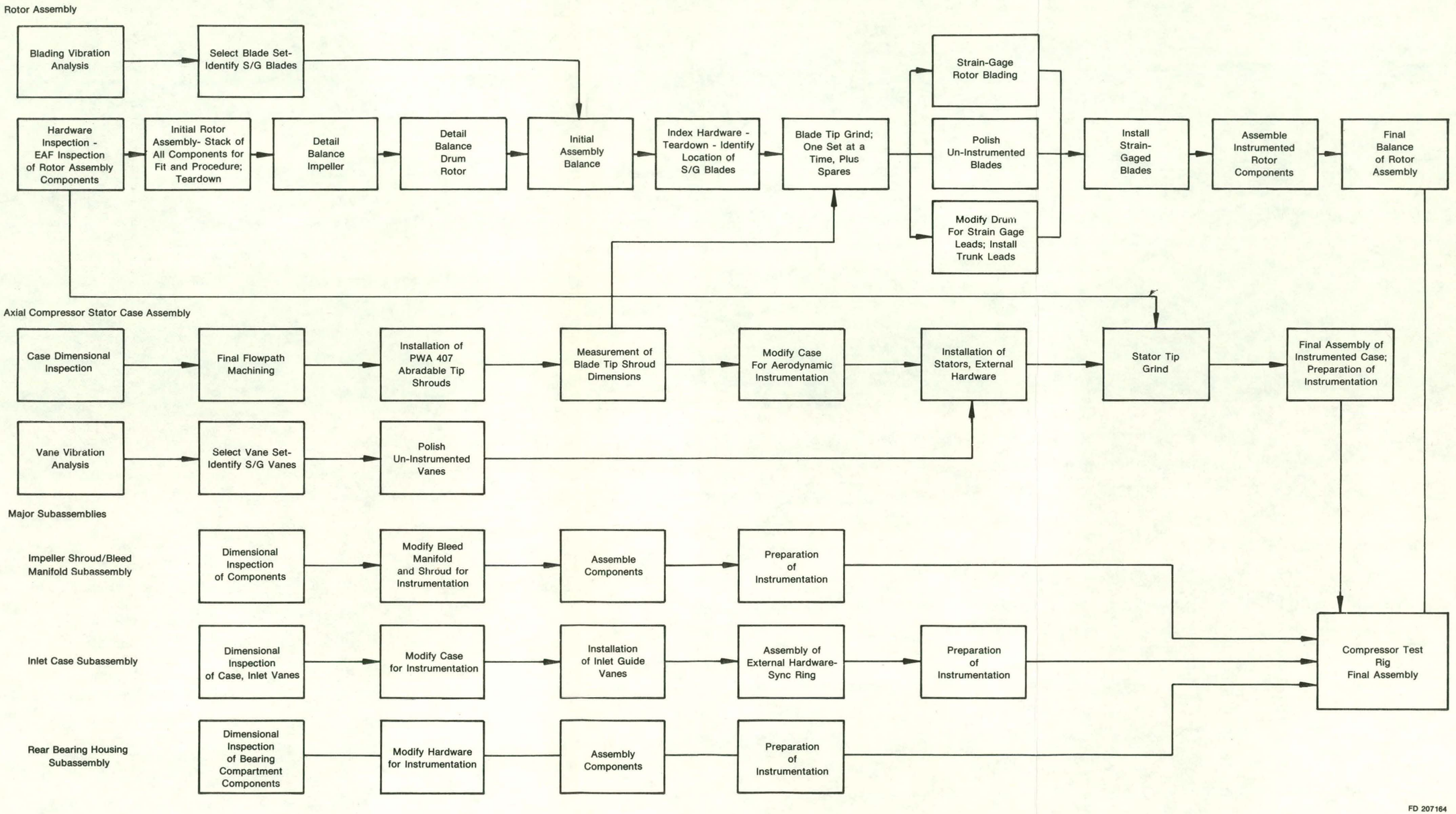

Figure III-11. Compressor Test Rig Assembly Plan

THIS PAGE

WAS INTENTIONALLY

LEFT BLANK

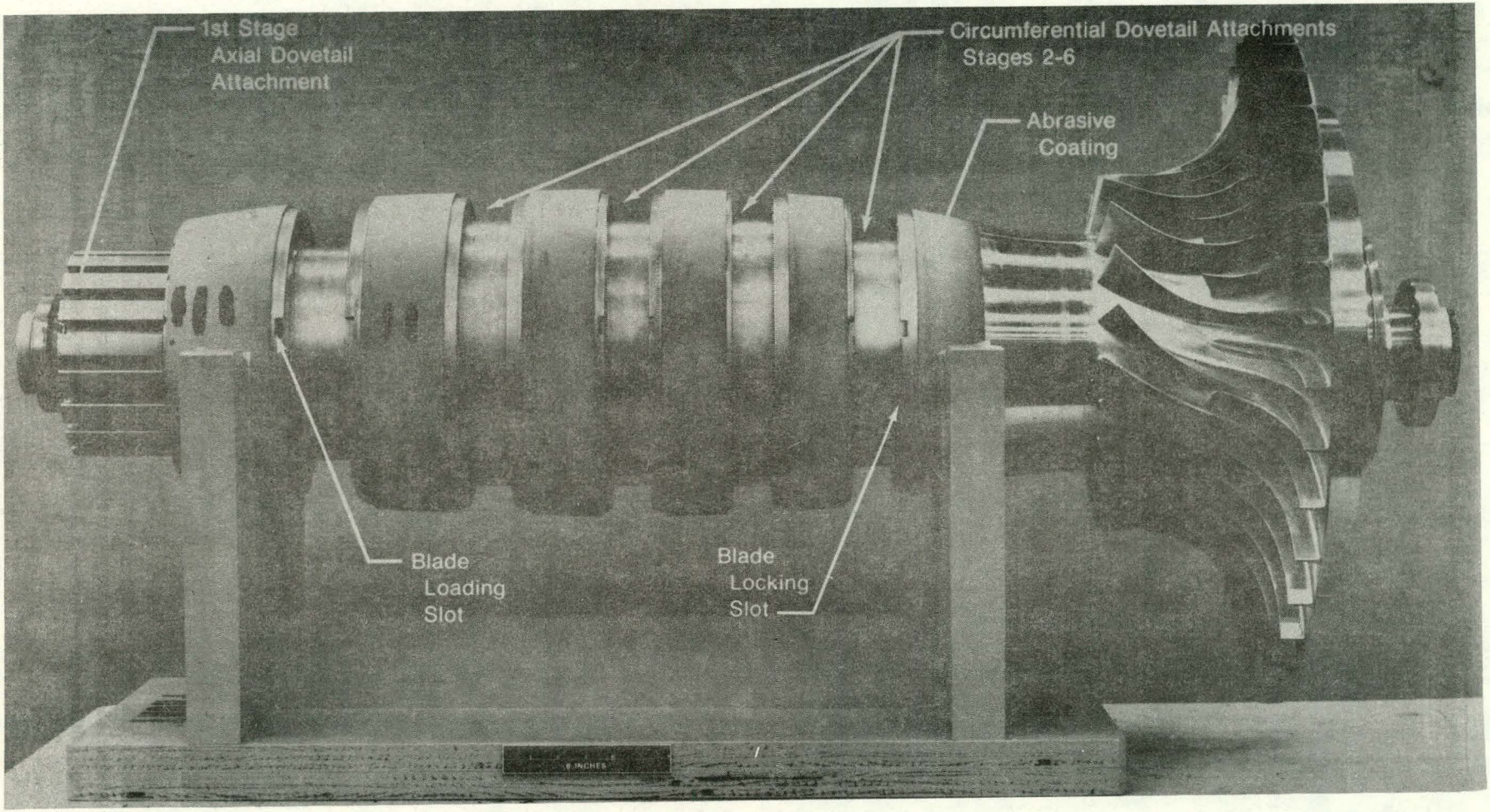

FE 179908
FD 207165

Figure III-12. Rotor Balance Assembly

With completion of the detailed balancing of the drum rotor and impeller, the axial compressor blading was installed. The circumferentially-loaded axial compressor blades (second through sixth stages) were installed in the drum rotor and the single wide-platform blade in each stage trimmed to provide the desired circumferential fit. All of the blades were then removed from the rotor, weighed, and paired by weight. Similarly, the first stage blades were moment-weighed and paired. Sets of paired blades were then selected and the blades in each set installed diametrically opposite each other in a sequence defined to minimize both the circumferential weight variation and the overall unbalance caused by the blading installation.

A check balance was subsequently completed to define the overall effect of the addition of the axial compressor blading. The blades in the second and sixth stages were then rearranged to minimize the unbalance of the entire assembly. Further reduction in the unbalance was achieved by adding balance weights, as required, between blade attachments in each of these two rows; an acceptable residual unbalance of 0.39 and 0.59 oz-in. was obtained in the front and rear balance planes, respectively. The relative position of all components was recorded and the entire rotor disassembled.

The axial compressor blade tips were subsequently ground to provide the desired blade assembly clearances. Factors taken into consideration in determining the required assembly clearance are outlined in table III-3; the resultant projected design speed running clearances are shown in table III-4. Clearances were selected so that the blade tips could potentially rub into the case abradable rub strip material by up to 0.008 under worst case transient conditions. All spare blades were also tipped in case they had to be substituted for one of the initially selected blades.

Table III-3. Factors Determining Blade Tip Assembly Clearance Requirements

Stage	Rotor Growth	Blade Growth	Case Growth	Active Clearance Control	Bearing Travel	Bearing Droop	Rotor Deflection and Tolerances	Case Ovalization
1	0.002	0.001	−0.002	0.006	0.002	0.002	0.006	0.008
2	0.012	0.002	−0.006	0.006	0.002	0.002	0.007	0.008
3	0.017	0.003	−0.012	0.006	0.002	0.002	0.008	0.008
4	0.020	0.005	−0.020	0.006	0.002	0.002	0.009	0.008
5	0.023	0.005	−0.024	0.006	0.002	0.002	0.010	0.008
6	0.026	0.006	−0.026	0.006	0.002	0.002	0.011	0.008

NOTE:
Figures represent maximum radial clearance decrement in inches anticipated at design rotor speed due to each factor

Table III-4. Blade Tip Clearance Summary

Stage	Maximum Projected Clearance Decrement	Assembly Clearance	Minimum Running Clearance	Nominal Running Clearance
1	0.025	0.017	−0.008	0.016
2	0.033	0.025	−0.008	0.017
3	0.034	0.026	−0.008	0.018
4	0.032	0.024	−0.008	0.019
5	0.032	0.024	−0.008	0.021
6	0.035	0.027	−0.008	0.021

After tip grinding, strain gages were installed on selected blades. The strain gage locations and installation details are provided in Section IV-C. Each strain gage was provided with sufficient length lead wires to allow splicing to trunk leads which were pre-installed in the inside of the drum rotor. Once the trunk leads and slip-ring adapting hardware were installed, reassembly of the axial compressor blading in the drum rotor was completed, and all instrumentation leads terminated and secured.

The centrifugal impeller was subsequently installed on the axial compressor rotor to check the rotor balance. A photograph of the final rotor assembly is shown in figure III-13. Final fine-tuning of the rotor balance was accomplished by repositioning the previously installed balance weights in the second and sixth stages. The final rotor residual unbalances were .39 oz-in. and .33 oz-in. in the front and rear balance planes, respectively. Upon completion of the final rotor balance, the centrifugal impeller was removed from the axial compressor rotor in preparation for the final test article assembly effort.

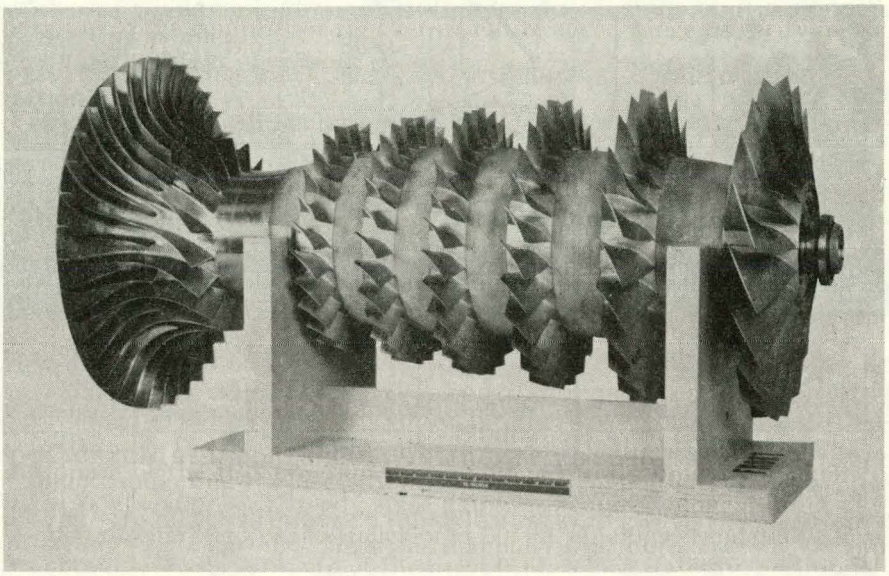

FE 181071
FD 207166

Figure III-13. Compressor Rotor Assembly

2. Axial Compressor Case Assembly

The variable stators were installed in the split stator case on a one-by-one basis, and the excess stock provided on the vane OD trailing edge was removed as required to obtain the range of variability desired (see Section II-A) while minimizing the end gaps in the nominal vane position. Upon completion of the installation of all the vanes, the vane sync ring assemblies were installed, the case halves joined together, and the circumferential variation in the nominal vane stagger angles checked for the first and sixth stages. A summary of the vane position variation measured for these two stages is presented in table III-5.

Table III-5. Variations in Nominal Vane Stagger

	Angle Deviation		
Stage	*Max*	*Min*	*Ave*
1	+38′	−22′	+10′
6	+20′	−10′	+2′

The stator tips were then ground as an assembly to provide the desired assembly clearances. Primary criteria for determining the vane tip clearances was that there should be no interference rub between the vane tips and drum rotor under worse case transient conditions over the entire range of variability for each vane row. The factors considered in determining the clearances and the estimated magnitude of the change in clearance from assembly through design speed due to each factor are summarized in table III-6. Implementation of the above clearance criteria, however, resulted in large running clearances under steady state operating conditions with the vanes in their design nominal position. An abradable coating of ekonol aluminum (PWA 255) was therefore flame sprayed on to the tips of the vanes to reduce the nominal running clearances to a level closer to the original design intent without risking a potentially catastrophic rub. The approximate thickness of the abradable tip coating for each vane row and the resultant final projected design speed average clearances are summarized in table III-7.

All remaining instrumentation installation and routing was next completed and the case readied for the final rig stack-up. A photograph of one of the completed case halves is shown in figure III-14.

Table III-6. Factors Determining Vane Tip Assembly Clearance Requirements

Stage	Rotor Growth	Vane and Case Growth	Active Clearance Control	Bearing Travel	Bearing Droop	Rotor Deflection and Tolerances	Case Ovalization
1	0.010	−0.002	0.003	0.003	0.002	0.006	0.008
2	0.015	−0.006	0.001	0.001	0.002	0.007	0.008
3	0.019	−0.010	0	0	0.002	0.008	0.008
4	0.021	−0.014	0.002	0.001	0.002	0.009	0.008
5	0.024	−0.017	0.004	0.002	0.002	0.010	0.008
6	0.027	−0.018	0.009	0.003	0.002	0.011	0.008

NOTE:
Figures represent maximum radial clearance decrement in inches anticipated at design rotor speed due to each factor.

Table III-7. Vane Tip Clearance Summary

Stage	Maximum Projected Clearance Decrement	Minimum Running Clearance to Vane Metal Surface	Abradable Coating Thickness	Average Nominal Running Clearance
1	0.030	0	0.019	0.030
2	0.028	0	0.011	0.020
3	0.027	0	0.009	0.017
4	0.029	0	0.013	0.018
5	0.033	0	0.019	0.020
6	0.042	0	0.024	0.030

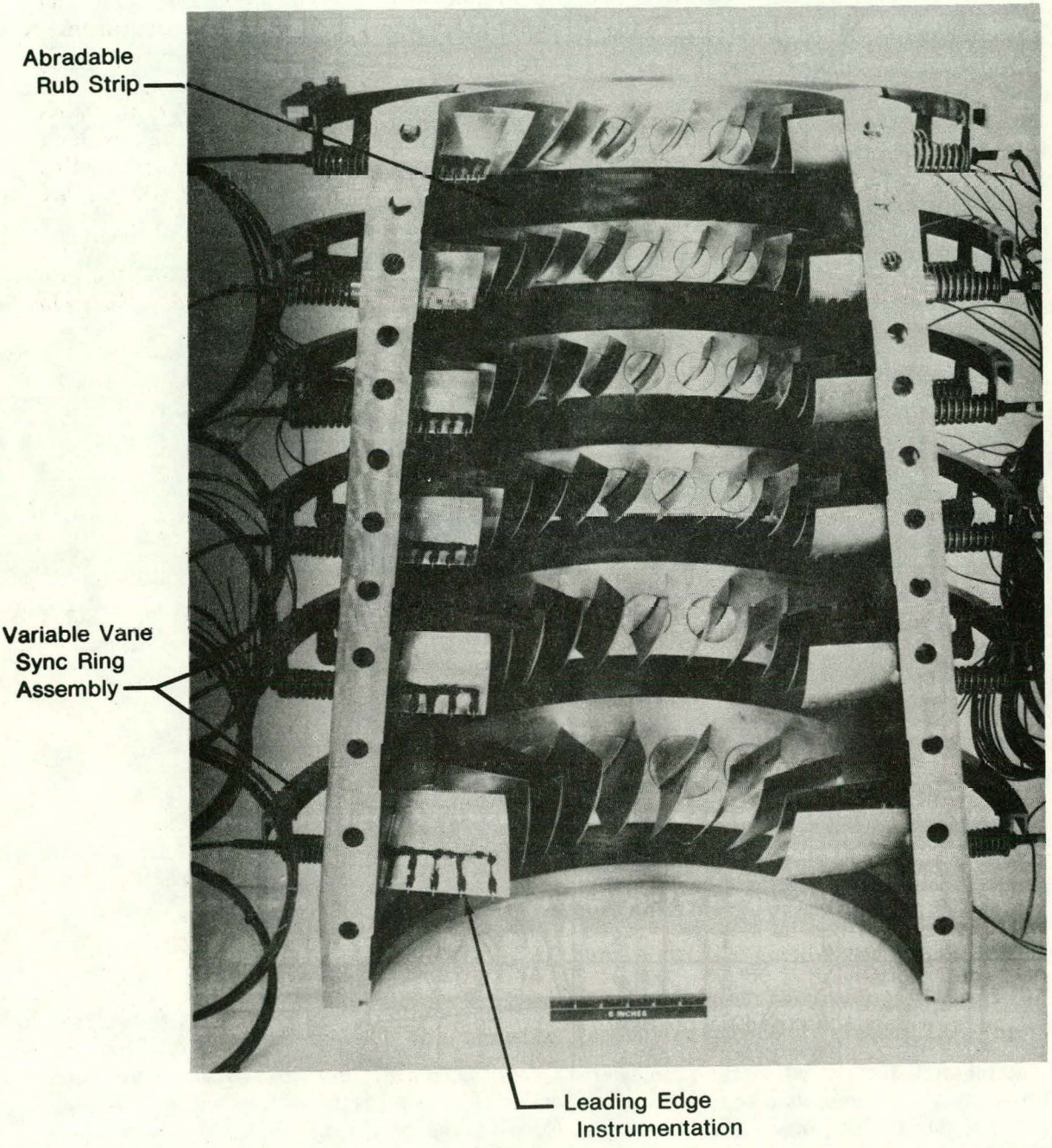

Figure III-14. Axial Compressor Split Stator Case Half Assembly

3. Test Rig Major Subassemblies

In addition to the compressor rig rotor and stator case assemblies, several other major subassemblies were completed prior to initiating the final compressor rig stackup. These included the inlet case, impeller shroud housing, and the rear bearing housing subassemblies.

The inlet case subassembly consisted of the inlet strut case, inlet guide vane (IGV) flaps, IGV sync ring assembly, and front bearing hairspring support. These components were assembled and all instrumentation installed, routed, and terminated. As with the axial compressor stator vanes, the IGV flaps required some blending on the OD surface to provide the desired range of variabilty.

The impeller shroud and the interstage bleed manifold housing were joined together to make the impeller shroud housing subassembly as shown in figure III-15. Two piston rings were used to seal the front end of the shroud which is allowed free axial movement to avoid thermal strains which could deflect the shroud into the rotating impeller.

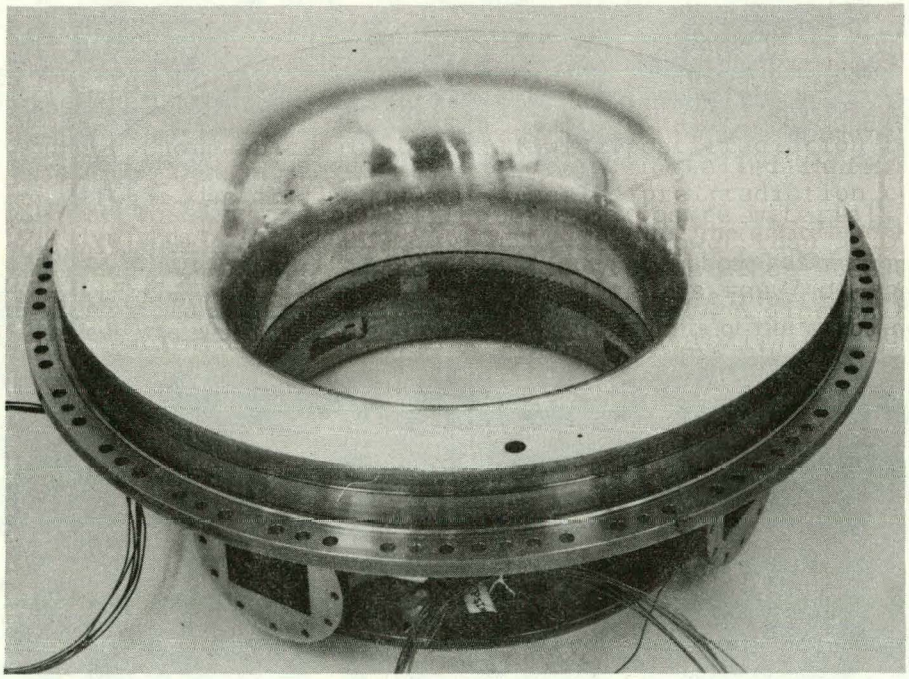

Figure III-15. Impeller Shroud Housing Assembly

The rear bearing housing subassembly consisted of the rear housing, impeller backface knife-edge seals, and the rear roller bearing hairspring support. All instrumentation, including that required for regulating the impeller backface leakage flow and thrust balance pressure, was installed. A preliminary assembly of the active clearance control system was additionally made to verify the internal dimensions and positioning of the thrust bearing outer race support.

4. Final Test Rig Assembly

The final test rig assembly sequence is outlined in figure III-16. The assembly sequence included stackup of all the compressor rig subassemblies and individual hardware items, installation of the rig in its transport stand, and final routing and terminating of all instrumentation.

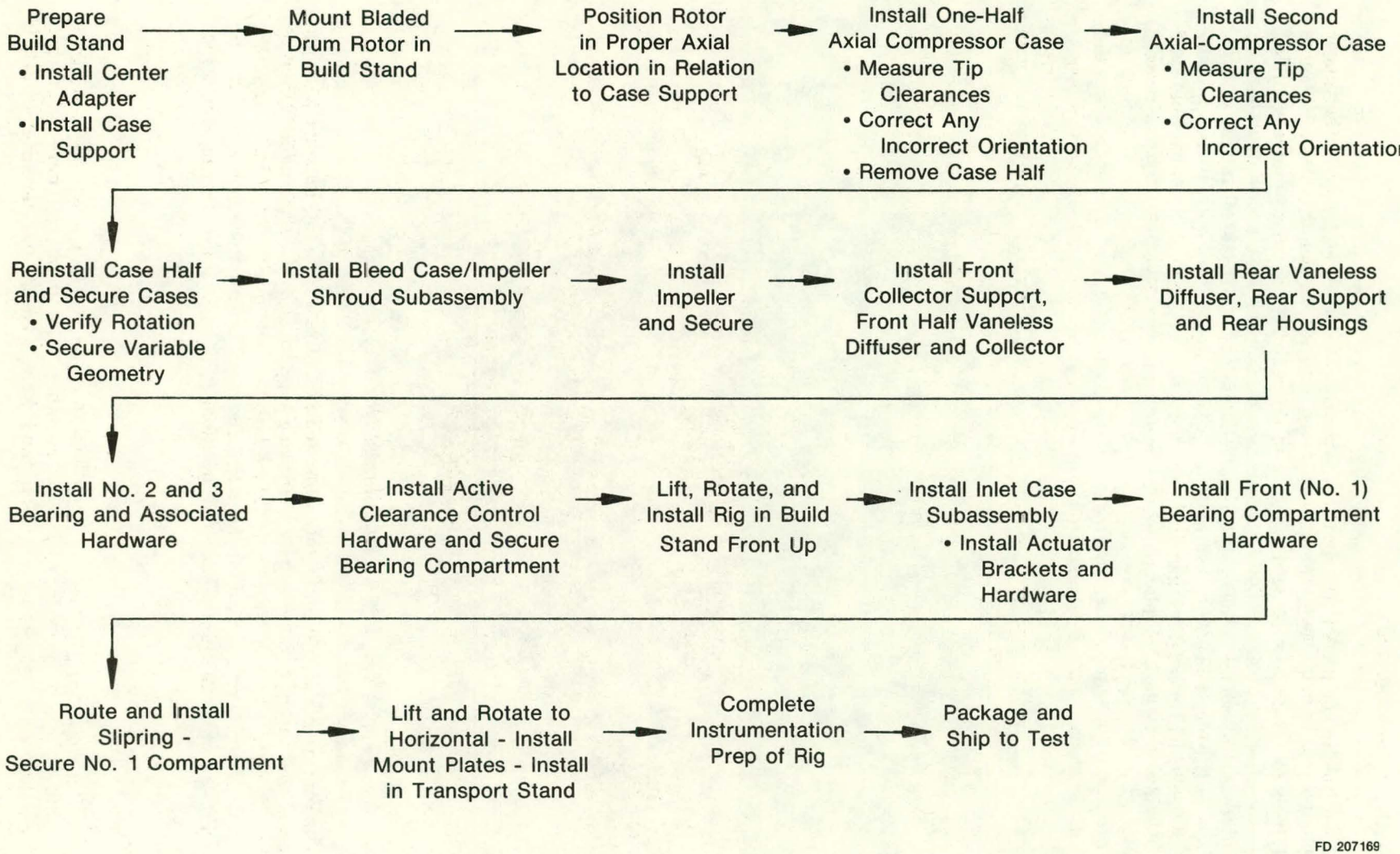

Figure III-16. Compressor Final Assembly Proceure

The bladed axial compressor rotor assembly was first mounted front-end-down in the compressor rig build stand. Each stator case half was then individually shimmed to the proper axial location, placed into position around the rotor, and all airfoil assembly clearances verified. A photograph of one of the cases in position around the rotor assembly is shown in figure III-17. Both case halves were subsequently placed into position and bolted together. After installation of the impeller shroud housing subassembly on the rear of the stator case, the centrifugal impeller was joined to the axial compressor drum rotor with twelve tiebolts. The vertical stackup of the rig cases then continued with addition of the vaneless diffuser assembly, discharge collector manifold, rear bearing housing subassembly, and the rear bearing compartment hardware. The compressor rig was then rotated 180°, placing the rig inlet up. The inlet strut case subassembly was then bolted to the front of the stator assembly and the remaining front bearing compartment hardware installed.

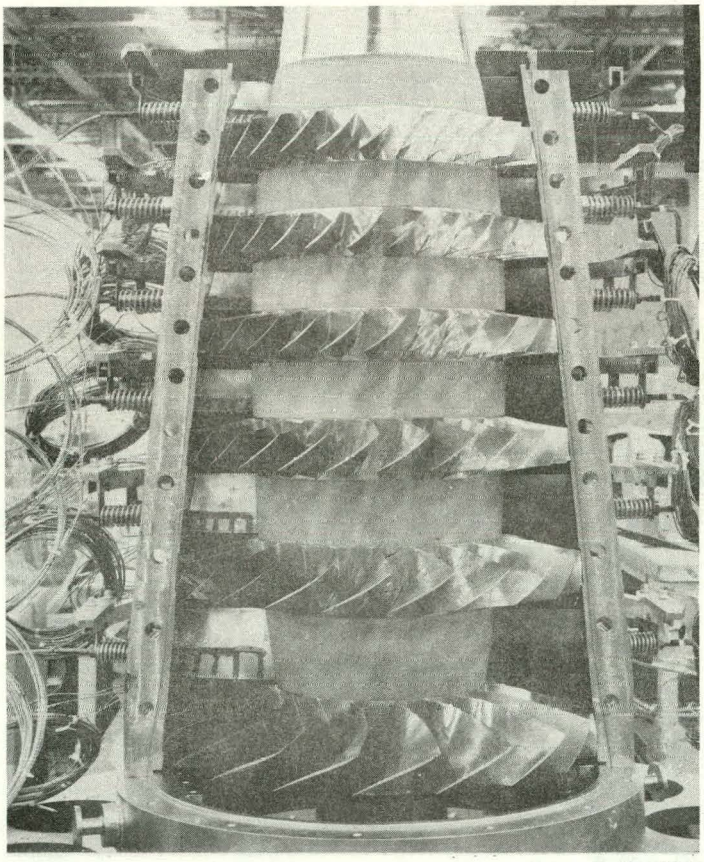

FE 186933
FD 207170

Figure III-17. Axial Compressor Rotor and Case Assembly

The compressor rig facility front and rear mount plates were next installed, aligned relative to the rig centerline, and dowelled into position. The rig was then turned horizontal and mounted in the rig mobile transport stand. Final preparation of the compressor rig for shipment to the test facility was then completed. All steady state pressure instrumentation was routed to a series of quick disconnect Hoke® panels. Performance thermocouple leads were continuously routed to one of six Uniform Temperature Reference (UTR) boxes. A photograph of the completed compressor rig assembly, ready for shipment to the test facility, is shown in figure III-18.

5. Diffuser Replacement Procedure

The compressor rig test program was structured such that two different diffuser configurations were utilized: a vaneless diffuser for the initial shakedown and axial compressor performance documentation testing, and a pipe diffuser for the overall compressor performance documentation testing. The compressor rig was specifically designed with sufficient flexibility such that the diffuser configurations could be changed without removing the compressor rig from the test facility. A brief summary of the diffuser change procedure follows.

Upon completion of the vaneless diffuser portion of the test program, the rig/turbine drive coupling and all rear plumbing and ducting were removed. A supplemental rig support bracket was then bolted to the axial compressor stator case rear flange. The compressor rig rotor was locked into position relative to the rig exterior cases with special supports which replaced the axial compressor discharge instrumentation probes. With the rig properly supported, the rear diffuser support housing and vaneless diffuser were removed and the pipe diffuser installed. Reassembly and preparation of the rig for further testing proceeded in an opposite fashion to the above.

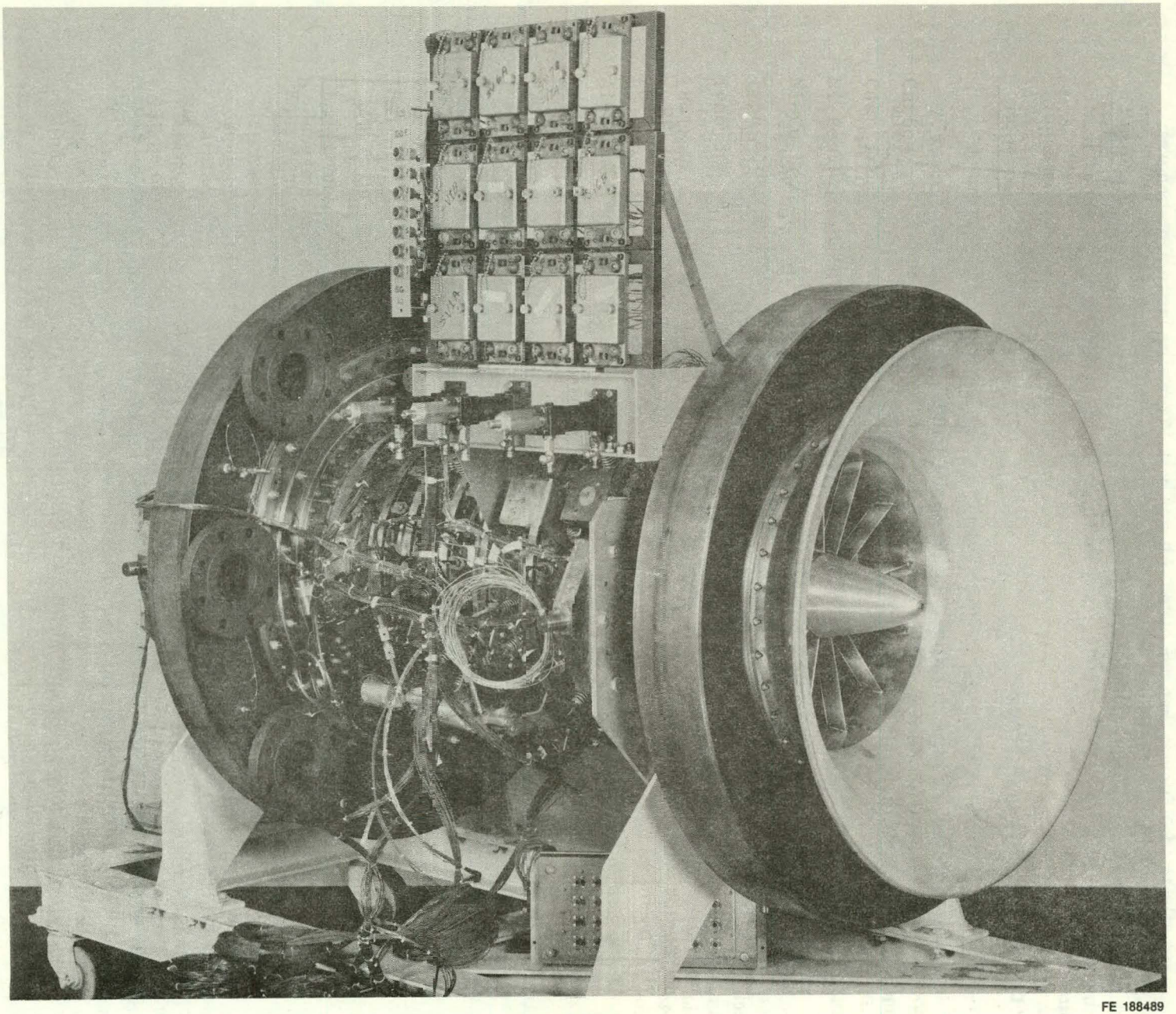

FE 188489
FD 207171

Figure III-18. Assembled Compressor Test Rig

SECTION IV
TEST EQUIPMENT AND FACILITIES

A. TEST FACILITY

The axial/centrifugal compressor rig was tested in the Full Scale Compressor Test Stand located in Pratt & Whitney Aircraft/Government Products Division's Turbojet Engine Altitude Test Facility. This stand has the capability of providing 26,000 horsepower at 16,200 rpm over a wide range of pressurized and heated inlet conditions. A brief summary of the stand's capability is presented in table IV-1; an overall schematic of the stand layout is shown in figure IV-1. Of the equipment available, only the atmospheric inlet/exit system, drive turbine, and stand data acquisition system were required for the compressor test program. A summary of each of these systems is presented below.

Table IV-1. P&WA/GPD Full Scale Compressor Test Stand Capabilities

Airflow:	Ram — 400 pps at 100 in HgA to 480 pps at 70 in HgA
	Exhaust — 20 pps at 1.5 in HgA to 120 pps at 15 in HgA
Air Temperature:	Up to 700°F at 250 pps and 120 in HgA
Drive System:	Direct-Drive Steam turbine, 3000-16,200 rpm operating range, 26,000 maximum horsepower
Data System:	Automatic Data Recording System
Support Systems:	Automatic Variable Geometry Control System, Automatic Surge Recovery System, Shop Air at 100 psig — 0.5 lb/sec, with 6 lb/sec supplement from other areas

1. Atmospheric Inlet/Exit System

A schematic of the test facility atmospheric inlet system is shown in figure IV-2. Air enters the compressor through a 132-ft long, 60-inch diameter duct which is connected to a 14-ft long, 144-inch diameter plenum chamber. A short 95-inch diameter transition duct provides the final transition to the rig inlet. A pneumatic tube seal is used to seal the inlet duct/rig bellmouth interface. At the compressor rig design flowrate, the Mach number at the rig bellmouth inlet was 0.02.

Flowrate is measured by means of a standard ASME thinplate orifice which is located in the 60-inch diameter duct section. Both 15-inch and 24-inch diameter orifices were used during the test program depending on the anticipated flow range of the particular test sequence scheduled.

The compressor rig discharge air was manifolded into a 60-inch duct which was vented to the atmosphere.

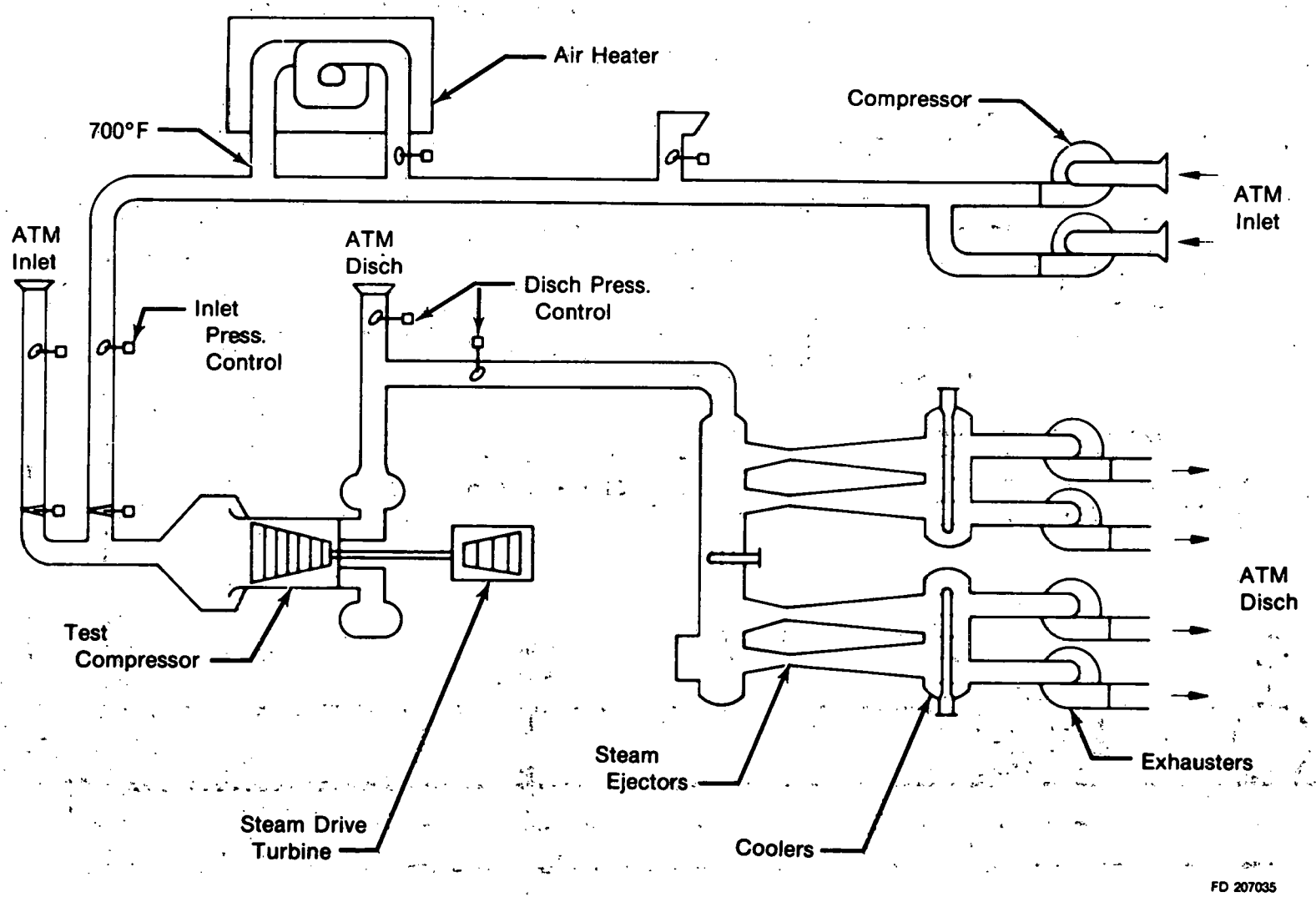

Figure IV-1. P&WA/GPD Full Scale Compressor Test Stand

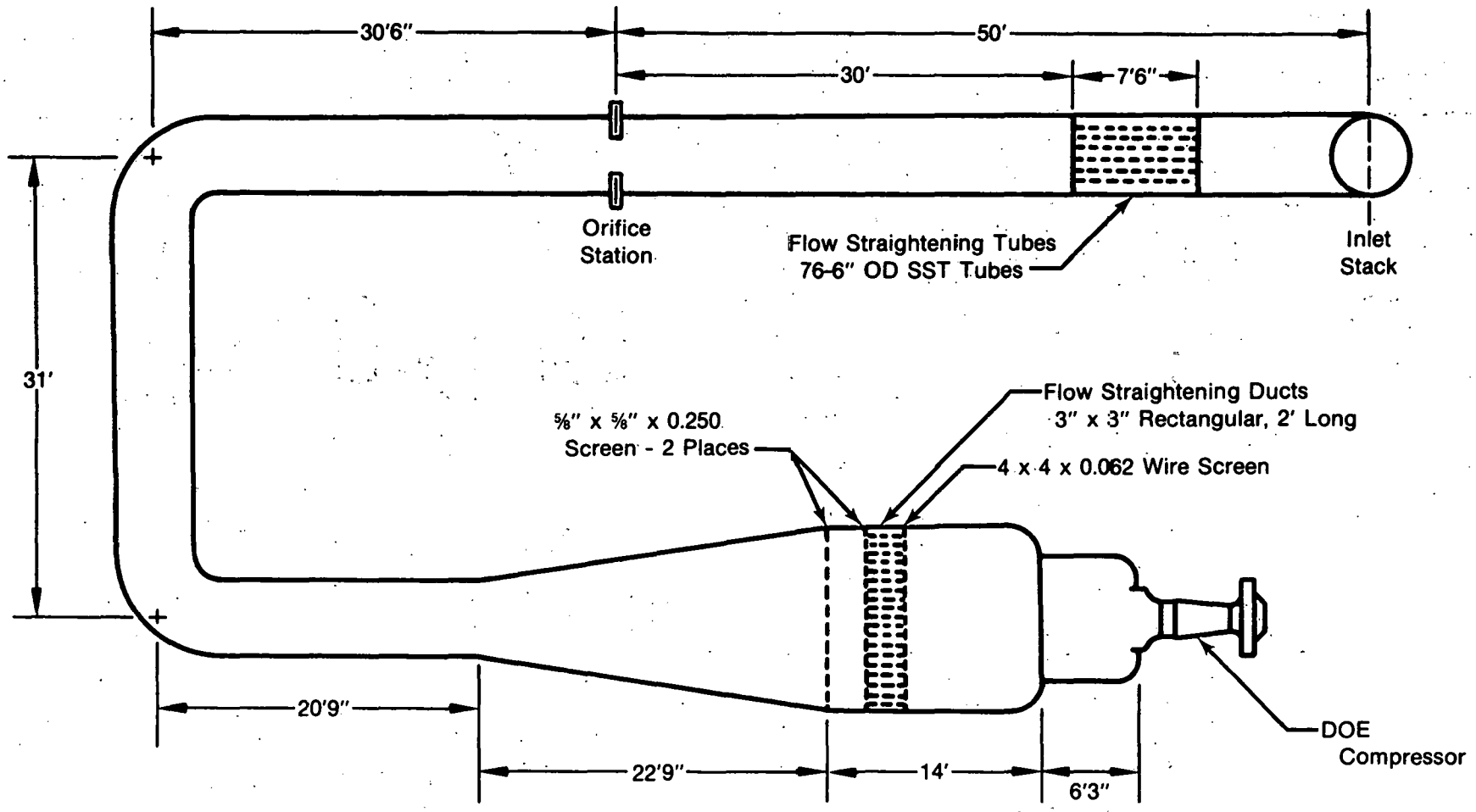

Figure IV-2. P&WA/GPD Full Scale Compressor Test Stand Inlet System

2. Drive Turbine

The drive system consists of a single-stage, direct drive TF30-P414A high turbine module which has been adapted to run on high pressure steam. The turbine speed is automatically controlled to within approximately ±20 rpm by an analog control system which operates the turbine main steam supply valve. A dual-priority abort system is provided to protect both the compressor rig and drive turbine from inadvertant overspeed conditions. The "Priority 2" abort system is designed to handle the majority of the facility problems normally encountered which would result in an overspeed indication. The Priority 2 abort initiates closure of the steam supply valve at its maximum rate, providing a rapid deceleration. In the rare event that the turbine rotor acceleration is so rapid that the main steam valve closure time response is insufficient to prevent a further increase in speed, the "Priority 1" abort system overrides and initiates firing of eleven explosively-driven relief valves to vent the turbine steam inlet manifold pressure.

3. Data System

The data system which services the Full Scale Compressor Test Stand consists of three subsystems. In addition to a digital automatic data acquisition system used for recording the majority of the compressor performance parameters, separate subsystems are provided for monitoring and recording rig vibration and strain gage data. A brief summary of each of these subsystems is presented below.

a. Automatic Data Recording System

The automatic data recording system is a computer controlled data acquisition and computation system. The system contains two computer systems for on-line data acquisition and rig performance calculations, a third computer for extensive rig performance analysis, and remote data acquisition subsystems (RDAS). Data acquisition is initiated through the RDAS, located in the test stand control room, which conditions and converts rig test measurements to computer compatible units. A summary of the data system's capability is presented in table IV-2.

Table IV-2. P&WA/GPD Full Scale Compressor Test Stand Data System Capability

Automatic Data Acquisition and Recording System

- 634 channels
  - 288 pressure (scanivalve) channels
  - 196 CA thermocouple channels
  - 100 pressure (transducer) channels
  - 36 low level millivolt channels
  - 10 speed/flow pulse train channels
  - 4 power supply monitor channels
- Recording Modes
  - — Static with two-48 header displays
  - — Monitor
  - — 3 transient modes
    - — 90 parameters max, 48 display max
    - — Scan rate of 200/No. parameters
    - — High speed transient of 28,000 samples/sec
  - — Teletype with 32 static and 48 performance parameters

The system has three basic modes of operation: static, monitor, and transient. The static mode consists of a full ten scan recording which is then averaged, and performance calculations completed. Up to 96 selected measurements or performance quantities can be presented on a cathode ray tube (CRT) display and printed out on a typewriter both of which are located in the test stand control room. The monitor mode provides a "snap-shot" single reading of selected measured parameters which are presented on the CRT display. The transient mode consists of repeated scanning of parameters with the data being recorded onto magnetic tape and selected parameters periodically updated on the CRT.

b. Vibration Data Acquisition System

The vibration data acquisition system consists of FM magnetic tape recording equipment, test stand control room vibration monitors, and on-line analysis equipment (spectrum and tracking analyzers). Cabling and patching capability is available to transmit up to twenty-four channels from the test stand to the centralized recording equipment. The system also includes equipment to allow scanning of all channels for monitoring and analysis of critical parameters.

c. Strain-Gage Data Acquisition System

The strain gage data acquisition system provides conditioning and recording equipment for a maximum of 96 strain gages. The system contains numerous monitor oscilloscopes for real-time evaluation of the blading's dynamic stress. In addition, the system contains FM magnetic tape recording equipment capable of processing 72 channels simultaneously.

B. COMPRESSOR RIG INSTALLATION

The axial/centrifugal compressor test rig installation is schematically presented in figure IV-3. The compressor test rig was installed in the test facility by means of a free-standing mount aligned to the rotating centerline of the drive turbine. Coupling of the compressor rotor to the drive turbine was accomplished utilizing a tight-fitting splined drive coupling. A photograph of the compressor rig test facility installation is shown in figure IV-4. The major rig test stand interfaces and support systems are summarized below.

1. Rig Mount

The compressor rig is bolted to front and rear support plates mounted normal to the rig axis. Each support plate contains three radial pins (two in the horizontal plane and one in the vertical plane) which are retained in spherical bearings located on the rig mount stand. The spherical bearings are designed to allow for radial thermal growths while maintaining rig alignment. In addition, the front spherical bearings are mounted in slide block supports to accommodate axial thermal growth. The rear holders are restrained to absorb rig-generated thrust loads. The rig rotor centerline was aligned in relation to the drive turbine centerline to within 0.002 inch by shimming the position of the rig mount stand relative to its support base.

2. Discharge System

The compressor discharge air was ducted from the rig discharge collector through six four-inch lines. Four of these lines were manifolded together into an 8-inch duct containing both an 8-inch main discharge control valve and a two-inch vernier control valve. These valves were regulated as required during the test program to vary the compressor back pressure. The remaining two lines were plumbed directly to the test facility 60-inch discharge duct. Each of these lines contained a manually-operated gate valve and a surge pop-bleed relief valve. The position of the gate valves was set prior to initiation of the test program to provide the best range of operation for the main discharge control valve.

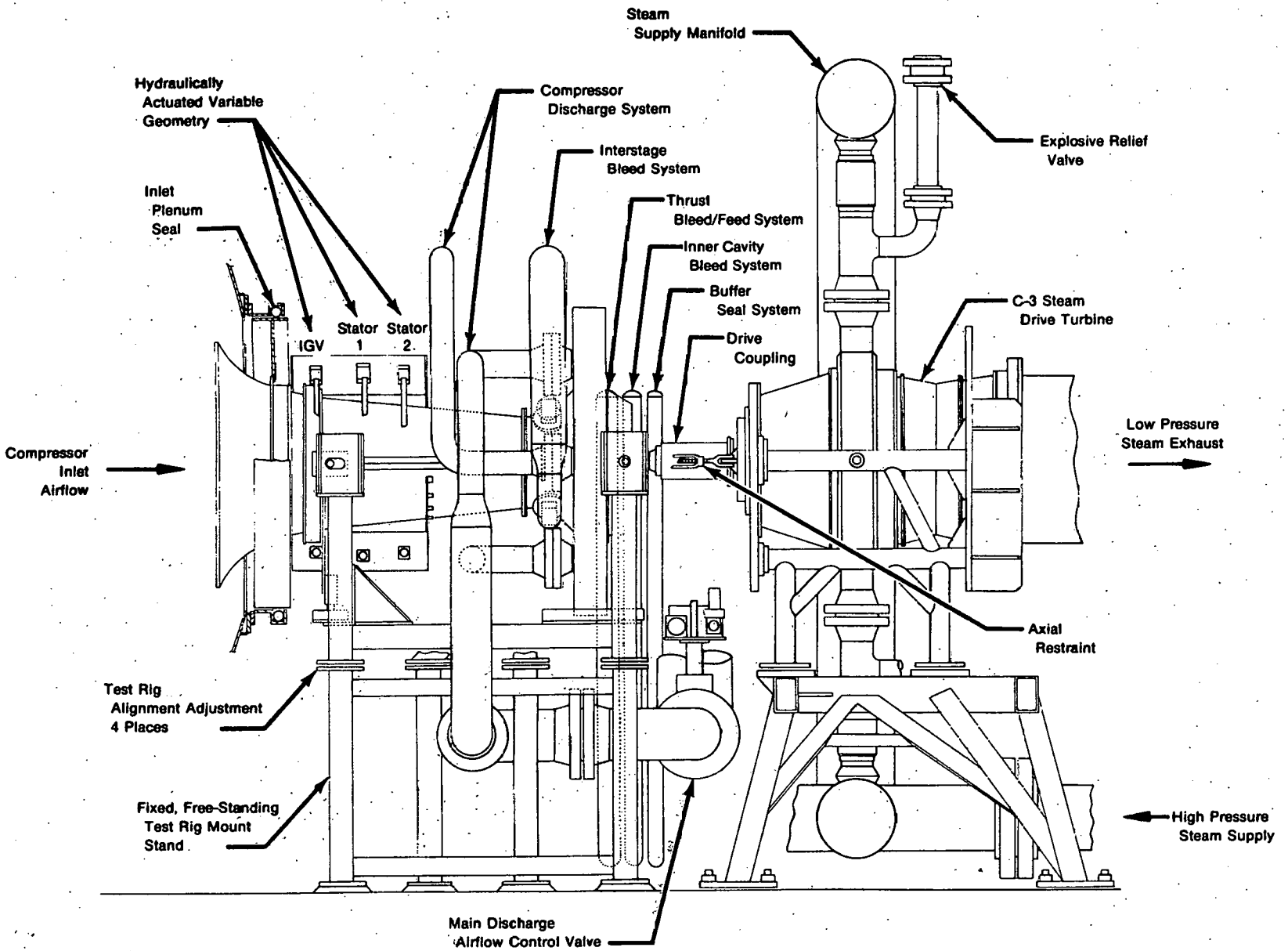

Figure IV-3. Schematic of Compressor Test Rig Installation

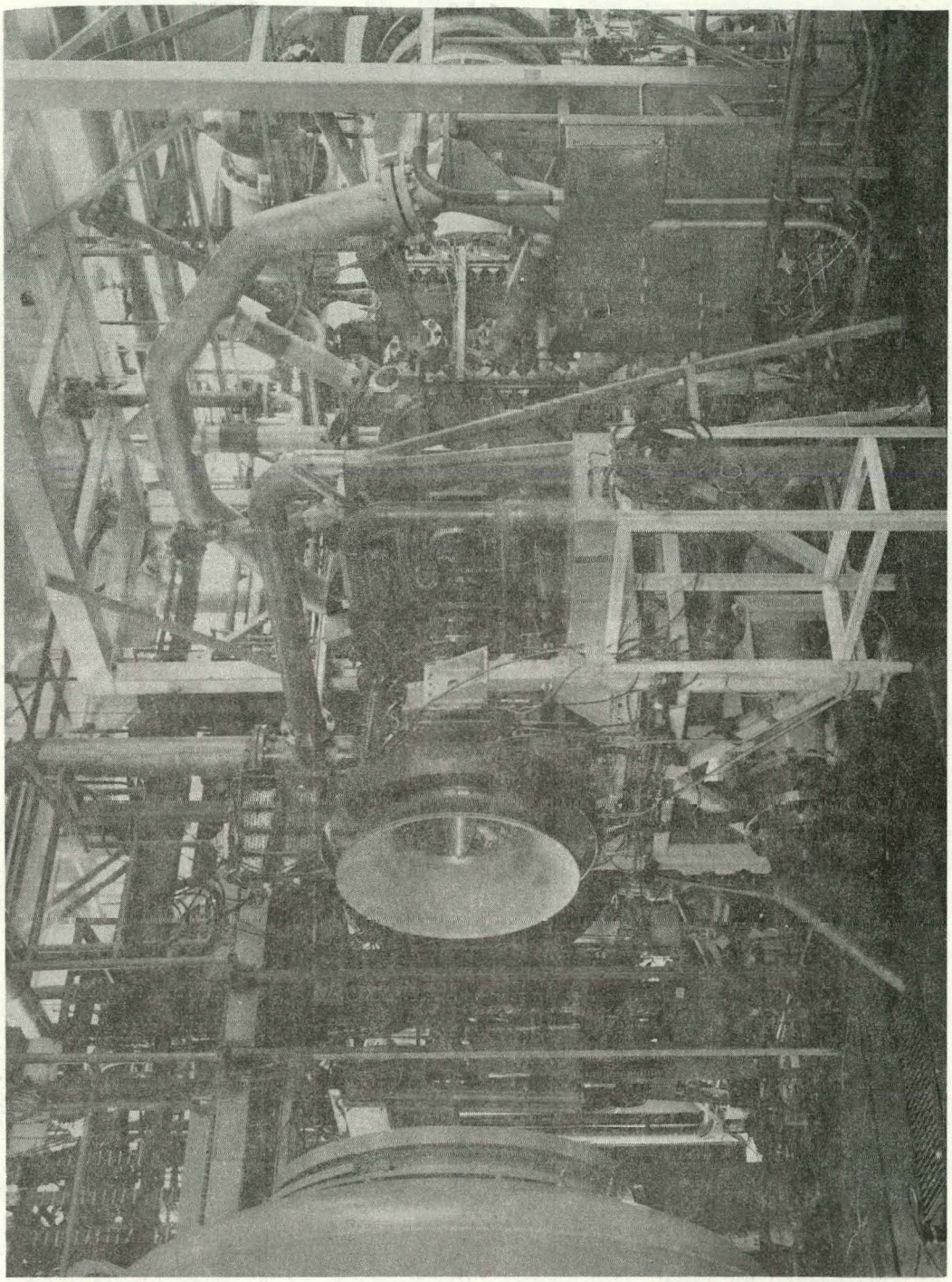

Figure IV-4. Compressor Test Rig Facility Installation

3. Interstage Bleed System

The four compressor rig interstage bleed lines were manifolded into a single eight-inch duct containing a pneumatic control valve and flow measuring orifice. The bleed line was then ducted to the test facility exhauster system to provide the capability of regulating the bleed downstream pressure.

4. Surge Recovery System

The test facility installation includes a system designed to ensure safe and rapid recovery from compressor surge. The system responds to input from any one of three transient detectors and can be programmed to initiate a number of various recovery sequences depending on the particular compressor test configuration. For this program, two transient pressure sensors (located at the rig inlet and discharge) and one transient temperature sensor (located at the centrifugal stage inlet) were utilized. The recovery sequence includes opening the rig main discharge valve, opening pop-bleed relief valves in the rig discharge and interstage bleed systems, slewing the variable stator vane rows to their fully closed position, and reducing rotor speed by 2000 rpm. A schematic of the surge recovery system is shown in figure IV-5.

5. Variable Vane Control

Two separate systems were used to control positioning of the compressor rig variable stator vane rows. The inlet guide vanes and first two stator rows were automatically regulated by means of a preprogrammed electro-hydraulic control system. This system provides the capability of independently scheduling vane position for each stage as a function of rotor speed and responding to compressor surge. In addition, a manual override option is available for each vane row. Positioning of the third through sixth stage stators was manually controlled through a remotely-operated electric motor driven actuation system.

6. Lubrication System

A standard external lubrication system utilizing MIL-7808 oil was used to lubricate the compressor rig bearing compartments. Separate supply and scavenge systems connected to a common oil reservoir were provided for the front and rear compartments. An air-motor system was available as a back-up to the primary electric motor driven supply and scavenge system to continue lubrication in the event of a power failure.

Lubrication and cooling for the Poly-Scientific slipring was provided by a separate external freon-oil system.

C. COMPRESSOR RIG INSTRUMENTATION

Instrumentation was provided to document both the compressor rig aerodynamic performance and its aero-mechanical operating characteristics. The instrumentation incorporated can be divided into three general categories: aerodynamic, structural, and rig operational support. A complete listing of all the rig instrumentation in each of these categories is included in Appendix B.

1. Aerodynamic Instrumentation

The aerodynamic instrumentation was selected to accomplish three primary objectives: (1) define the overall compressor performance, (2) allow definition of the axial compressor and centrifugal stage component performances, and (3) provide interstage measurements for diagnostic purposes to aid in performance optimization if required. A summary of the location

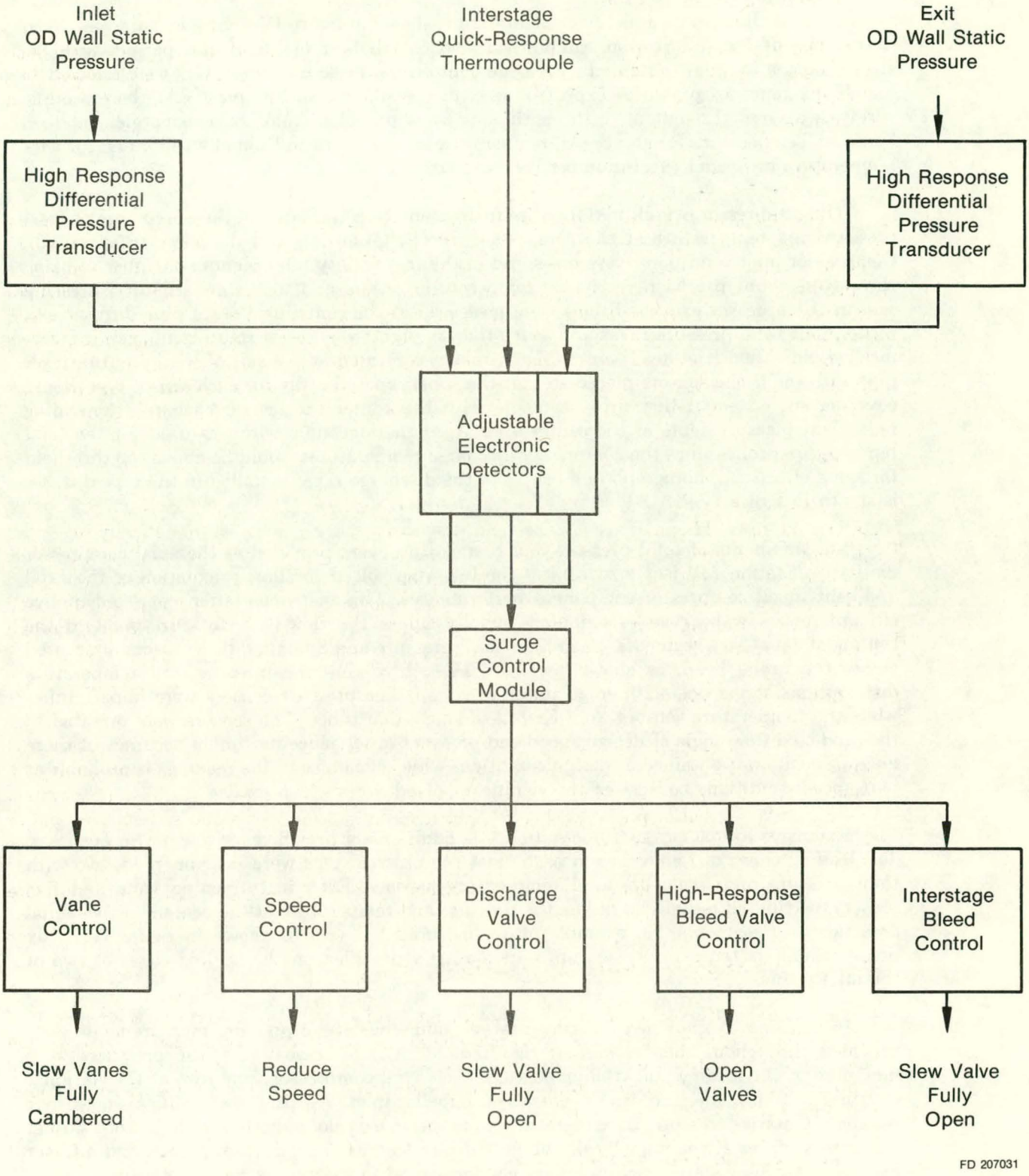

Figure IV-5. P&WA/GPD Compressor Test Stand Surge Recovery System

and extent of the aerodynamic instrumentation is shown in figure IV-6. Special care was taken during the design, fabrication, calibration, and installation of all of the performance instrumentation in order to minimize measurement errors. Pressure transducers were selected to match the range of pressures expected. Premium grade chromel-alumel (CA) thermocouple wire was utilized throughout, with continuous leads provided from the sensing element to a Uniform Temperature Reference. All temperature sensors were additionally calibrated for wire temperature error and Mach number recovery error.

The compressor overall performance instrumentation consisted of measurements of total pressure and temperature at the compressor inlet (Station 1.0) and discharge (Station 3.0). Compressor inlet conditions were measured in the test facility inlet plenum chamber utilizing three Rosemount precision resistance temperature sensors and four standard total pressure sensors. Compressor exit conditions were measured at the centrifugal stage pipe diffuser exit plane. Four total pressure rakes and four total temperature rakes were utilized, each containing five individual Kiel-head sensors. Each rake was located at the exit of a different diffuser pipe with the probe sensors placed so that the superimposed array for each sensor type would cover seventeen equal flow area segments with the center sensors on each rake providing redundant measurements of the center area. Aged thermocouple wire was used for the total temperature probes since the compressor discharge temperatures would be above the threshold for aging effects. A photograph of a couple of the discharge rakes installed in the pipe diffuser is shown in figure IV-7.

Measurements of total pressure and temperature were provided at the axial compressor discharge (Station 2.0) just upstream of the interstage bleed to allow calculation of the axial and centrifugal compressor component performances. This instrumentation consisted of five circumferential wake rakes distributed radially across the flow-path to correspond to the centers of equal area segments. Each rake has 8 pressure and 8 temperature sensors alternated across the probe head, as shown in figure IV-8, to define the pressure and temperature distributions across one sixth stage stator vane gap. The pressure sensors were impact tubes while the temperature sensors were Kiel-head stagnation tubes. The sensors were oriented to the predicted flow angle at design speed and pressure ratio, hence maximum accuracy of these measurements was obtained at design conditions while some bias in the readings is probable at part speed conditions because of the significant bleed flows which existed.

Extensive interstage instrumentation was additionally provided for diagnostic purposes. The leading edges of four vanes in each axial compressor stage were instrumented, two with total pressure and two with total temperature sensors. Each instrumented vane had five sensors distributed radially to define the pressure and temperature at the centers of five equal area flowpath segments. An example of an instrumented vane is shown in figure IV-9. Six pressure and six temperature sensors were similarly provided on the leading edges of two of the inlet struts.

In addition to the above instrumentation, numerous static pressure measurements were provided throughout the compressor rig. Redundant outer case wall static pressures were measured at the leading and trailing edges of each axial compressor vane row, at the station 2 instrumentation plane, and at the centrifugal impeller inlet. Within the centrifugal stage, four redundant static pressure measurements were provided along both the hub and shroud flowpath surfaces at the impeller discharge, diffuser leading edge, diffuser throat, and diffuser exit sections. Four static pressures were also measured in the rig discharge collector.

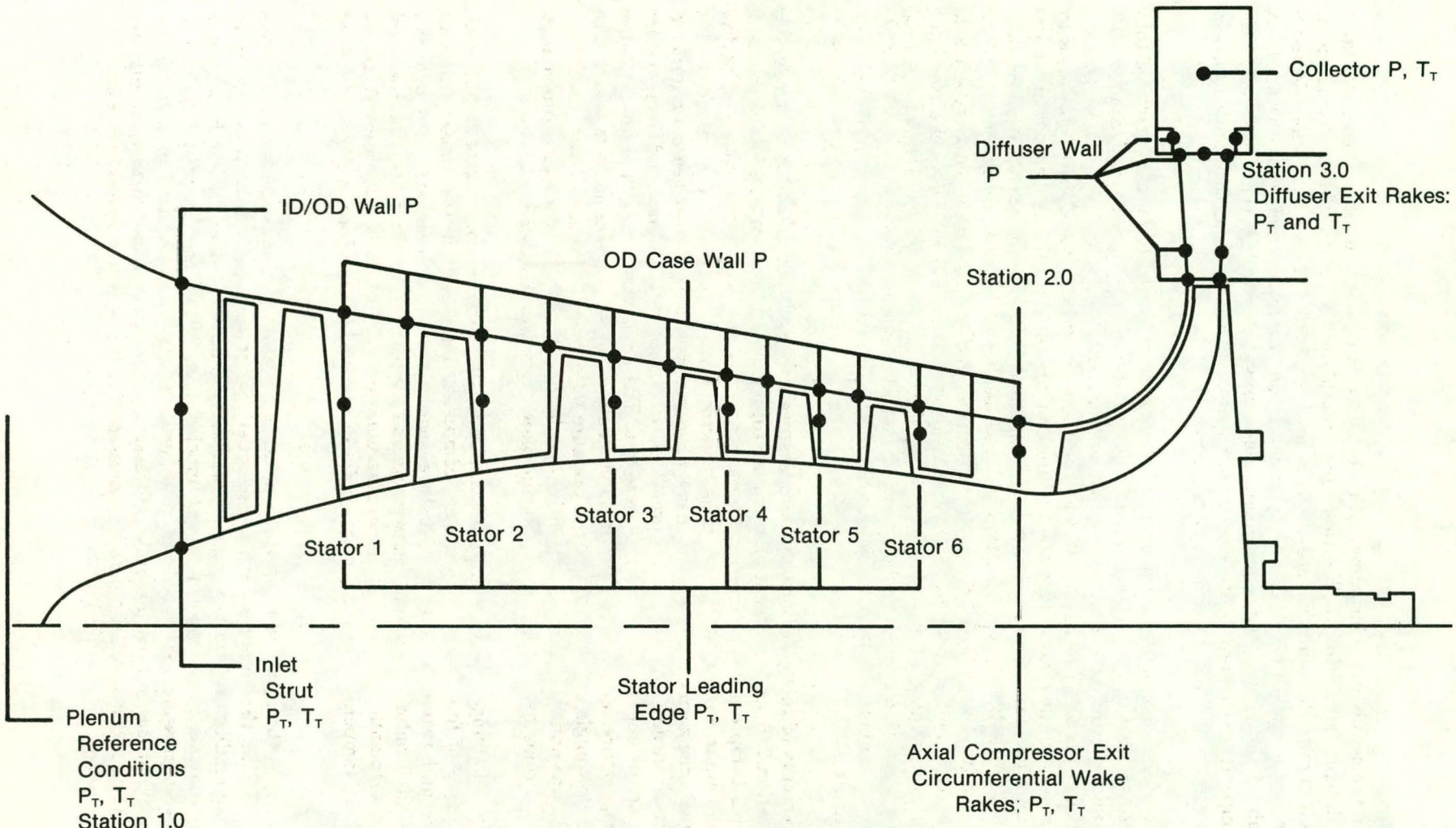

Figure IV-6. Compressor Aerodynamic Instrumentation Schematic

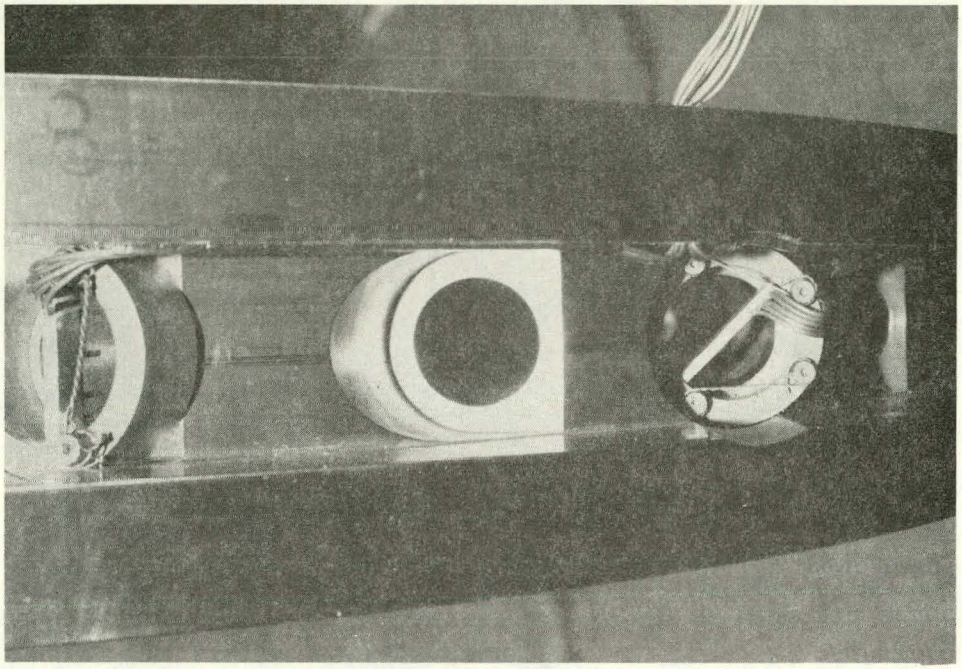

FE 348864

Figure IV-7. Pipe Diffuser Discharge Rake Installation

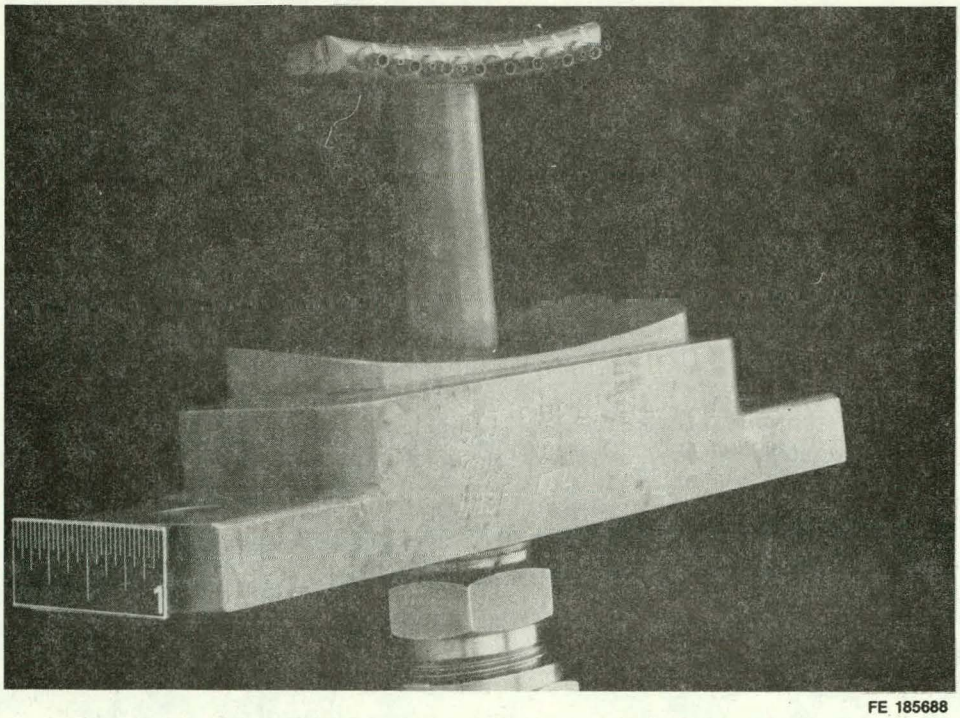

FE 185688

Figure IV-8. Axial Compressor Exit Circumferential Wake Rake

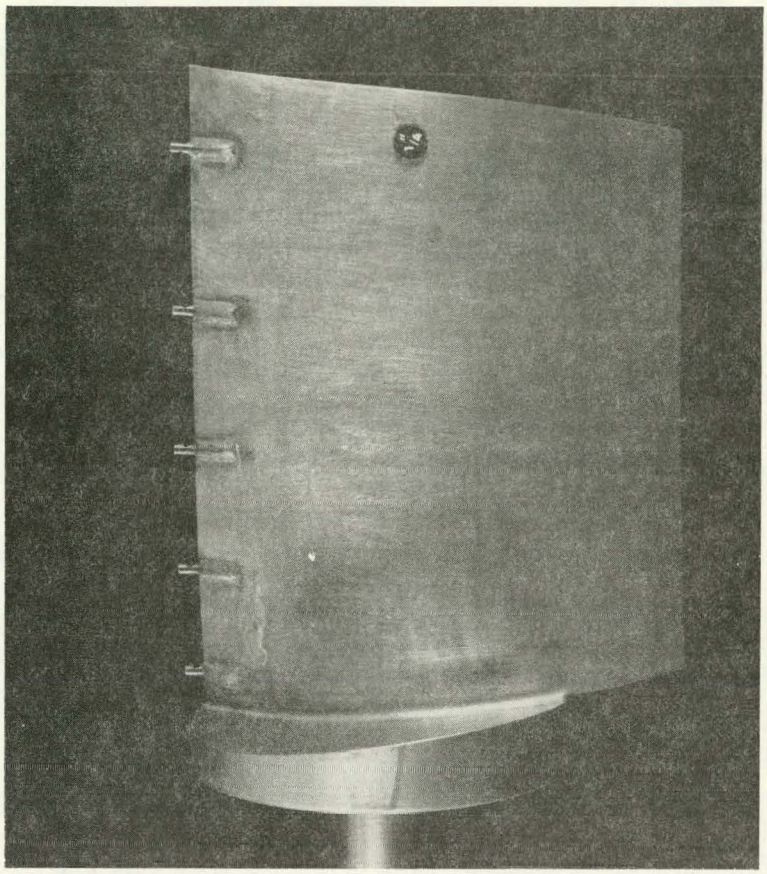

FE 185548

Figure IV-9. Instrumented Axial Compressor Vane

2. Structural Instrumentation

Structural instrumentation was provided primarily to monitor and evaluate the vibratory characteristics of the axial compressor airfoils as indicated in figure IV-10. A total of sixty strain gages were utlized for this purpose including 34 dynamic gages located on the blades and 26 dynamic gages located on the vanes.

The precise locations of the strain gages on each airfoil were determined based on stress-coat and holographic vibratory analyses. For each airfoil row, selected blades/vanes were stress-coated and excited by a shaker test to define the maximum stress locations and relative stress ratios. Subsequent holographic analysis was used to define mode shapes for each airfoil row. Examples of the stress-coat and holographically defined mode shapes for the first stage blade are presented in figures IV-11 and IV-12, respectively.

Based on the above tests, strain gage locations were defined to document all major vibratory modes for which potential excitation sources had been identified. A summary of the number of strain gages, location, and stress limit for each vibratory mode instrumented is presented in table IV-3. Since the stress coat and holographic analyses were conducted prior to final tip grinding of the airfoils, a small correction was applied to the lab test defined natural frequencies to account for the airfoil length change due to the tip grinding. Table IV-4 summarizes the natural frequencies for each airfoil row both as lab tested and with the tip grinding correction.

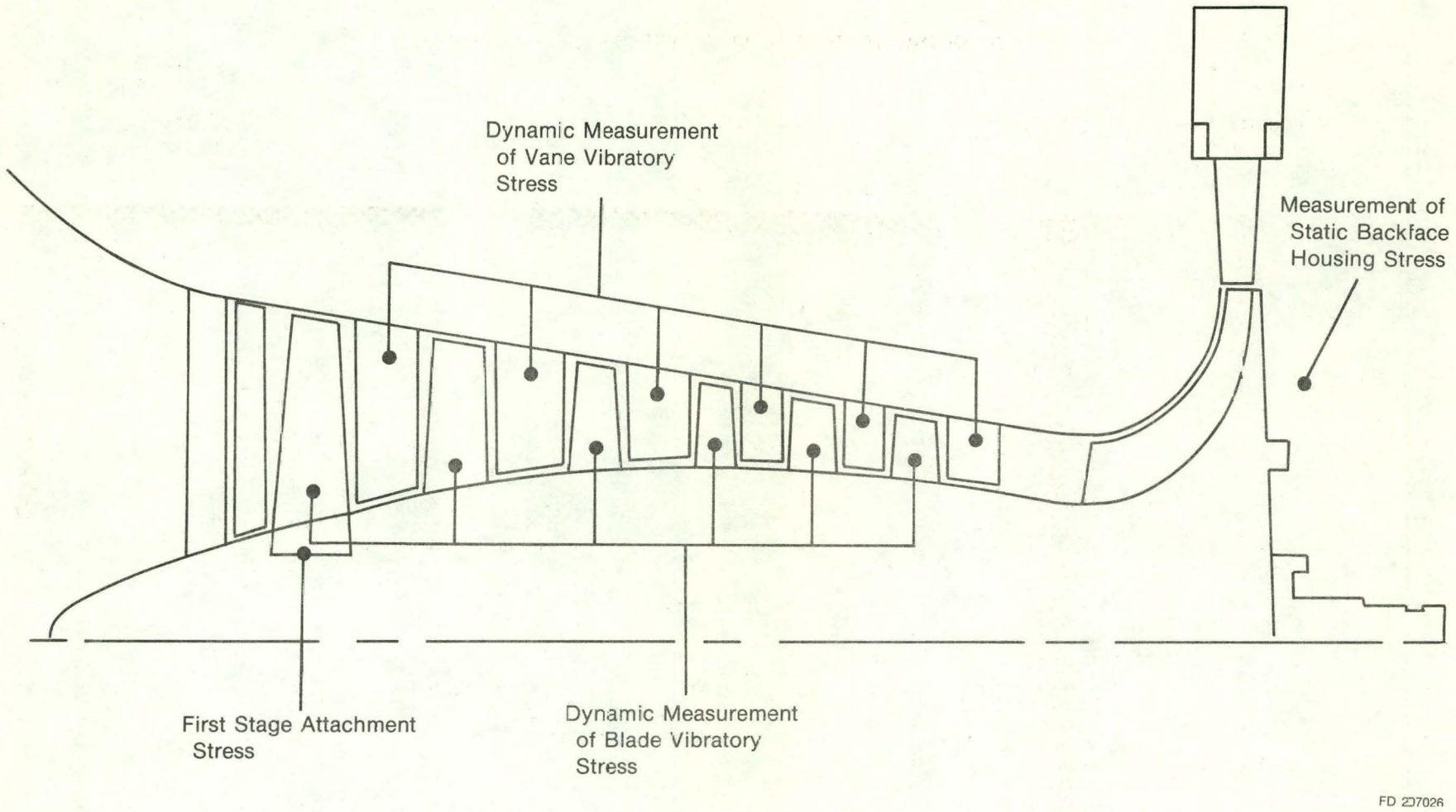

Figure IV-10. Compressor Structural Instrumentation Schematic

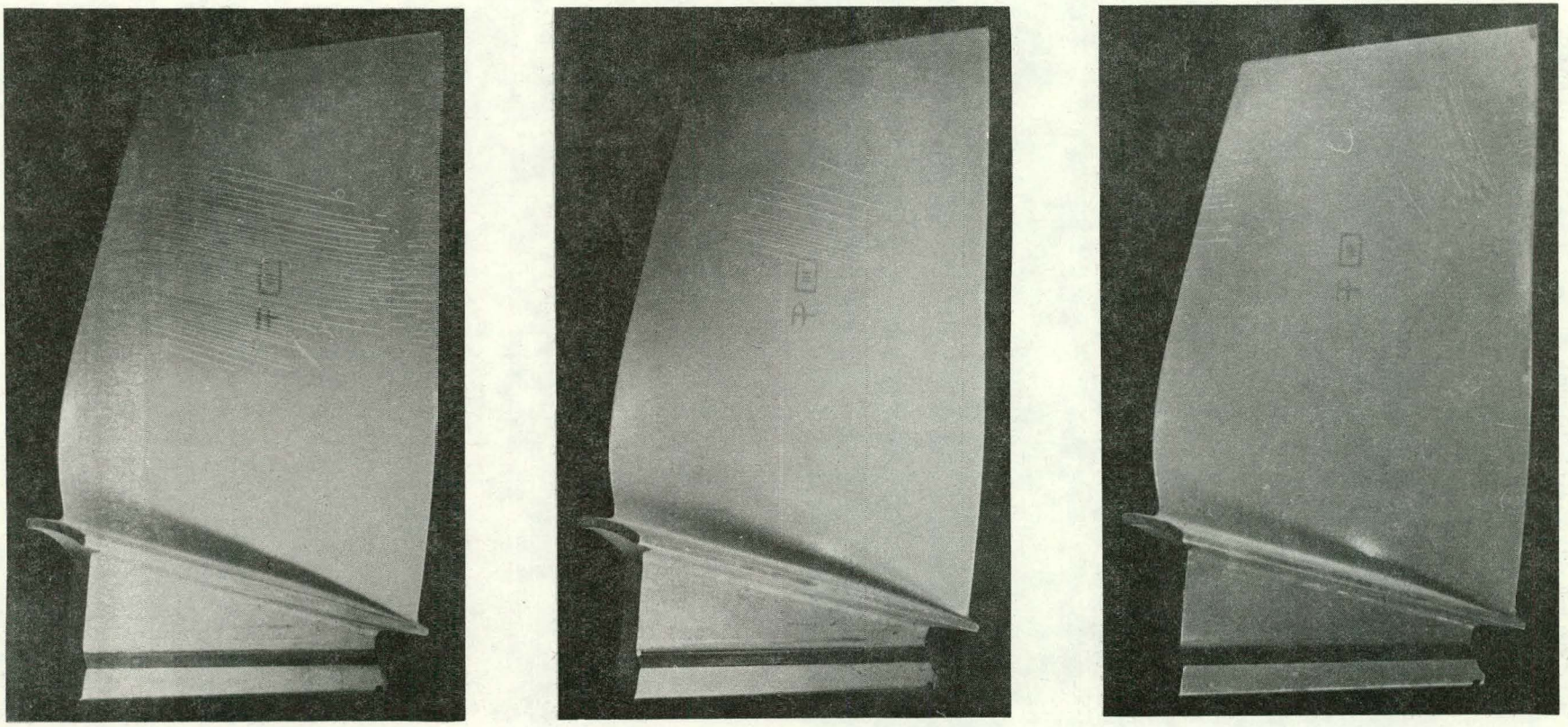

407 Hz
First Bending

916 Hz
Second Bending

1649 Hz
First Torsion

FD 207025

Figure IV-11. First Stage Blade Stress-Coat Test Results

407 Hz
First Bending

916 Hz
Second Bending

1649 Hz
First Torsion

FD 212963

Figure IV-12. First Stage Blade Holograms

Table IV-3. Airfoil Strain Gage Summary

Stage	Gage Number	Gage Location	Vibratory Mode	Vibratory Stress Limit ksi, p-p Steady State	Vibratory Stress Limit ksi, p-p Transient
Rotor Blades					
1	1	MRT-CV	FIRST BENDING	27	40
	2	MRT-CV	FIRST BENDING		
	3	MRT-CV	FIRST BENDING		
	4	ATTACHMENT-CV	FIRST BENDING		
	5	ATTACHMENT-CC	SECOND BENDING		
	6	50% SPAN-CC	FIRST BENDING		
	7	TRAILING EDGE-CC	FIRST TORSION		
2	8	MRT-CV	FIRST BENDING	26	39
	9	70% SPAN, 40% CHORD-CC	SECOND BENDING		
	10	MRT-CV	FIRST BENDING		
	11	70% SPAN, 40 CHORD-CC	SECOND BENDING		
	12	ROOT, TRAILING EDGE	FIRST/SECOND TORSION		
	13	60% SPAN, 90% CHORD-CC	FIRST TORSION		
3	14	MRT-CV	FIRST BENDING	29	44
	15	MRT-CV	FIRST BENDING		
	16	MRT-CV	FIRST BENDING		
	17	80% SPAN, 30% CHORD-CC	SECOND BENDING		
	18	60% SPAN, 70% CHORD-CC	2 NODAL CHORDWISE BENDING		
4	19	MRT-CV	FIRST BENDING	30	44
	20	MRT-CV	FIRST BENDING		
	21	MRT-CV	FIRST BENDING		
	22	50% SPAN, 15% CHORD-CC	SECOND BENDING		
	23	ROOT, LEADING EDGE-CC	2 NODAL CHORDWISE TORSION		
5	24	MRT-CV	FIRST BENDING	34	50
	25	MRT-CV	FIRST BENDING		
	26	70% SPAN, 70% CHORD-CC	SECOND BENDING		
	27	50% SPAN, 50% CHORD-CC	FIRST TORSION		
	28	25% SPAN, TRAILING EDGE-CC	THIRD BENDING		
6	29	ROOT, 30% CHORD-CV	FIRST BENDING	38	57
	30	ROOT, 30% CHORD-CV	FIRST BENDING		
	31	ROOT, 30% CHORD-CV	FIRST BENDING		
	32	ROOT, 70% CHORD-CV	FIRST TORSION		
	33	50% SPAN, 60% CHORD-CC	FIRST TORSION		
	34	20% SPAN, 70% CHORD-CC	2 NODAL CHORDWISE BENDING		
Stator Vanes					
1	1	MRT-CV	FIRST BENDING	49	73
	2	MRT-CV	FIRST BENDING		
	3	MRT-CC	FIRST BENDING/TORSION		
	4	ROOT, LEADING EDGE-CC	SECOND TORSION		
	5	60% SPAN, TRAILING EDGE-CC	2 NODAL CHORDWISE BENDING		
2	6	MRT-CV	FIRST BENDING	49	73
	7	ROOT, 20% CHORD-CC	FIRST TORSION		
	8	ROOT, 35% CHORD-CC	FIRST BENDING		
	9	30% SPAN, 90% CHORD-CC	2 NODAL CHORDWISE BENDING		

Table IV-3. Airfoil Strain Gage Summary (Continued)

3	10	MRT-CV	FIRST BENDING	49	73
	11	MRT-CV	FIRST BENDING		
	12	25% SPAN, 80% CHORD-CC	2 NODAL CHORDWISE BENDING		
	13	40% SPAN, TRAILING EDGE-CC	FIRST TORSION		
	14	MRT-CV	FIRST BENDING		
4	15	MRT-CV	FIRST BENDING	49	73
	16	MRT-CC	FIRST BENDING		
	17	ROOT, 25% CHORD-CC	FIRST TORSION		
	18	ROOT, LEADING EDGE-CC	2 NODAL CHORDWISE BENDING		
5	19	MRT-CV	FIRST BENDING	49	73
	20	MRT-CC	FIRST BENDING		
	21	10% SPAN, LEADING EDGE-CC	2 NODAL CHORDWISE BENDING		
6	22	MRT-CV	FIRST BENDING	49	73
	23	MRT-CC	FIRST BENDING		
	24	10% SPAN, 60% CHORD-CV	FIRST TORSION		
	25	10% SPAN, 60% CHORD-CC	TRAILING EDGE TORSION		
	26	20% SPAN, LEADING EDGE-CC	2 NODAL CHORDWISE BENDING		

CC	Concave Surface
CV	Convex Surface
MRT	Maximum Root Thickness

Table IV-4. Natural Frequencies of Blades and Vanes

Airfoil	*Vibratory Mode*	*Measured Frequency (Holography)*	*Corrected Frequency for Tipped Airfoil*	*Airfoil Length Reduction*
ROTOR 1	FIRST BENDING	407	419	0.060
	SECOND BENDING	916	944	
	FIRST TORSION	1649	1700	
ROTOR 2	FIRST BENDING	708	741	0.050
	SECOND BENDING	1662	1741	
	FIRST TORSION	2540	2661	
	SECOND TORSION	3210	3362	
ROTOR 3	FIRST BENDING	970	1021	0.055
	SECOND BENDING	2057	2165	
	2 NODAL CHORDWISE BENDING	4386	4615	
ROTOR 4	FIRST BENDING	978	1043	0.046
	SECOND BENDING	3973	4239	
	2 NODAL CHORDWISE TORSION	4788	5109	
ROTOR 5	FIRST BENDING	1329	1463	0.060
	FIRST TORSION	3206	3530	
	SECOND BENDING	4241	4669	
	THIRD BENDING	6100	6715	
ROTOR 6	FIRST BENDING	1670	1884	0.084
	FIRST TORSION	3638	4104	
	2 NODAL CHORDWISE BENDING	7355	8296	
STATOR 1	FIRST BENDING	636	704	0.226
	FIRST TORSION	1335	1478	
	SECOND TORSION	2765	3062	
	2 NODAL CHORDWISE BENDING	3397	3762	
STATOR 2	FIRST BENDING	505	589	0.226
	FIRST TORSION	1131	1319	
	2 NODAL CHORDWISE BENDING	4412	5145	
STATOR 3	FIRST BENDING	1050	1242	0.187
	FIRST TORSION	1619	1916	
	2 NODAL CHORDWISE BENDING	4117	4872	
STATOR 4	FIRST BENDING	972	1169	0.171
	FIRST TORSION	1777	2138	
	2 NODAL CHORDWISE BENDING	5173	6224	
STATOR 5	FIRST BENDING	1128	1373	0.150
	2 NODAL CHORDWISE BENDING	4861	5919	
STATOR 6	FIRST BENDING	1352	1646	0.134
	FIRST TORSION	2202	2681	
	TRAILING EDGE TORSION	4574	5596	
	2 NODAL CHORDWISE BENDING	5378	6547	

3. Operational Support Instrumentation

Additional instrumentation was incorporated to monitor operation of the compressor rig and to provide the input required for regulating the various rig auxiliary systems. This instrumentation is summarized in figure IV-13.

Bearing compartment instrumentation included compartment pressure, oil inlet and outlet temperature and pressure, and bearing outer race temperatures. Accelerometers were mounted in the horizontal and vertical planes of each of the roller bearing supports to measure rotor vibration levels. Additionally, the slipring coolant inlet pressure and temperature, outlet temperature, and flowrate were measured. The differential seal pressures across the multi-element knife edge seals provided adjacent to each bearing compartment were monitored to ensure minimal oil leakage out of the compartments.

Static pressures and air temperatures were measured in all of the rig internal cavities to allow calculation of the rotor thrust loads and secondary leakage flows. Those compartment pressures that could be regulated on the test stand were displayed on digital readouts in the facility control room.

Three transient detectors were utilized to provide input to the facility surge recovery system. These included two high response static pressure sensors, located in the rig outer case wall at the axial compressor first rotor inlet and centrifugal stage exit, and a quick response temperature sensor at the centrifugal stage inlet.

A combination of position potentiometers and dial indicators were utilized to monitor and record vane position for the seven rows of variable axial compressor vanes. Vane position instrumentation for the automatically-controlled first three vane rows (IGV, stators 1 and 2) included dual resolvers (vane control system input), position potentiometers (data system input), and dial indicators (back-up). The remaining four variable vane rows were instrumented solely with dial indicators which were viewed in the control room via a television monitor for remote manual position control.

Blade tip clearances were measured using a series of removable aluminum-tipped rub probes installed over the first, third, and sixth stage axial compressor blade tips, and at the centrifugal impeller inlet and exit. These probes were removed from the rig, measured, and recorded after each successively higher speed operating point to determine the minimum clearance during that portion of the run program. A single laser clearance probe was additionally installed at the impeller exit to provide a real-time indication of clearance changes at this station.

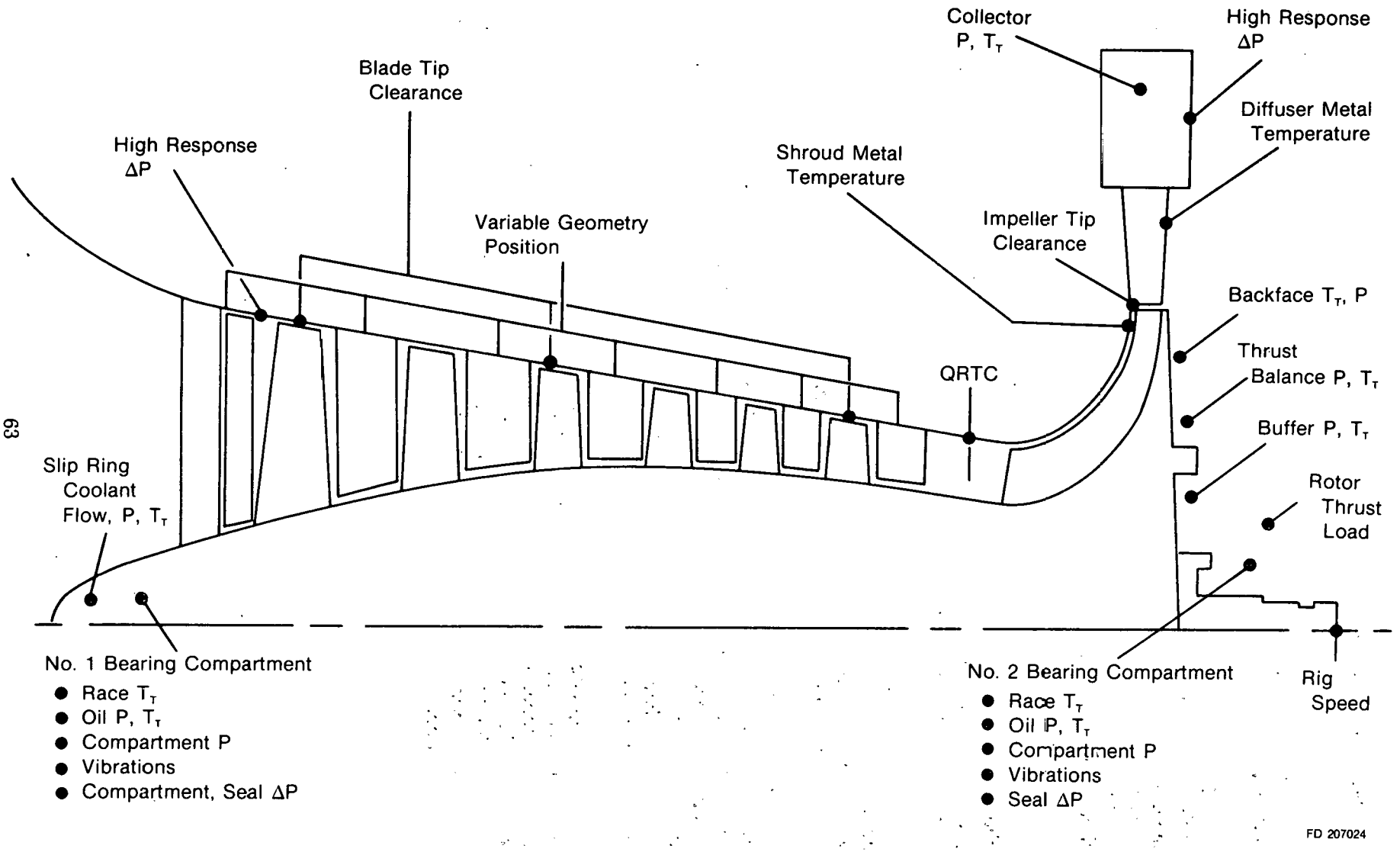

Figure IV-13. Operational Support Instrumentation Schematic

THIS PAGE

WAS INTENTIONALLY

LEFT BLANK

SECTION V
PROCEDURES

A. TEST PROCEDURES

1. Pre-run

Prior to each compressor rig test sequence, all stand support, instrumentation, and data systems were activated and a series of pre-run checks made to ensure proper operation. The final phase of the countdown procedure was initiated with the preparation and installation of the facility overspeed abort system explosive relief valves. Once the relief valves were installed, the steam, air, hydraulic, and lubrication systems for both the compressor rig and drive systems were activated. All instrumentation was then calibrated and verified through the data system, including setup of the dynamic strain and vibration data acquisition systems. Once all system checks were complete, the explosive valves were armed and the steam supply system brought up to starting temperature.

2. Rig Operation

The procedures adopted for the actual operation of the test facility were primarily oriented toward maintaining both the compressor rig and drive turbine operating characteristics within design specifications. While the rotor speed and variable geometry position controls were automatically regulated, the compressor rig interstage bleed flow, thrust balance pressure, backface buffer cavity pressure, bearing compartment pressure, and discharge valve controls were all manually operated. Speed transients were therefore conducted in stepped fashion, with adjustments of the manually-controlled systems made as required.

The initial step in the starting procedure for the drive turbine was to bleed a small amount of steam through the main supply valve to elevate the turbine to a satisfactory starting temperature. Upon completing the necessary preheat, the condenser system ejector located in the turbine discharge system was activated creating a sufficient differential pressure across the turbine to initiate rotation. Turbine speed was manually controlled up to 3,000 rpm, at which time the control was switched to automatic.

The general procedure utilized for operating the rig and obtaining the desired data was as follows:

(a) Select desired operating point (corrected speed and pressure ratio)

(b) Calculate actual rotor speed required based on inlet temperature

(c) Accelerate the rig to the required speed with the discharge valve(s) fully open

(d) Set the interstage bleed to the desired level

(e) Close discharge valve(s) to establish the desired rig pressure ratio.

Acceleration of the rig from the 3000 rpm turbine idle to the desired rpm was completed in 1500 rpm increments to permit adjustment of the rig support systems as discussed above. Upon reaching 9000 rpm (rig idle), a 5 minute hold was imposed prior to accelerating to higher speeds to provide sufficient time for the rig to reach thermal equilibrium. Acceleration rates for all speed transients were held to less than 1000 rpm/minute to reduce the risk of thermally-induced airfoil tip rubs.

In addition to the above procedure, operation of the compressor rig above 95% design speed required a throttled inlet (approximately 10 psia) due to a facility power limit at the time the test program was being conducted.

After all the required data was obtained for any particular test sequence, the compressor rig discharge valves were fully opened and the rig decelerated at a maximum rate of 2000 rpm/minute. Temporary holds were imposed at 9000 rpm and 3000 rpm to allow both the rig and turbine to thermally stabilize.

3. Test Program

The compressor test program was conducted in three phases. The objectives for each of these phases in the sequence conducted were to (1) verify the rig operation and structural integrity, (2) document the axial compressor performance, and (3) document the overall compressor performance. A brief summary of the test program conducted, including the extent of the data obtained in each phase, is presented in table V-1 and is discussed below.

Table V-1. Compressor Test Synopsis

Date	*Run Hr*	*Max rpm*	*Performance Data Acquired*
I. Rig Shakedown/Stress-Survey Program (With Vaneless Diffuser)			
5/7	0.9	6,000	Wide Open Discharge Steady State Points
5/9	0.4	6,000	Wide Open Discharge Steady State Points
5/15	0.4	4,000	Wide Open Discharge Steady State Points
5/19	0.8	6,000	Wide Open Discharge Steady State Points
5/28	2.8	7,500	Wide Open Discharge Steady State Points
5/30	3.7	12,000	Partial Speedlines at 50% and 60% Speeds
6/6	4.4	14,500	Speedlines Defined to Peak Efficiency at 80% and 90% Speeds
II. Axial Compressor Performance Documentation (With Vaneless Diffuser)			
6/16	1.8	14,600	2 Data Points at 95% Speed
6/17	6.8	15,400	95% and 100% Speedlines Defined up to Peak Efficiency 70% Speed Data Taken up to Approx. 20% Stall Margin
III. Overall Compressor Performance Documentation (With Pipe Diffuser)			
8/11	1.0	7,500	—
8/12	7.3	7,700	Full Speedline Definition at 20%, 30%, 40%, and 50% Speeds Including Stalls
8/15	4.1	15,400	Full Speedline Including Surge at 70% Speed; Partial Speedlines Defined at 80% and 90% Speeds
8/21	2.3	10,400	Additional Low Speed Data at 30% and 40% Speeds
9/11	3.2	16,600	Backface Leakage Variation at 70% and 100% Speeds; Full Speedline Including Surge at 100% Speed

(a) Rig shakedown/stress-survey program

The initial phase of the compressor test program was structured so as to verify satisfactory operation of the compressor rig and all of its auxiliary support systems over the entire rig operating range. The test program consisted of a sequence of six steps to establish proper facility/compressor operation:

- Static check-out of all facility and rig support systems;
- Static check-out of the data aystem and calibration of all required equipment;
- Static check-out of the facility abort system;
- Operation of the facility at low speed to verify manual and automatic operation of the speed control;
- Operation of the compressor rig over its entire speed range to verify mechanical, structural, and support system operation;
- Check-out of all instrumentation and the data system.

During this test sequence, vibration and strain gage data were monitored and recorded continuously. Transient performance and rig operational status data were recorded during all rig accels/decels. Steady-state data was obtained periodically during this sequence to be used in evaluating the rig's operational characteristics. In addition, a limited amount of preliminary axial compressor performance data was obtained in the 50% to 90% design speed range.

(b) Axial Compressor Performance Documentation

The second phase of the test program was conducted to document the axial compressor performance. Axial compressor steady-state data was acquired along a series of speedlines from wide-open discharge to peak efficiency at 50, 70, 80, 90, 95, and 100% design speed. In order to obtain an early estimate of the axial compressor stability, additional data was obtained at 50 and 70% speed above the nominal operating line to approximately 20% stall margin; this was achieved without surging the compressor. All data acquired during this phase was obtained with the variable geometry at the design setting.

(c) Overall Compressor Performance

The final phase of the test program was conducted to document the overall compressor performance over the complete operating range.

For this phase, the vaneless diffuser, which had been intalled for the prior two phases, was replaced with a pipe diffuser. The test sequence was specifically conducted to obtain the following data:

- Starting and low speed aerodynamics;
- Interstage bleed requirement definition;
- Aerodynamic design point performance;

- Axial, centrifugal, and overall compressor performance (pressure ratio, speed-flow, and efficiency characteristics);

- Surge line definition.

Acquisition of the desired data for this phase of the program was completed in two parts. The initial test sequence was to acquire data to document the compressor's starting characteristics. Low speed data was acquired at 20, 30, 40 and 50% design speed from wide-open discharge to stall. Due to the low pressure and flow generated by the compressor at these low speeds, the pressure transducers and the inlet orifice were changed to provide improved measurement accuracies for these test conditions.

The subsequent high speed test sequence acquired data at 70, 80, 90 and 100% design speeds. Full speedlines, including surges, were recorded at 70 and 100% speeds, with partial speedlines to above peak efficiency recorded at 80 and 90% speeds. The pressure transducers and the inlet orifice were sized to minimize measurement uncertainty.

B. DATA REDUCTION AND ANALYSIS PROCEDURES

Data obtained from the axial/centrifugal compressor rig was recorded, corrected for probe calibration, reduced into engineering units, and preliminiary performance calculations performed using an on-line data reduction program. The data was subsequently reduced in terms of the axial compressor, centrifugal compressor, and combined axial/centrifugal compressor performances and compared to design goals.

The data reduction procedures and significant equations utilized are summarized below.

1. Flow Calculation

The compressor rig inlet flowrate and interstage bleed flowrate were measured using standard ASME thin-plate orifices located in the rig inlet ductwork upstream of the plenum chamber and in the bleed discharge plumbing respectively. The flow calculations were of the form:

$$W = K_1 \left[C_o - K_2 \left(\frac{\Delta P}{P} \right) \right] [K_3 T + K_4] \sqrt{\frac{P \Delta P}{T}} \qquad (1)$$

where: W — actual flowrate, lbm/sec
P — orifice upstream pressure, psia
ΔP — orifice differential pressure, psi
T — orifice upstream temperature, °R
C_o, K_1, K_2, K_3, K_4 — constants

Two different inlet orifices were used to obtain the desired flow accuracy at both high and low flow conditions: a 24-in. diameter orifice for all testing above 50% design rotor speed, and a 15-in. diameter orifice for all data acquisition at 50% speed and lower. Table V-2 presents the values of the flow equation constants for each of the orifices used.

Flows were corrected to a standard day inlet based on plenum conditions as follows:

$$W_{COR} = \frac{W \sqrt{\theta}}{\delta} \qquad (2)$$

where: $\theta = T_1/518.688$
$\delta = P_{T_1}/14.696$

Table V-2. Flow Orifice Equation Constants

Station	Orifice	Constants C_v	K_1	K_2	K_3	K_4
INLET	24"	1.0	302.44	0.2993	0.0000204	0.9985
	15"	1.0	125.13	0.2940	0.0000132	0.9985
INTERSTAGE BLEED	6"	1.0234	11.5973	0.3794	0.0000204*	1.000

*K_3 = 0.0 if T is less than 200°F

When testing was initiated with reduced inlet pressure an approximate 3% reduction in the measured inlet orifice flow was noted relative to previous data at the same speed and flow. No other changes in performance or in the rig operating characteristics was apparent. Cause of the flow shift was attributed to leakage through the plenum pneumatic seal aggrevated by the increased pressure differential. Since no replacement seal was available, testing was continued and the inlet flow rates for subsequent data points determined from a correlation of the inlet corrected flow versus the measured value of P_T/P_S at the inlet strut leading edge for the initial data points. The flow correlation is presented in figure V-1.

2. Temperature Calibrations and Corrections

Wire calibrations and Mach number recovery corrections were applied to all performance temperature measurements. The wire calibrations were experimentally determined in the P&WA instrumentation lab for each batch of thermocouple wire used and were of the form:

$$T_{corrected} = T_{measured} - \Delta T \tag{3}$$

where ΔT was specified as a function of the measured temperature. Copies of the wire calibration data for the axial compressor discharge (station 2) and pipe diffuser exit (station 3) probes are shown in figures V-2 and V-3.

Temperature recovery corrections were applied as:

$$T_{actual} = T_{measured}/R \tag{4}$$

where the recovery (R) is calculated from:

$$R = 1 - \left[K \left(\frac{P_T}{14.7}\right)^{-0.58} \left(\frac{540}{T}\right)^{0.25} (1 - X) \right] \tag{5}$$

and $X = 0.00076\ M_n^3 - 0.001025\ M_n^2 - 0.00763 M_n + 1.000029$ (6)

M_n = Mach Number
P_T = sensor total pressure (psia)
T = sensor total temperature (°R)
K = sensor scale factor (determined from calibration data)

Value of the scale factor (K) determined for the axial compressor discharge and pipe diffuser discharge temperature sensors was 0.30336.

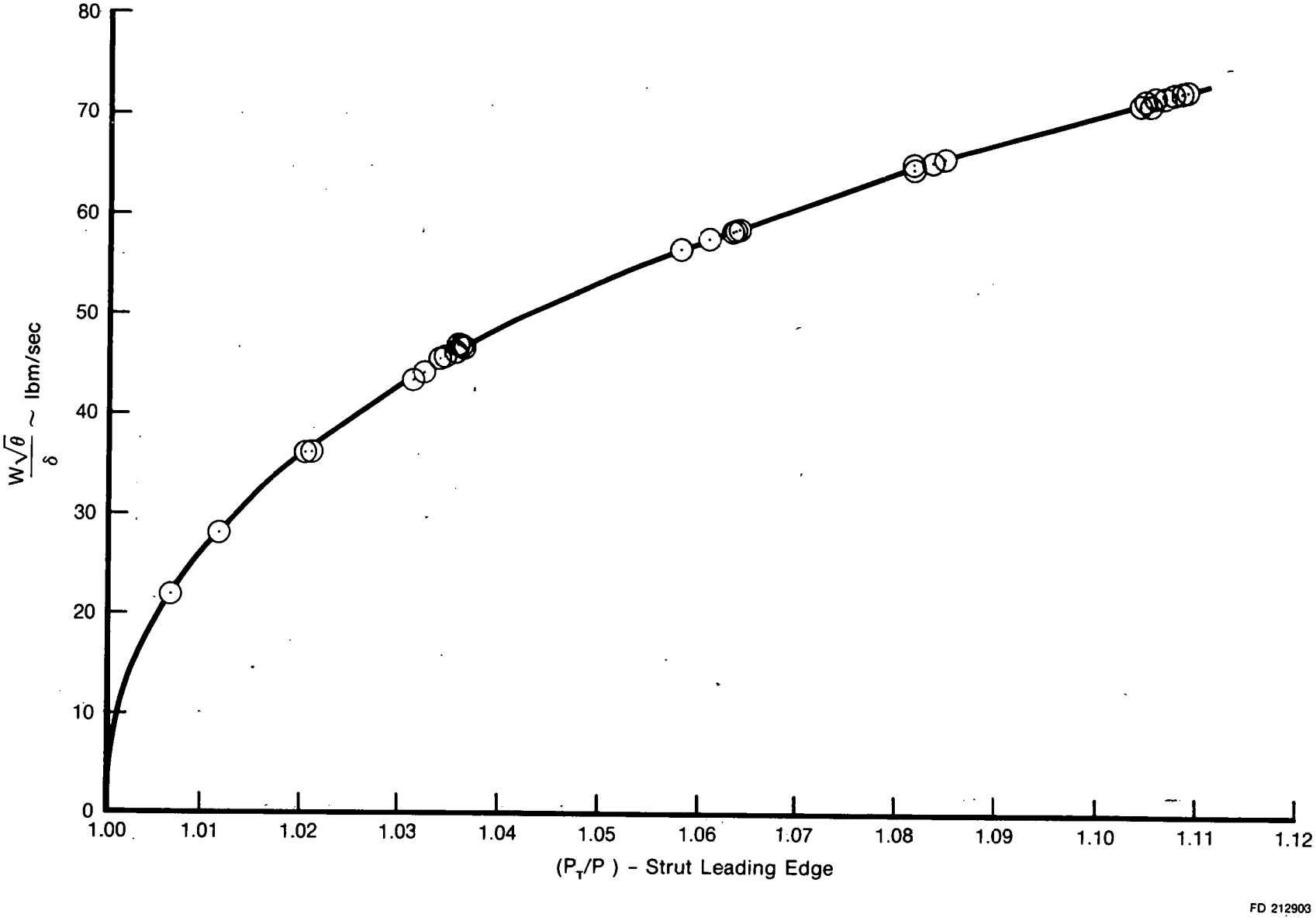

Figure V-1. Inlet Flow Correlation

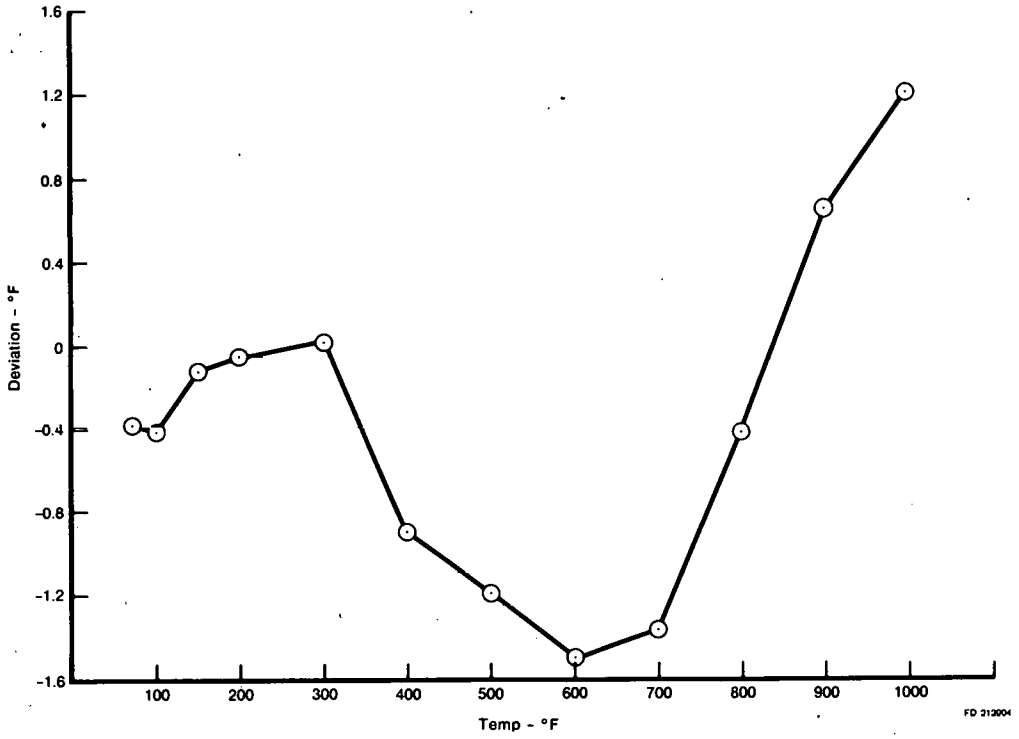

Figure V-2. Axial Compressor Discharge Wake Rake Thermocouple Wire Calibration Data

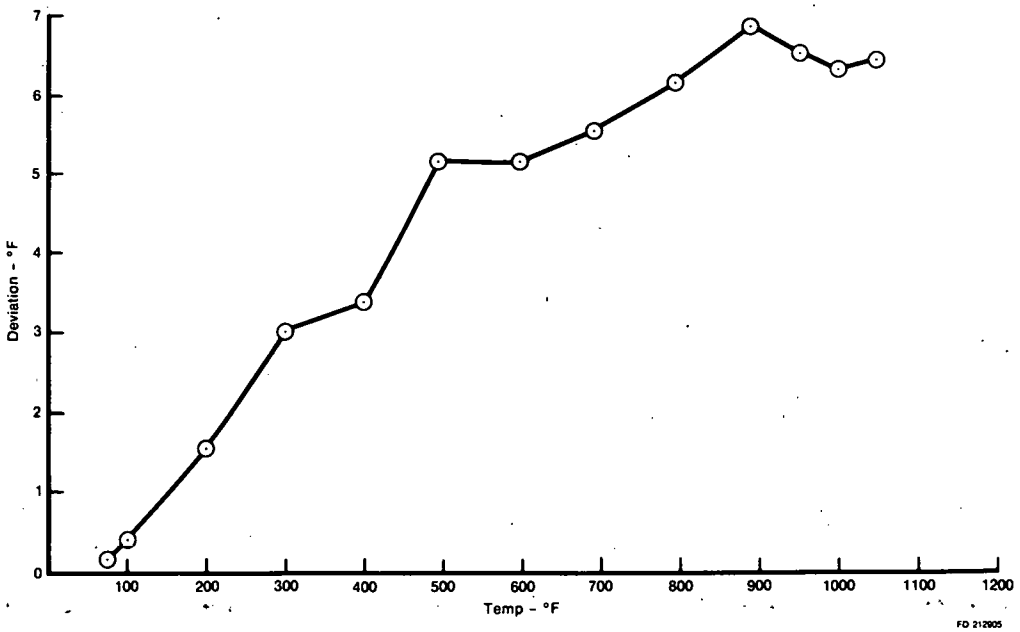

Figure V-3. Pipe Diffuser Exit Rake Thermocouple Wire Calibration Data

In addition to the wire calibration and recovery corrections a slight correction was also applied to the measured pipe diffuser exit average temperature to account for the effects of the impeller backface leakage flow. The estimated magnitude of the leakage flowrates at design speed as a function of the buffer seal differential pressure is shown in figure V-4. During the test program, data was acquired at both 70% and 100% design speed in which the buffer seal ΔP was varied over a range from 0 to approximately 1.5 psia while all other rig operating conditions were held constant. The resulting effect on the measured rig discharge temperature is shown in figure V-5. All of the subsequent design speed data was acquired with the buffer seal ΔP maintained at less than 0.5 psia (backface leakage flow less than 0.2%) and a small correction made based on the figure V-5 correlation to adjust the temperature to an equivalent zero leakage flow. The effect of this correction was to reduce the quoted design speed efficiencies by less than 0.25%.

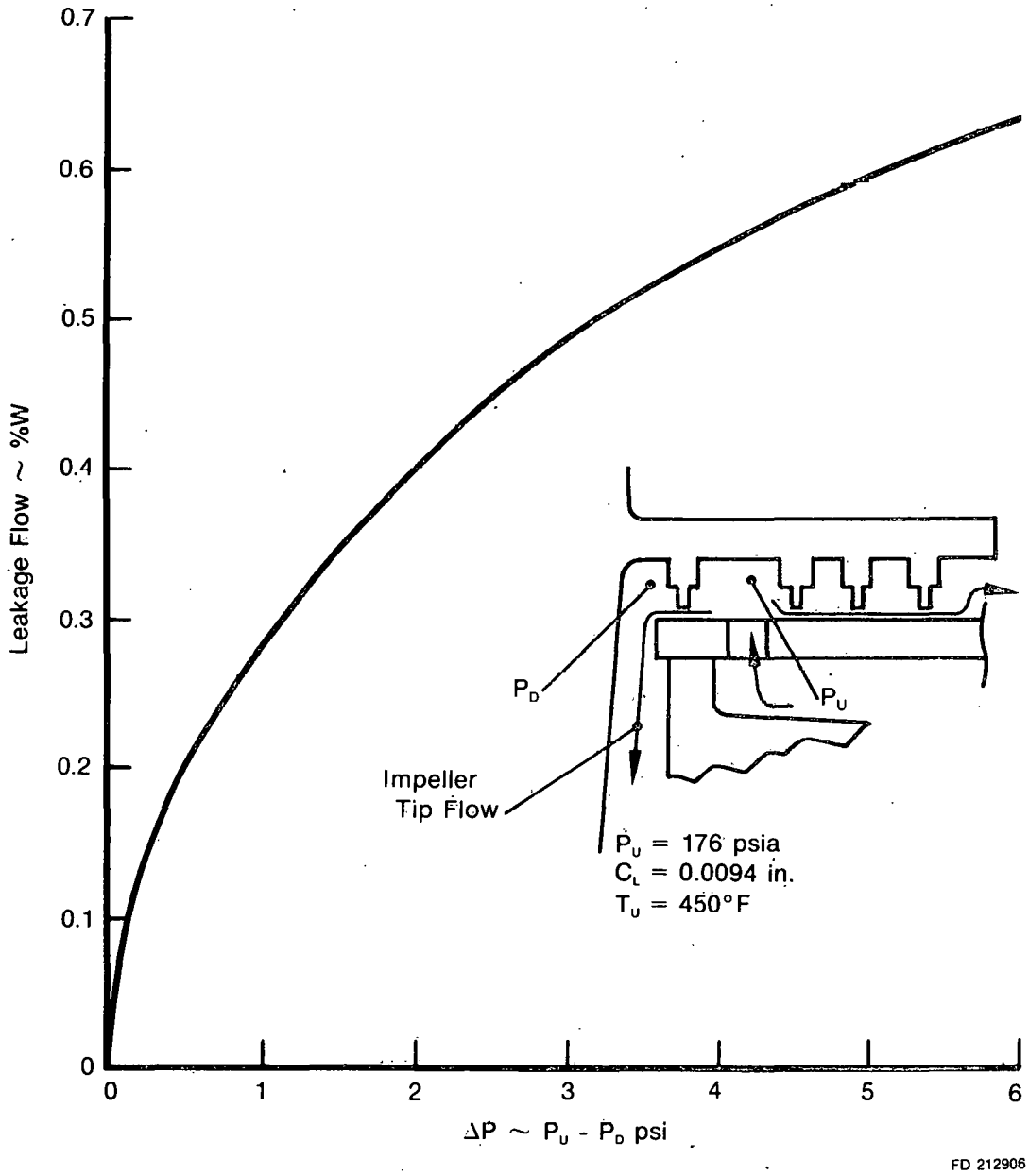

Figure V-4. Impeller Backface Leakage Flow Curve

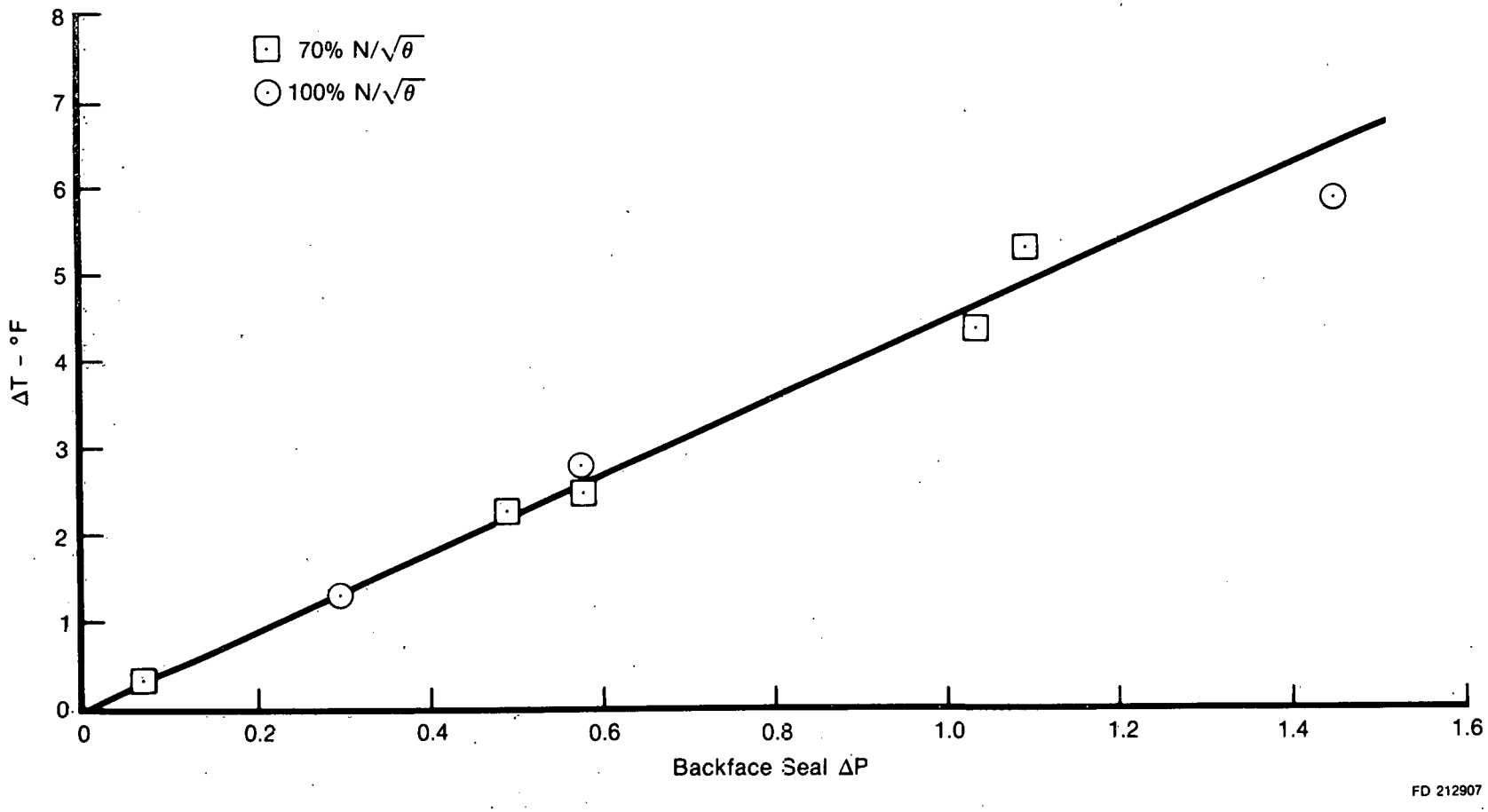

Figure V-5. Effect of Impeller Backface Seal Leakage on Measured Rig Discharge Temperature

3. Averaging Techniques

Two averaging methods were used during the compressor rig data reduction: 1) standard arithmetic averaging and 2) mass-averaging. Arithmetic averaging was used for the axial compressor discharge circumferential pressure and temperature profiles and to average all redundant interstage measurements at the same radial position but at more than one circumferential location. The resultant radial profiles at each axial compressor instrumentation station were then mass-averaged and these mass-averaged values used for all subsequent performance calculations.

The mass-average of a given number (n) of values of an arbitrary parameter (P) is defined as

$$\bar{P} = \frac{\sum_{i=1}^{n} \Delta W_i P_i}{\sum_{i=1}^{n} \Delta W_i} \tag{7}$$

where $\Delta W_i = \frac{k_i A_i P_{T_i}}{\sqrt{T_i}}$ (8)

Since the compressor rig instrumentation sensors were generally located at the centers of equal area segments of the flow-path, the area term in equation (8) usually cancelled out. The flow parameter (k) values were calculated from the ratio of the local total pressure (P_{T_i}) and the measured OD wall static pressure ($P_{s_{OD}}$) as follows:

$$k_i = M_i \sqrt{\frac{\gamma g}{R}} \left(1 + \frac{\gamma - 1}{2} M_i^3\right)^{-\frac{\gamma + 1}{2(\gamma-1)}} \tag{9}$$

where

$$M_i = \left\{ \left(\frac{2}{\gamma-1}\right) \left[\left(\frac{P_{T_i}}{P_{s_{OD}}}\right)^{\frac{\gamma-1}{\gamma}} - 1 \right] \right\}^{1/2} \tag{10}$$

The pipe diffuser exit pressure and temperature measurements (20 measurements each obtained over 4 pipes) were superimposed so as to result in an array of 17 measurement locations in the centers of equal area flowpath segments with the center area defined by four repeat readings from each of the instrumented pipes. The entire array was then mass-averaged to yield the final compressor discharge average pressure and temperature values.

4. Performance Calculations

Overall compressor performance was defined from the inlet plenum (Station 1) to the pipe diffuser exit plane (Station 3). Measurements obtained at the axial compressor discharge wake rake plane (Station 2) were used to divide the axial compressor and centrifugal stage component performances. All calculations were performed on a total-to-total basis using average values as defined in Section 3. Pressure ratios were therefore defined as:

$$PR_{axial} = P_{T_2}/P_{T_1} \tag{11}$$

$$PR_{centrifugal} = P_{T_3}/P_{T_2} \tag{12}$$

$$PR_{overall} = P_{T_3}/P_{T_1} \tag{13}$$

Corresponding adiabatic efficiencies were calculated based upon the pressure rise and dry air values of enthalpy and are in agreement with values obtained using Reference 6:

$$\eta_{ad_{1,2}} = \frac{\Delta h'}{\Delta h} = \frac{f\,(PR_{1,2}\ T_1)}{f\,(T_1,\ T_2)} \tag{14}$$

A net adiabatic efficiency was also calculated for the part-speed overall compressor performance which accounts for the work done on the interstage bleed flow. The net efficiency is defined as:

$$(\eta_{ad})_{net} = \frac{(W - W_{bl})\ \Delta h'_{1,3}}{(W - W_{bl})\ \Delta h_{1,3} + W_{bl}\ \Delta h_{1,2}} \tag{15}$$

Polytropic efficiency was calculated from the adiabatic efficiency and pressure ratio per the following assuming a γ of 1.4:

$$\eta_p = \left[\frac{\gamma-1}{\gamma}\ \ell n\ PR\right] \Big/ \left[\ell n\left(1 + \frac{PR^{\frac{\gamma-1}{\gamma}} - 1}{\eta_{ad}}\right)\right] \tag{16}$$

A constant flow stall margin definition was used as follows:

$$SM\% = \frac{PR_{Surge} - PR_{OP}}{PR_{OP}} \times 100$$

C. DATA VALIDATION

Data acquired from the compressor rig was examined for consistency and validity and a detailed uncertainty analysis performed. The uncertainty analysis included an evaluation of potential sources of error due to the measurement sensors, the data acquisition and recording equipment, calibration data curve fits, data reduction procedures, sampling rates, and run-to-run measurement variations. The predicted uncertainties in the compressor rig inlet and discharge measurements used in the determination of the overall compressor performance are shown in table V-3. The resultant estimated uncertainty of the overall compressor efficiency is 1.31%. Uncertainty of the measured uncorrected compressor rig inlet flowrate is approximately 1.84%.

Table V-3. Uncertainty Estimates

Variable	*No. of Sensors*	*Units*	*Bias +−*	*Precision +−*	*Uncertainty +−*
Plenum P_T	4	psia	0.047	0.014	0.061
Plenum T_T	3	°F	0.37	0.47	0.84
Discharge P_T	20	psia	3.23	0.294	3.52
Discharge T_T	20	°F	7.60	0.82	8.42
Efficiency	—	%	1.13	0.18	1.31

THIS PAGE

WAS INTENTIONALLY

LEFT BLANK

SECTION VI
RESULTS AND DISCUSSION

Overall axial/centrifugal compressor performance, as well as axial and centrifugal stage component performances, were acquired during the pipe diffuser portion of the test program. Additional axial compressor performance data was obtained during the initial vaneless diffuser test series. A complete summary of the compressor rig aerodynamic performance data is tabulated in Appendix A. The Appendix A data tabulations and the ensuing discussion of the test data are accordingly divided into three sections: 1) overall compressor performance, 2) axial compresor performance, and 3) centrifugal stage performance. A summary of the significant compressor rig mechanical/structural data and teardown observations is also included in this section.

A. OVERALL COMPRESSOR PERFORMANCE

An overall compressor performance map is presented in figure VI-1. Full speedline definition, including surge points, was obtained at 50%, 70%, and 100% design rotor speeds with partial speedlines obtained to above peak efficiency at 80% and 90% speeds. All data was acquired with the variable axial compressor vane rows in their nominal positions per the design vane angle schedule. Part-speed interstage bleed flow rates were selected to ensure adequate flow range capability at each of the speeds documented. No attempt was made to optimize or minimize the bleed flows. The approximate percent bleed at peak efficiency for each speedline is indicated in figure VI-1. The exact bleed flow for each data point are included in the Appendix A tabulations. Since the overall performance data was acquired at slightly reduced inlet pressure, the value of the test Reynolds number index ($\delta/\theta^{1.74}$) is also included on the figure for each speed-line. The efficiency values quoted are not corrected for Reynolds number effects (the effect of correcting the design speed performance to a Reynolds index of 1.0 would be to increase the quoted adiabatic efficiencies by approximately 0.3%).

The peak design speed overall performance measured was 87.8% adiabatic efficiency at 18.45:1 pressure ratio and approximately 10% stall margin. Performance for the data point closest to the 18:1 pressure ratio design point was 87.6% adiabatic efficiency and 14% stall margin. The demonstrated performance for these two points is compared to the contract goals in table VI-1. Performance for the data point closest to the design pressure ratio exceeds the contract efficiency goal by 2.0% and exceeds the contract minimum stall margin goal by 4%. The highest efficiency measured at any speed (neglecting bleed effects) was 88.76% adiabatic efficiency at 12:1 pressure ratio and 90% rotor speed.

Table VI-1. Design Speed Overall Performance Summary

	Demonstrated		
	Peak Efficiency	*Closest to Design PR*	*Program Goal*
Flow, lbm/sec	70.7	70.5	70
Pressure Ratio	18.45	17.81	18
Adiabatic Efficiency, %	87.8	87.6	85.6
Polytropic Efficiency, %	91.7	91.5	90
Stall Margin, %	10	14	10

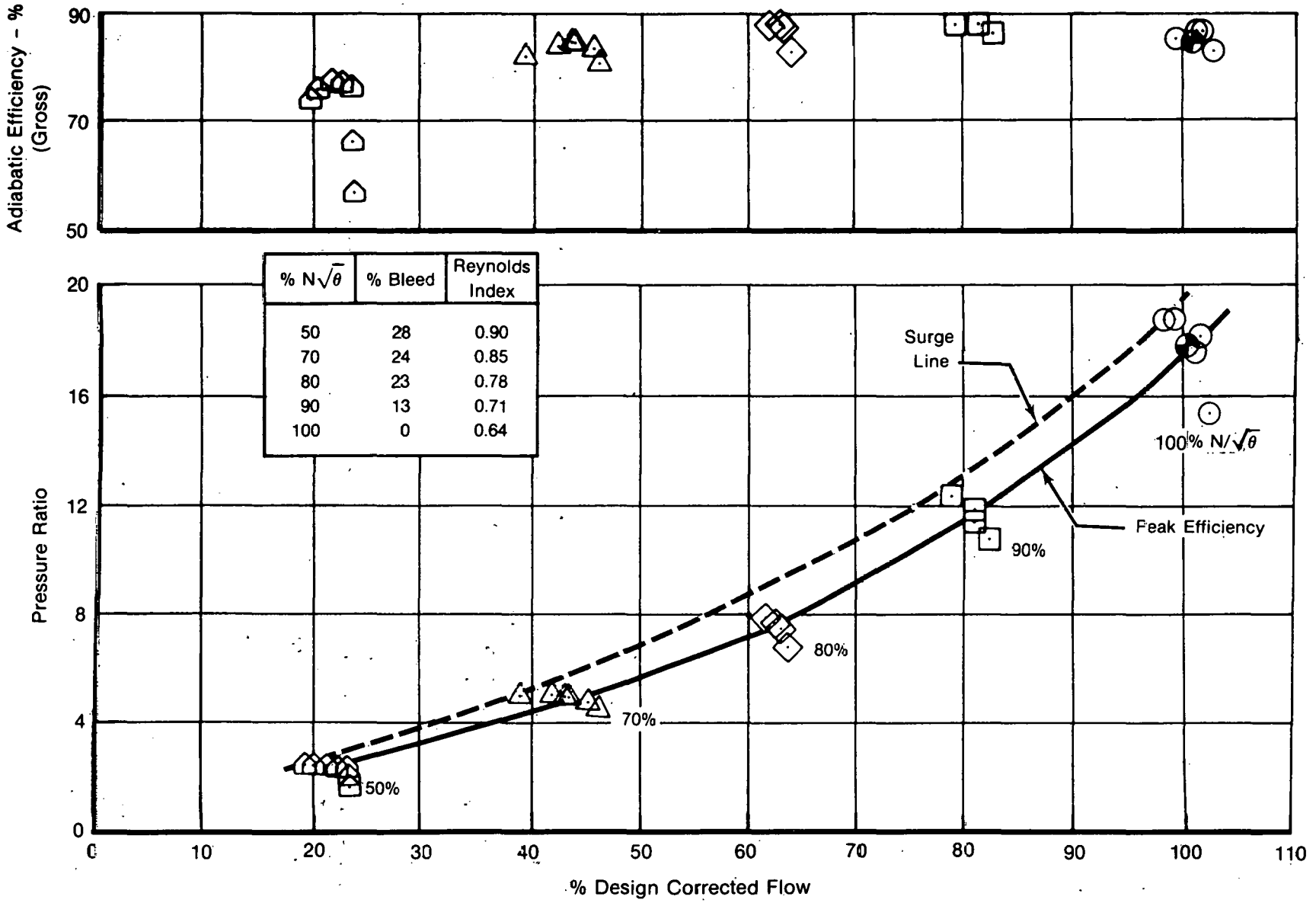

Figure VI-1. Overall Compressor Performance Map

The compressor performance demonstrated not only exceeded the program goals but even more significantly represents the highest known single spool compressor performance demonstrated to date in this pressure ratio and flow class. This performance can be directly translated into equivalent benefits in terms of gas turbine engine performance potential. For the conceptual engine cycle defined in Phase I (18:1 pressure ratio and 2500°F CET) each percent increase in compressor adiabatic efficiency can be equated to an approximate 1.0% improvement in simple cycle engine SFC and an approximate 1.4% increase in shaft horsepower.

Part speed efficiency values were also calculated with a correction to account for the work done on the interstage bleed flow. The resultant "net" overall performance map, which is useful for simplified cycle analyses which cannot separately book-keep the bleed flow, is presented in figure VI-2. It should be reiterated that no attempt was made to minimize the part speed bleed flow rates, hence some improvement in the part-speed "net" performance may be feasible.

An axial/centrifugal matching analysis was undertaken based on the available interstage data to determine the minimum bleed flow requirements at any given rotor speed. The results of the analysis are shown in figure VI-3, in which the corrected flow at the axial/centrifugal interface is plotted versus the corrected speed at the same location for both the axial and centrifugal components. The indicated flow difference between the axial compressor surge line and the centrifugal stage choke line represents the required bleed flow. The excellent flow range potential demonstrated by the axial compressor at part speed resulted in less interstage bleed requirement than originally anticipated. Figure VI-4 summarizes the actual minimum bleed flows required as compared to the range of bleed flow utilized for the compressor test program.

In addition to the data shown on figures VI-1 and VI-2, additional low speed performance data was obtained to document the compressor starting characteristics. Data was obtained along constant speed lines from a wide open discharge valve setting into stall at 20%, 30%, 40% and 50% speeds as shown in figure VI-5. The stall line was defined by the initiation of a static pressure oscillation at a frequency of approximately ½ rotor speed at the axial compressor discharge (indicative of an axial compressor rotating stall condition). Analysis of the low speed data acquired has indicated no starting or axial/centrifugal matching problems which would complicate use of this compressor configuration in an engine application.

B. AXIAL COMPRESSOR PERFORMANCE

Axial compressor performance data was acquired from both the vaneless diffuser and pipe diffuser portions of the test program. A composite performance map showing the axial compressor performance data from both test sequences is shown in figure VI-6. A complete tabulation of the axial compressor performance data is included in Appendix A.

The highest axial compressor performance was measured during the initial vaneless diffuser test sequence. Peak design rotor speed performance was 89.47% adiabatic efficiency at 6.5:1 pressure ratio (as compared to design goals of 89.0% adiabatic efficiency at 6.67:1 pressure ratio). The design rotor speed performance acquired at the same pressure ratio during the subsequent pipe diffuser testing was approximately 0.7% lower in efficiency. Cause of the performance deterioration can be primarily attributed to slightly increased "nominal" airfoil running tip clearances for the later test runs due to wearing away of the abradable rub materials during transient operating conditions (see Section II.B.4).

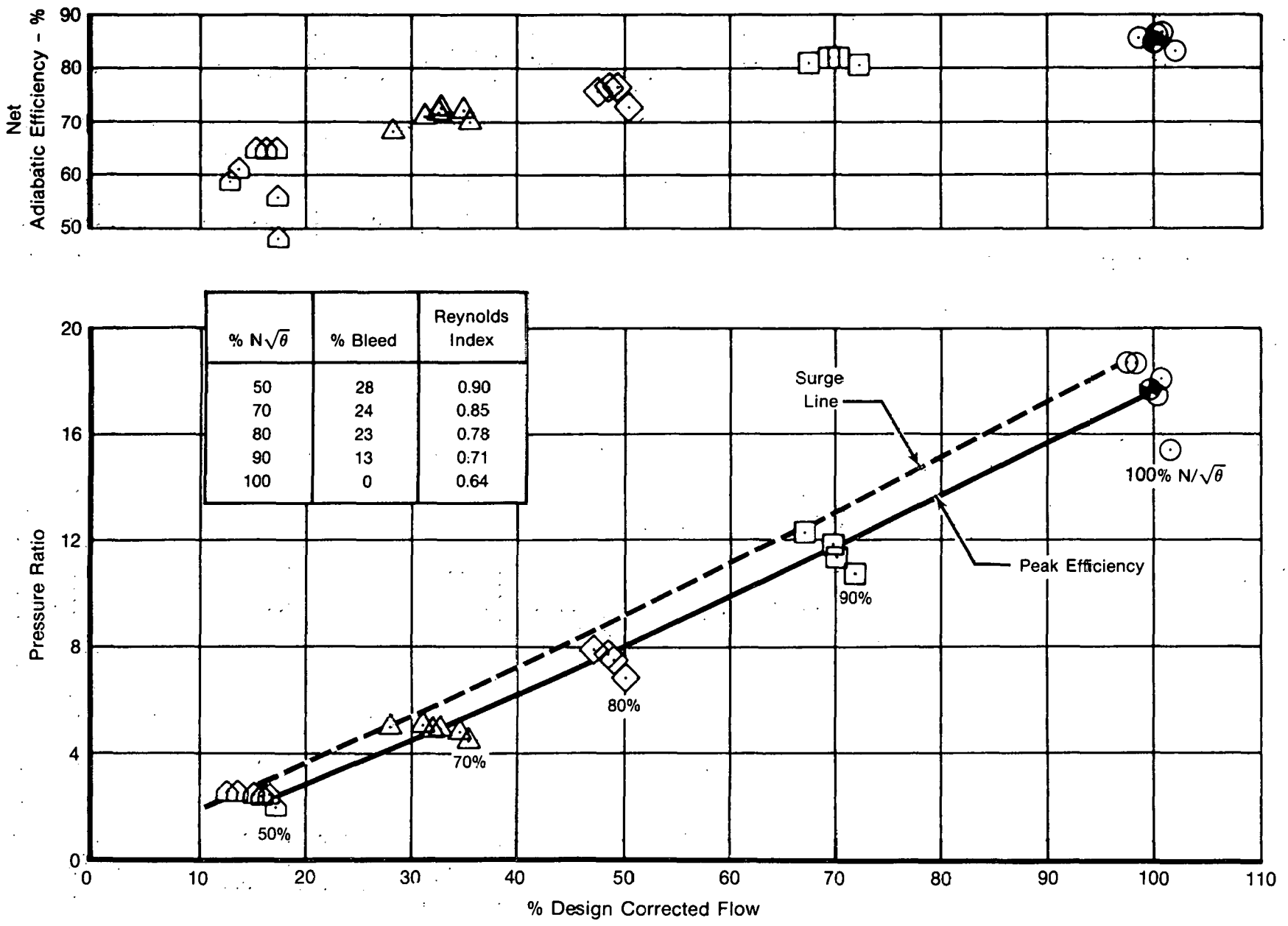

Figure VI-2. Net Overall Compressor Performance

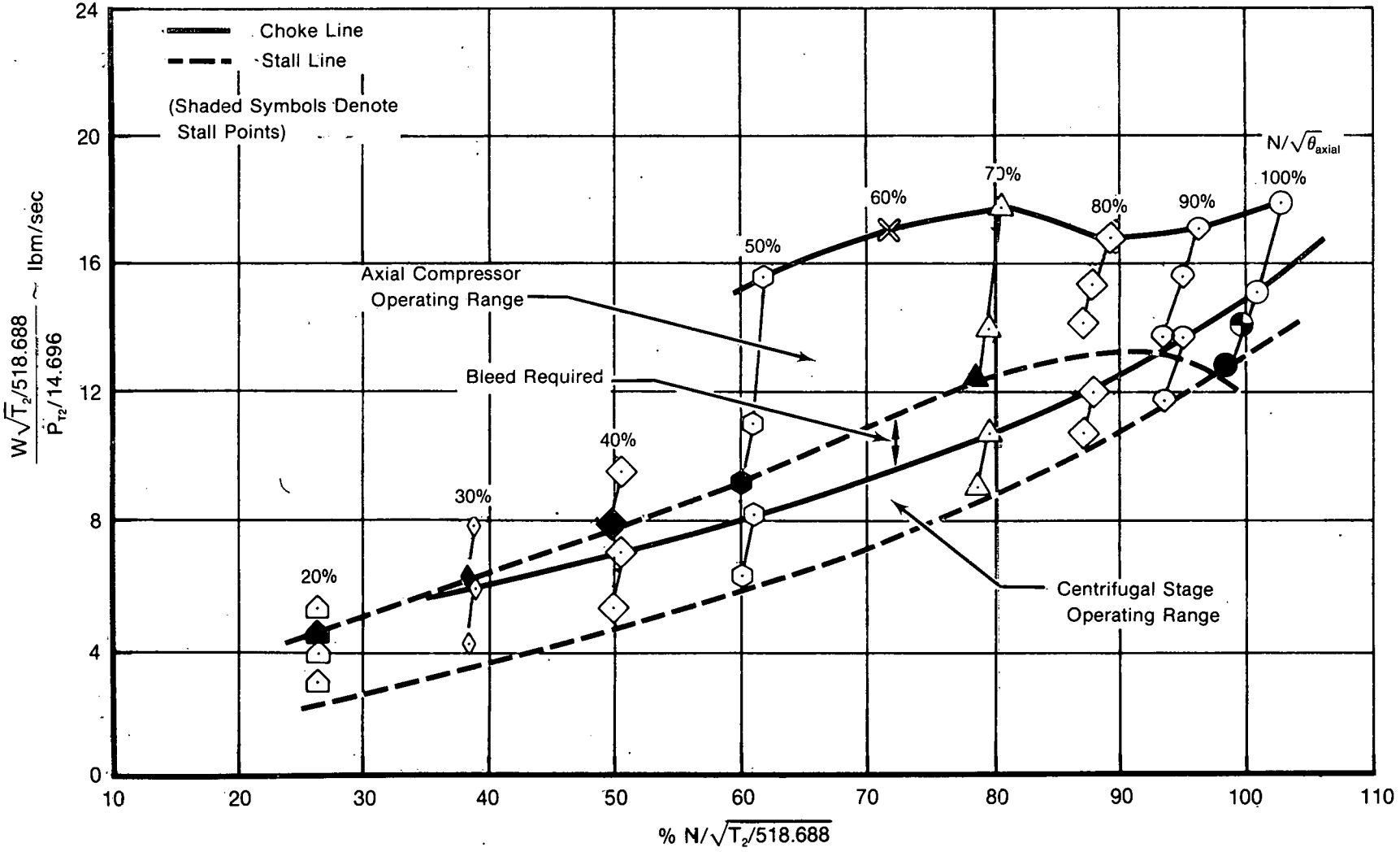

Figure VI-3. Compressor Off-Design Matching Analysis

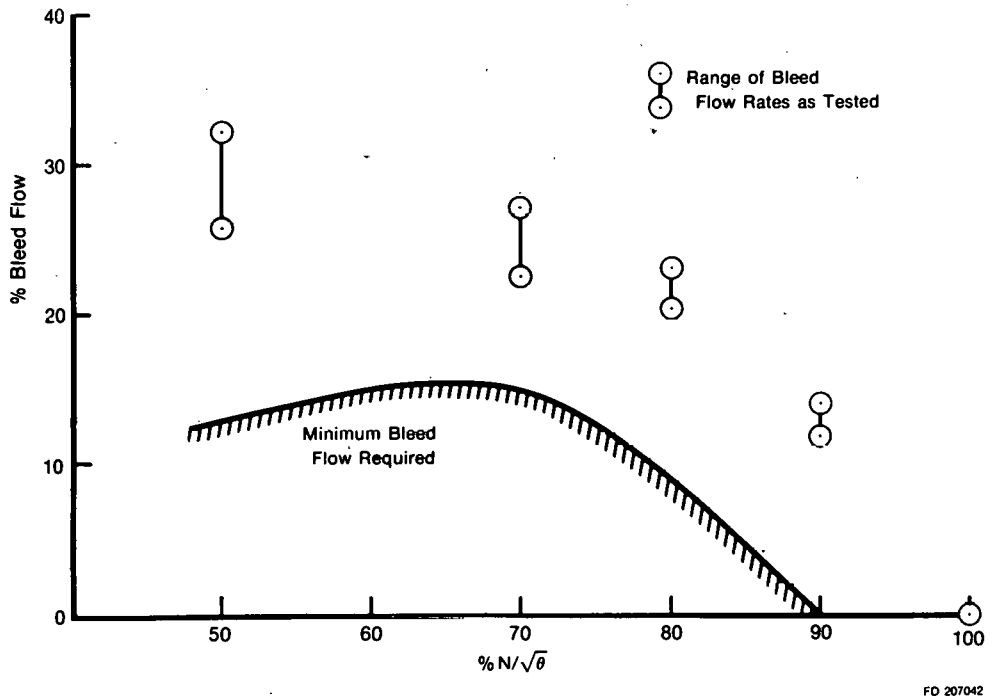

Figure VI-4. Interstage Bleed Flow Requirement

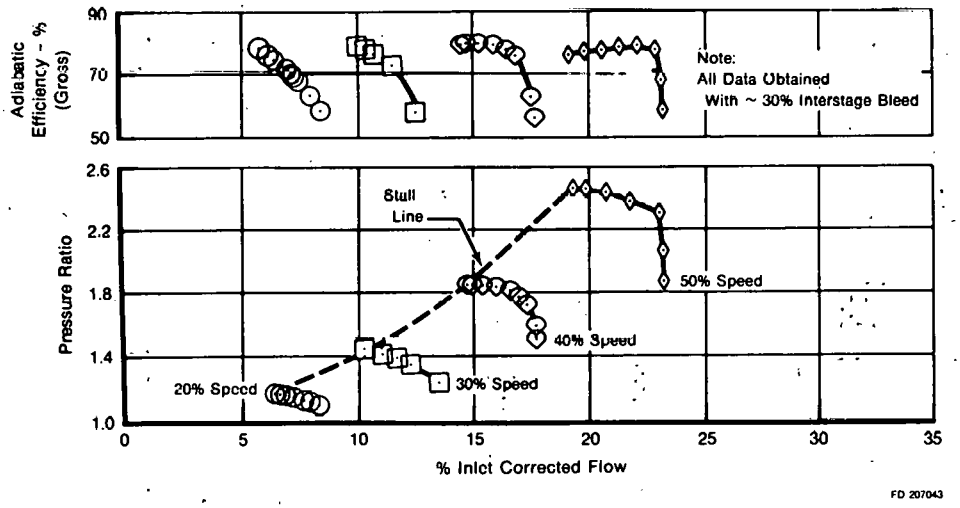

Figure VI-5. Overall Compressor Low Speed Performance Map

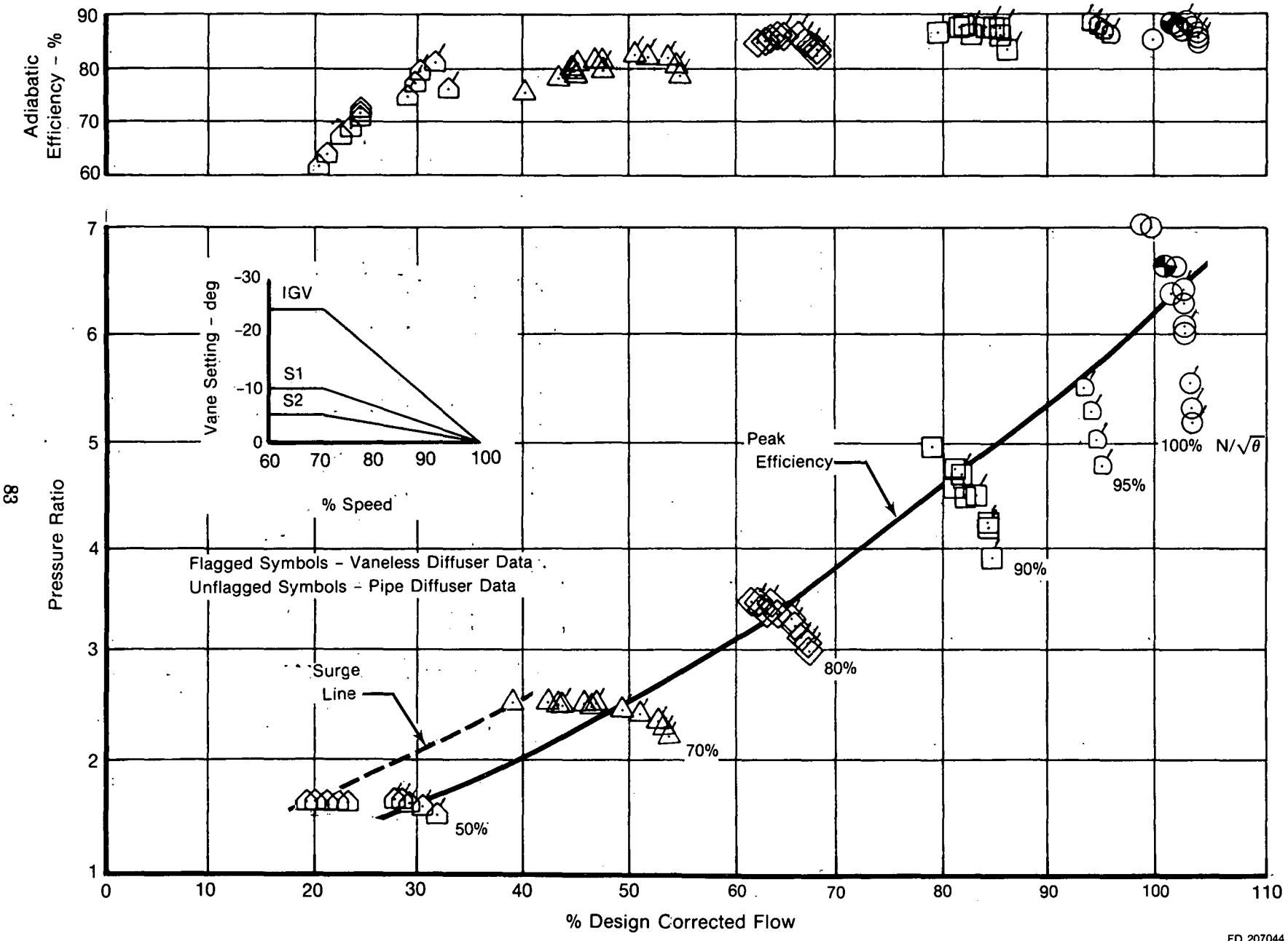

Figure VI-6. Axial Compressor Performance Map

The axial compressor performance was characterized by broad efficiency islands (i.e., high efficiency was obtained over a wide range of pressure ratio and rotor speeds). The measured peak efficiencies were essentially constant from 100% down to 90% rotor speed falling off slightly at 80% speed and lower. In actuality, the axial compressor measured performance at the lower rotor speeds is probably conservative due to the likely influence of the relatively large (greater than 20%) interstage bleed flows on the discharge measurements at these speeds (sensors are aligned to the design flow angles). Especially when viewed in conjunction with the trend of increasing centrifugal stage efficiency at the lower rotor speeds (see next section), a bias in the interstage measurements at the lower rotor speed/high bleed flow conditions appears likely.

A cursory analysis of the axial compressor stage characteristics indicates the compressor surges recorded at 50% and 70% rotor speeds were initiated in the axial compressor front end stages. Insufficient high response instrumentation was included in the test rig to distinguish in which component (the axial or centrifugal stages) the design speed surge initiated. Stall margin for the axial compressor at design speed from the axial compressor peak efficiency point to the overall compressor surge point was approximately 14%. The axial compressor stall margins at 50% and 70% rotor speeds were approximately 30% and 26%, respectively.

The combination of excellent efficiency and good stability demonstrated at the high axial compressor design loading levels provides conclusive verification for the low aspect ratio blading design philosophy.

C. CENTRIFUGAL STAGE PERFORMANCE

The centrifugal stage performance map derived from the interstage instrumentation measurements is shown in figure VI-7. All of the stage design goals (PR, η, flow) were either met or exceeded. A summary of the stage design speed performance relative to the program minimum goals is presented in table VI-2.

Table VI-2. Centrifugal Stage Design Speed Performance Summary

	Demonstrated		
	Peak Efficiency	*10% Stall Margin*	*Program Goal*
Pressure Ratio	2.76	2.70	2.70
Airflow, lb_m/sec	14.19	15.20	14.10
Adiabatic Efficiency, %	92.7	88.3	85.8
Exit Mach Number	0.32	0.35	0.35
Stall Margin, %	2.3	10.0	10.0

An analysis of the design rotor speed centrifugal stage performance at peak efficiency was conducted to divide the measured stage performance into impeller and diffuser component performances. Impeller exit conditions were calculated from the continuity and momentum equations based on the measured impeller exit static pressure and stage temperature rise. Design blockages were assumed. The resultant component performances are summarized in table VI-3 relative to the design goals. As can be seen, the excellent stage performance demonstrated is the result of both higher than predicted impeller efficiency and lower than predicted diffuser total pressure loss.

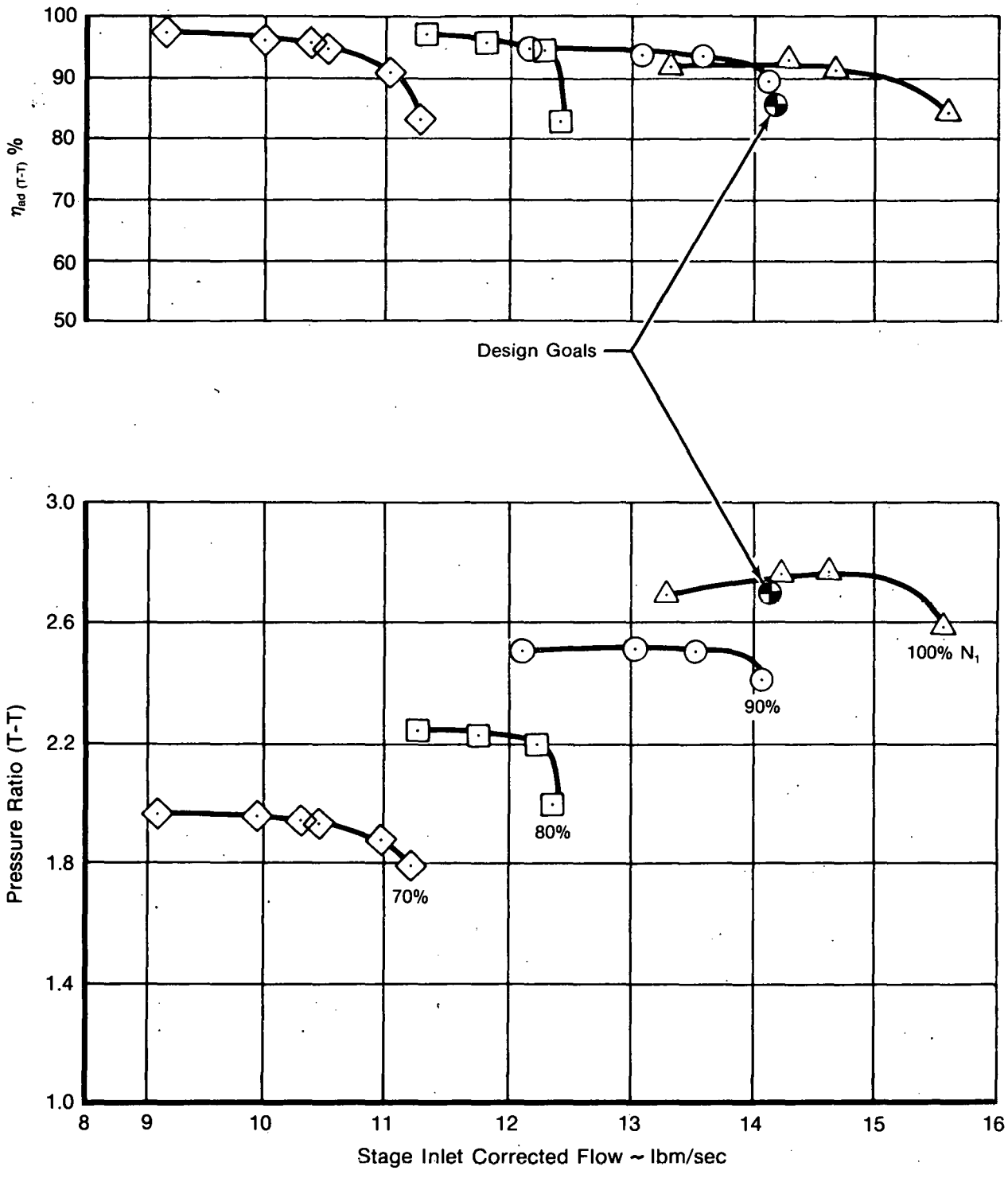

Figure VI-7. Centrifugal Stage Performance Map

Table VI-3. Impeller/Diffuser Design Point Performance Summary

		Demonstrated	Program Goal
Impeller			
	Pressure Ratio	2.82	2.82
	Adiabatic Efficiency, %	94.7	90.0
Diffuser			
	Total Pressure Loss, %	2.1	4.2

As discussed in the previous section, the indicated trend of increasing centrifugal stage efficiency to unrealistically high values as rotor speed is decreased is due to the influence of the bleed flow at part speed on the interstage measurements.

D. COMPRESSOR MECHANICAL PERFORMANCE

In general, the mechanical operating characteristics of the compressor were excellent, particularly with respect to rotor dynamics and blade vibratory behavior. A summary of the compressor mechanical behavior and teardown inspection is presented in the following text.

1. Compressor Rotor Dynamics

The rotor dynamics of the compressor were excellent over the entire operating range. During the operation of the compressor, a series of minor critical speeds were identified, the majority of which were predicted. In all cases, the magnitude of the rotor response at each of these critical speeds was well within the allowable operating limits of the rig bearings. All of the responses occurred at low speeds and could be accelerated/decelerated through without impact on the test rig operation. A summary of the compressor rotor response for both the resonance and normal operating conditions is presented in table VI-4. The maximum deflections were 0.4 mils at 13,400 RPM and 0.6 mils at 7500 RPM for the front and rear bearings, respectively.

Table VI-4. Compressor Test Rig Rotor Vibration Summary

	Front Bearing		Rear Bearing	
Speed	Vertical (mils)	Horizontal (mils)	Vertical (mils)	Horizontal (mils)
1500	0.05	0	0.05	0.05
3000	0.20	0.10	0.10	0.10
4500	0.20	0.30	0.20	0.10
6000	0.10	0.20	0.20	0.10
7500	0.10	0.20	0.6*	0.10
8500	0.20	0	0.10	0
9530	0.20	0.20	0.10	0.10
10450	0.20	0.20	0.30	0.10
10780	0.20	—	0.10	0.10
12000	0.20	—	0.20	0.20
13400	0.40	—	0.20	0.20
14700	0.30	—	0.20	0.30
15400	0.30	—	0.30	0.30

*Resonance Peak

2. Blading Vibratory Stress

The blading vibratory stress levels observed during the compressor test program were well below allowable limits and, thus, did not limit operation of the rig. A summary of the observed stress levels for each of the blades and vanes is presented in figures IV-8 and IV-9, respectively.

In general, the vibratory data revealed good correlation between the predicted natural frequencies and the observed resonance conditions, particularly for first bending and first torsional mode response. Most of the observed resonances were produced by low order excitations (<10E) resulting in first bending mode response. Several of the expected high order drivers (upstream and downstream vanes/blades) also produced resonant conditions. A summary of these high order drivers, their predicted resonances, and their observed resonances is presented in table VI-5.

Table VI-5. Summary of Observed Blade Resonances for High Order Drivers

Stage	*Excitation Source*	*Frequency*	*Predicted Mode*	*Resonance Observed*
Rotor 1	Upstream	13E	First Torsion	—
	Downstream	20E	—	
	Difference	7E	First Torsion	—
Rotor 2	Upstream	20E	First Torsion	First Torsion
	Downstream	22E	First Torsion	—
	Difference	2E	—	—
Rotor 3	Upstream	22E	—	—
	Downstream	24E	—	—
	Difference	2E	—	—
Rotor 4	Upstream	24E	First Torsion	First Torsion
	Downstream	26E	First Torsion	—
	Difference	2E	—	—
Rotor 5	Upstream	26E	First Torsion	—
	Downstream	26E	Second Bending	—
	Difference	—	—	—
Rotor 6	Upstream	26E	First Bending	—
	Downstream	20E	First Torsion	First Bending/Torsion
	Difference	6E	—	—

The observed vibrational behavior of the blading clearly illustrates the ruggedness of low aspect ratio blading. The use of this type of blading offers the potential for a significant improvement in durability as compared to current state-of-the-art industrial gas turbines.

3. Rig Teardown Inspection

Upon completion of the test program, the compressor rig was dismounted from the test stand, disassembled, inspected, and placed in storage. In general, the hardware was in excellent condition after 40 hours of testing, with no major structural problems evident. A brief summary of several items of interest are discussed in the following paragraphs.

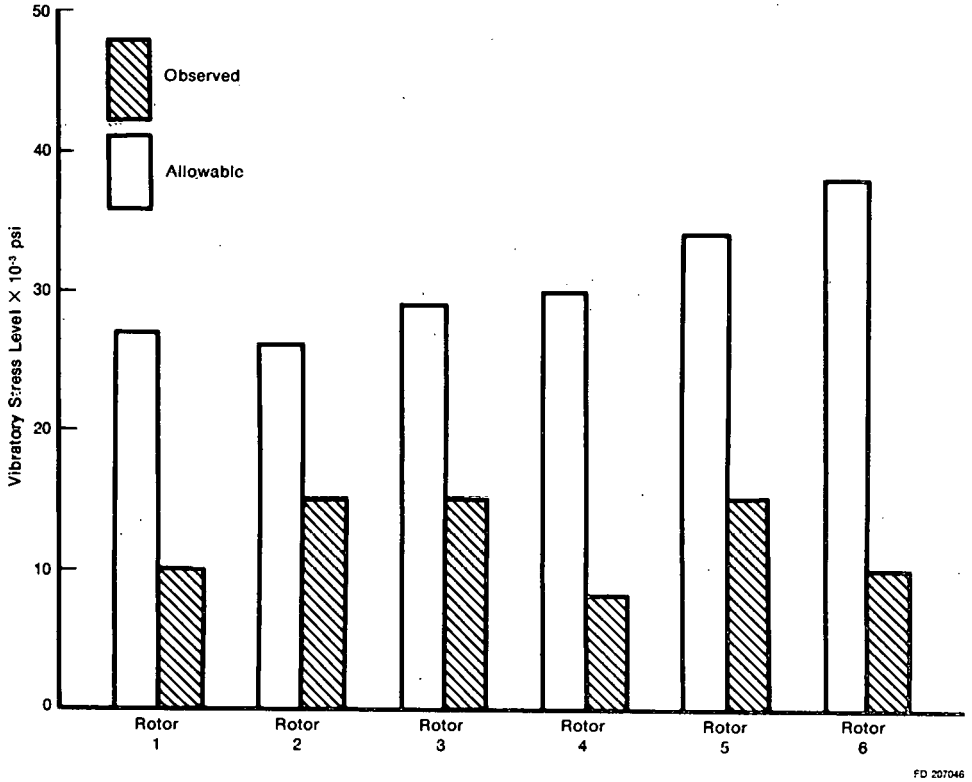

Figure VI-8. Comparison of Maximum Observed Vibratory Stress and Allowable Limit for Compressor Test Rig Blades

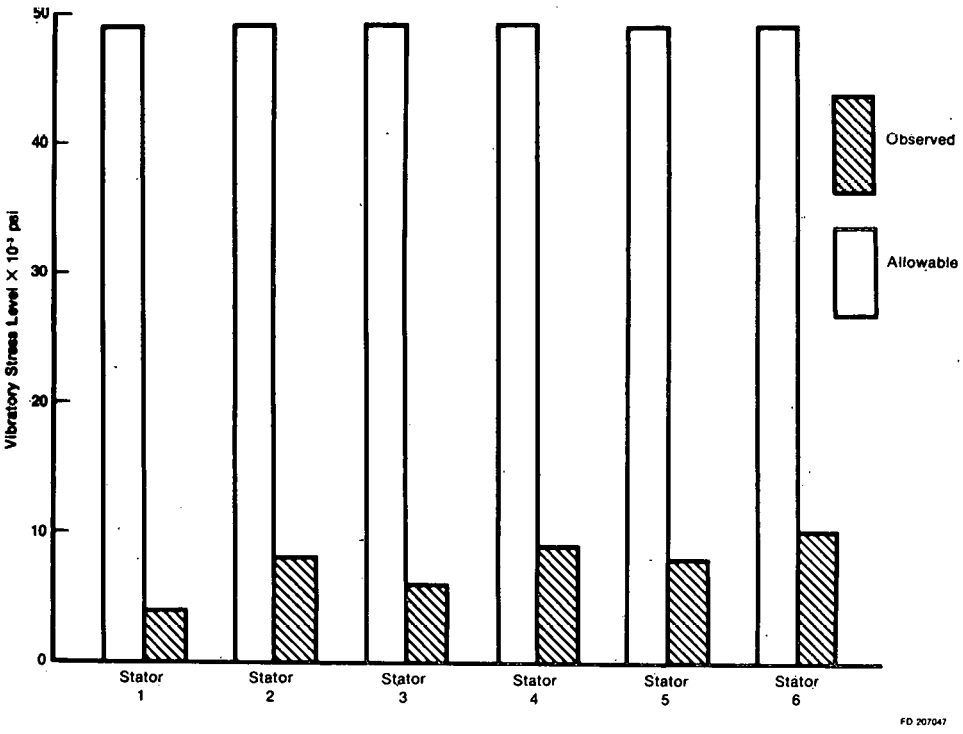

Figure VI-9. Comparison of Maximum Observed Vibratory Stress and Allowable Limit for Compressor Test Rig Vanes

After removal of the axial compressor case, three of the variable vanes were found to be out of position. A single loose inlet guide vane could be rotated nine degrees independent of the sync ring; this was due to a loose sync arm retaining bolt, the lock washer not having secured the bolt. Two first-stage stator vanes could be moved ± ten degrees independent of the sync ring; this was due to damaged keyways at the vane spindle/sync arm interface. Both of these problems were considered to be minor.

During the initial operation of the test rig after installing the pipe diffuser, an impeller tip/shroud interference rub occurred at very low speed operation (~900 RPM); the damage to the impeller and shroud is shown in figures VI-10 and VI-11, respectively. Fluorescent penetrant inspection of the tip region of the impeller was made and no cracks were found. The small heat-affected zone indicated a very minor rub, not affecting the strength of the impeller material. Dimensionally, the tip contour is within 0.002 inch of its original profile. Upon completion of the detailed impeller inspection, it was concluded that the impeller was structurally sound and could be utilized in future tests, if desired.

Figure VI-10. Impeller Tip Damage Due to Interference Rub

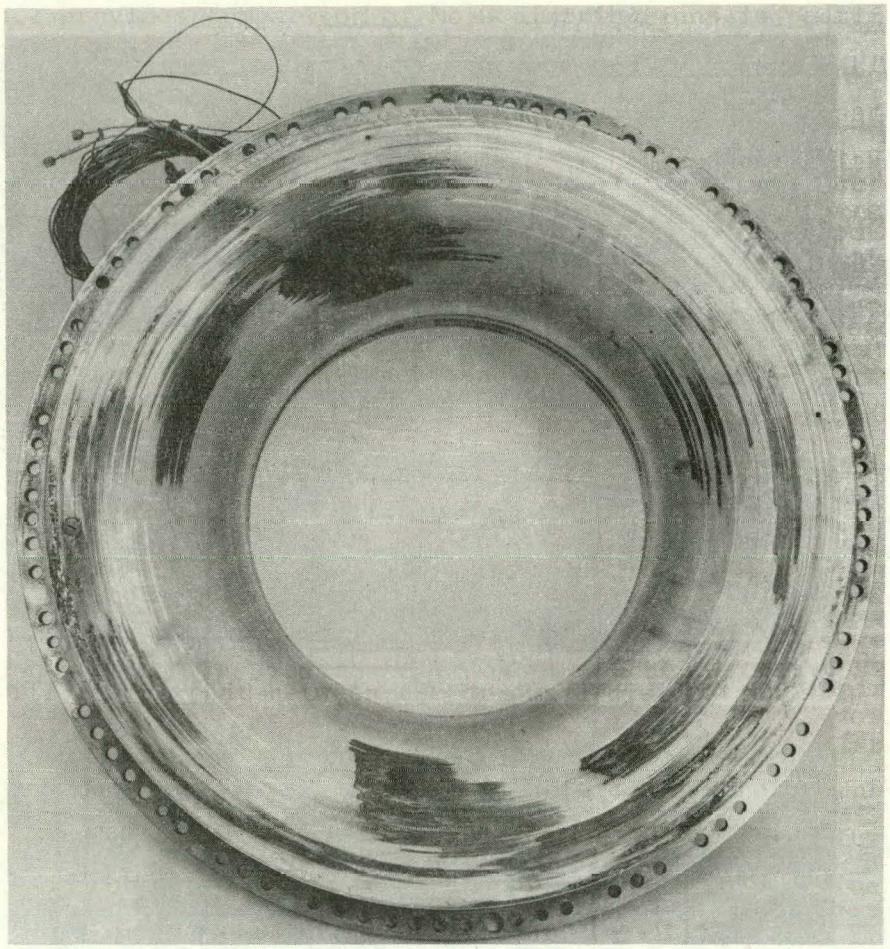

Figure VI-11. Impeller Shroud Damage Due to Interference Rub

In addition to the impeller/shroud rub, a number of nondestructive interference rubs occurred between the stator tip/drum rotor and the blade tip/shroud. In each case, the rub was very minor and did not impact operation of the compressor. The stator tip/drum rotor rubs involved only several vanes per stage, the abrasive coating on the drum removing only a small amount of the vane tip abradable coating (ekonol-aluminum). An example of this type of rub condition is shown in figure VI-12. The use of the abradable coating was successful, as the coating remained intact except where abraded away. None of the vanes were sufficiently contacted to remove the entire thickness of abradable material. All in all, this appears to be a satisfactory means of reducing rig operating clearances while minimizing the risk of a catastrophic rub. Further testing would be required to determine the feasibility of using this type of coating in an engine application.

On the average, the blade tip/shroud rubs were approximately 0.016 deep. Based upon the dimensional analysis done at assembly, a maximum rub of 0.008 would have been expected. Since the rig was operated over the range of conditions which were addressed in the analysis, it is hypothesized that the rig was operating with clearances approximately 0.009 less than design. This is consistent with the stator behavior, as clearances on the order of 0.009 tighter would result in the partial abradable rubs discussed above.

Initially, actual blade tip assembly clearances were slightly less than the desired clearances. After operation of the test rig through the initial series of transients, the nominal running clearances were effectively increased by the depth of the interference rubs. A summary of the estimated actual blade tip running clearances for normal operation is presented in table VI-6.

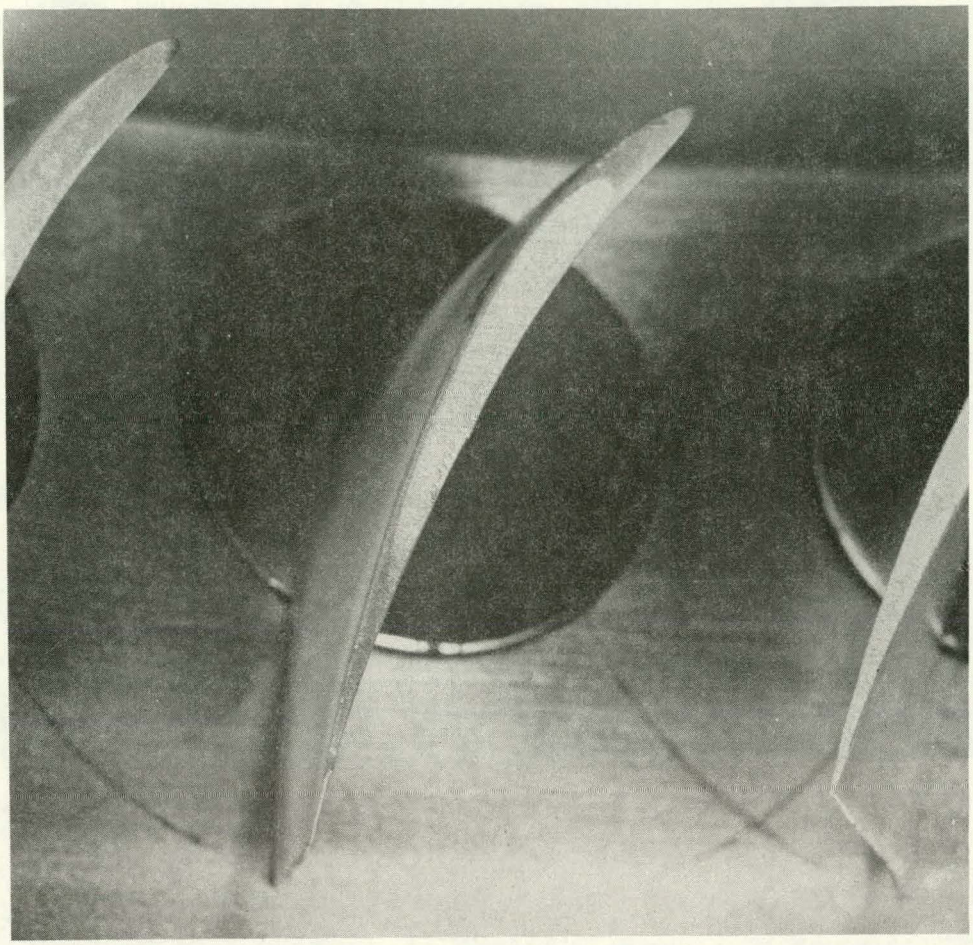

FD 212902

Figure VI-12. Example of Stator Tip/Drum Rotor Rub

Table VI-6. Estimated Actual Running Clearances for Axial Compressor Blades

Stage	Design Nominal Running Clearance	Actual Running Clearances	
		Initial	Final
1	0.016	0.013	0.030
2	0.017	0.007	0.022
3	0.018	0.007	0.019
4	0.019	0.010	0.022
5	0.021	0.010	0.027
6	0.021	0.009	0.035
Ave	0.019	0.010	0.026

THIS PAGE

WAS INTENTIONALLY

LEFT BLANK

SECTION VII
CONCLUDING REMARKS

- The combined axial/centrifugal compressor demonstrated 91.5% polytropic efficiency at 18:1 pressure ratio and 14% surge margin which is the highest known compressor performance demonstrated in this pressure ratio and flow class. The demonstrated performance is particularly significant in that it was achieved at airfoil loading levels approximately 15% above current production engine practice.

- The program performance objectives were achieved in this initial compressor rig test with the original design nominal variable vane settings and pipe diffuser throat sizing.

- The test results conclusively verify the readiness of the advanced low aspect ratio axial compressor and centrifugal backend stage technologies for incorporation in future industrial gas turbine applications. In addition, the technologies demonstrated could potentially be beneficially utilized in a wide range of compressor applications including marine propulsion systems, small gas turbines, and large turbofan aircraft engines.

- The low speed performance data acquired indicate no starting or part speed matching problems with this type of compressor configuration.

- No mechanical or structural problems were encountered which would preclude use of this compressor configuration in an engine application. The excellent rotor dynamics and blade vibratory characteristics exhibited by the single spool drum rotor/low aspect ratio blading configuration could potentially result in improved bearing life and/or minimize the required number of bearings in a particular engine application.

THIS PAGE

WAS INTENTIONALLY

LEFT BLANK

SECTION VIII
REFERENCES

1. Schweitzer, J. K., and B. T. Brown, "Advanced Industrial Gas Turbine Technology Readiness Demonstration Program, Final Report, Phase I Design Study," DOE HCP/T 5035-0001, October 1977.

2. Roe, L. A., B. T. Brown, and J. K. Schweitzer, "Advanced Industrial Gas Turbine Technology Readiness Demonstration Program, Interim Report, Phase II, Turbine Cascade Airfoil Fabrication and Test," P&WA FR-9981, 20 October 1978.

3. Cheatham, J. G., et.al., "Single-Stage Experimental Evaluation of Low Aspect Ratio, Highly Loaded Blading for Compressors, Part IX Final Report, Stage F and G, Volume I," NASA CR-134993, May 1976.

4. Reid, L., and R. D. Moore, "Experimental Study of Low Aspect Ratio Compressor Blading," NASA TM 79280, March 1980.

5. Reddy, J. L., and J. F. Klapproth, "Advanced Fan Development for High Bypass Engines," AIAA Paper No. 68-563.

6. Keenan, J. H., and J. Kaye, "Gas Tables," John Wiley & Sons, Inc., New York, 1948.

APPENDIX A. PERFORMANCE TABULATIONS

1. Overall Compressor Performance

%N	ADR No.	$W\sqrt{\theta/\delta}$	$PR_{T\text{-}T}$	η_{ad} — %	% Bleed	W_{net}	(η_{ad}) net — %
20	194	5.642	1.117	63.26	27.13	4.111	50.83
	196	5.459	1.127	67.32	28.09	3.925	53.40
	198	5.267	1.137	70.79	29.66	3.705	55.34
	200	5.115	1.143	73.24	30.50	3.554	56.64
	202	5.003	1.149	75.44	31.51	3.427	57.39
	204	4.745	1.158	78.18	33.48	3.156	57.89
30	210	9.051	1.245	57.51	25.06	6.783	47.29
	213	8.336	1.337	72.73	28.22	5.984	57.80
	215	7.943	1.372	76.99	30.41	5.527	59.74
	217	7.651	1.390	78.79	31.90	5.210	59.97
	219	7.283	1.404	79.16	33.99	4.808	58.63
40	225	12.329	1.484	55.59	26.23	9.096	45.52
	227	12.369	1.548	60.86	26.15	9.134	50.03
	229	11.996	1.712	75.19	27.17	8.737	61.14
	231	11.706	1.751	76.86	28.08	8.419	61.91
	233	11.265	1.789	78.08	29.65	7.925	61.89
	235	10.989	1.804	78.17	30.44	7.645	61.40
	237	10.718	1.821	78.23	31.32	7.362	60.71
	239	10.506	1.829	77.47	32.39	7.104	59.36
	241	10.351	1.837	77.09	32.73	6.964	58.81
	243	10.285	1.838	77.00	32.96	6.895	58.49
50	249	16.253	1.881	57.10	25.89	12.045	47.17
	251	16.234	2.068	66.38	25.82	12.042	54.49
	253	16.126	2.310	76.25	26.02	11.930	63.04
	255	15.584	2.366	77.32	27.05	11.368	63.30
	257	14.923	2.408	77.47	28.20	10.715	62.62
	259	14.018	2.438	76.03	30.72	9.713	59.72
	261	13.493	2.443	74.17	32.12	9.159	57.26
70	319	32.20	4.592	80.98	22.48	24.96	69.70
	321	31.54	4.835	83.94	23.01	24.28	71.97
	323	30.31	4.974	84.93	24.10	23.01	72.14
	325	30.16	4.985	84.71	24.23	22.85	71.86
	327	30.12	5.000	84.69	24.29	22.81	71.78
	329	29.23	5.041	84.22	25.10	21.89	70.88
	331	27.10	5.053	82.23	27.17	19.74	67.85
80	334	44.53	6.874	83.42	21.06	35.15	72.67
	338	43.98	7.603	87.99	21.63	34.47	76.33
	340	43.71	7.796	88.44	22.19	34.01	76.37
	342	43.14	7.991	88.14	23.09	33.18	75.47
90	352	57.30	10.904	86.93	12.06	50.39	80.92
	355	56.33	11.562	88.47	12.65	49.21	82.02
	357	56.38	12.005	88.76	13.16	48.96	81.95
	359	54.84	12.501	88.39	14.06	47.13	80.99

APPENDIX A. PERFORMANCE TABULATIONS

1. Overall Compressor Performance (Continued)

100	412	71.40	15.710	84.17	0	71.40	84.17
	414	70.45	17.809	87.56	0	70.45	87.56
	416	70.68	18.451	87.84	0	70.68	87.84
	418	68.89	19.011	86.33	0	68.89	86.33
	Stall	68.37	19.000	—	0	68.37	—

APPENDIX A. PERFORMANCE TABULATIONS

2. Axial Compressor Performance

a. Vaneless Diffuser Data

$\%N$	*ADR No.*	$W\sqrt{\theta/\delta}$	*PR*	$\eta_{ad}\%$
50	70	21.978	1.514	76.58
	48	21.084	1.615	81.67
	47	20.127	1.637	79.43
	50	19.865	1.654	77.68
	52	19.352	1.662	74.82
70	180	37.20	2.260	79.05
	181	36.97	2.330	80.66
	182	36.52	2.411	82.61
	183	35.31	2.474	82.83
	185	34.17	2.522	83.36
	187	32.19	2.555	81.52
	189	30.39	2.561	79.19
80	76	46.902	3.028	83.23
	78	46.924	3.107	84.55
	80	46.399	3.219	85.66
	82	45.834	3.367	86.32
	84	45.630	3.414	86.95
	86	43.450	3.578	85.72
	87	44.162	3.546	86.81
90	92	58.691	3.965	85.16
	94	58.507	4.234	87.54
	96	58.569	4.299	88.11
	98	57.814	4.542	88.23
	100	56.640	4.729	87.92
95	134	65.834	4.828	87.73
	136	65.451	5.088	88.07
	138	65.169	5.342	88.84
	140	64.675	5.569	89.14
100	158	71.856	5.223	85.96
	160	71.913	5.380	86.48
	162	71.786	5.603	87.44
	166	71.370	6.140	88.30
	168	71.371	6.366	88.87
	177	71.181	6.478	89.47

APPENDIX A. PERFORMANCE TABULATIONS

2. Axial Compressor Performance

b. Pipe Diffuser Data

%N	ADR No.	$W\sqrt{\theta/\delta}$	PR	η_{ad}%
70	319	32.20	2.576	82.59
	321	31.54	2.575	82.33
	323	30.31	2.574	81.16
	327	30.12	2.575	80.32
	329	29.23	2.576	79.29
	331	27.10	2.571	76.18
80	334	44.53	3.440	86.87
	338	43.98	3.463	86.39
	340	43.71	3.511	86.40
	342	43.14	3.567	85.27
90	352	57.30	4.528	88.59
	355	56.33	4.616	88.35
	357	56.38	4.784	88.52
	359	54.84	4.995	87.53
100	412	71.40	6.086	88.28
	414	70.45	6.446	88.68
	416	70.68	6.690	88.23
	418	68.89	7.072	86.69
	Stall	68.37	7.090	—

APPENDIX A. PERFORMANCE TABULATIONS

3. Centrifugal Stage Performance

$\%N$	ADR No.	$W\sqrt{\theta/\delta}$	PR	$\eta_{ad}\%$	$N/\sqrt{\theta_2}$	$\%N/\sqrt{\theta_2}$
70	319	11.22	1.7825	83.16	8945	79.99
	321	10.97	1.8778	90.60	8942	79.97
	323	10.45	1.9322	94.93	8923	79.80
	327	10.32	1.9420	95.84	8905	79.64
	329	9.93	1.9568	96.05	8887	79.48
	331	9.08	1.9650	97.17	8841	79.06
80	334	12.35	1.9984	82.99	9864	88.21
	338	12.22	2.1952	94.57	9847	88.06
	340	11.74	2.2206	95.77	9818	87.80
	342	11.25	2.2400	97.09	9773	87.40
90	352	14.04	2.4095	89.38	10663	95.35
	355	13.50	2.5051	93.40	10622	94.99
	357	13.01	2.5095	93.83	10576	94.58
	359	12.09	2.5029	94.81	10483	93.75
100	412	15.54	2.5812	84.02	11331	101.33
	414	14.59	2.7626	91.25	11239	100.51
	416	14.19	2.7579	92.70	11180	99.98
	418	13.25	2.6881	91.90	11039	98.72

APPENDIX B
COMPRESSOR INSTRUMENTATION

1. COMPRESSOR AERODYNAMIC INSTRUMENTATION SUMMARY

Title	*No.*	*Range*	*Units*	*Type*
Inlet Orifice Upstream Pressure	4	0-15	PSIA	Wall taps
Inlet Orifice Differential Pressure	4	0-5	PSID	Pressure taps (delta transducer)
Inlet Orifice Temperature	4	0-100	°F	C/A thermocouple
Plenum Total Pressure	4	0-15	PSIA	Wall taps
Plenum Total Temperature	4	0-100	°F	Rosemount Resistance thermometers
Strut L.E. Total Pressure	6	0-15	PSIA	Kiel-head pressure sensors
Strut L.E. Total Pressure	6	0-100	°F	Stagnation tube C/A thermocouples
Strut L.E. OD Static Pressure	4	0-15	PSIA	Wall taps
Strut T.E. OD Static Temperature	4	0-15	PSIA	Wall taps
Stator 1 L.E. Total Pressure	10	0-50	PSIA	Kiel-head pressure sensors
Stator 1 L.E. Total Temperature	10	0-150	°F	Stagnation tube C/A thermocouples
Stator 1 L.E. Static Pressure	4	0-25	PSIA	Wall taps
Stator 1 T.E. Static Pressure	4	0-25	PSIA	Wall taps
Stator 2 L.E. Total Pressure	10	0-50	PSIA	Kiel-head pressure sensors
Stator 2 L.E. Total Temperature	10	0-250	°F	Stagnation tube C/A thermocouples
Stator 2 L.E. Static Pressure	3	0-50	PSIA	Wall taps
Stator 2 T.E. Static Pressure	4	0-50	PSIA	Wall taps
Stator 3 L.E. Total Pressure	10	0-100	PSIA	Kiel-head pressure sensors
Stator 3 L.E. Total Temperature	10	0-400	°F	Stagnation tube C/A thermocouples
Stator 3 L.E. Static Pressure	3	0-50	PSIA	Wall taps
Stator 3 T.E. Static Pressure	4	0-50	PSIA	Wall taps
Stator 4 L.E. Total Pressure	10	0-100	PSIA	Kiel-head pressure sensors
Stator 4 L.E. Total Temperature	10	0-500	°F	Stagnation tube C/A thermocouples
Stator 4 L.E. Static Pressure	3	0-100	PSIA	Wall taps
Stator 4 T.E. Static Pressure	4	0-100	PSIA	Wall taps
Stator 5 L.E. Total Pressure	10	0-100	PSIA	Kiel-head pressure sensors
Stator 5 L.E. Total Temperature	10	0-600	°F	Stagnation tube C/A thermocouples
Stator 5 L.E. Static Pressure	3	0-100	PSIA	Wall taps
Stator 5 T.E. Static Pressure	4	0-100	PSIA	Wall taps
Stator 6 L.E. Total Pressure	10	0-150	PSIA	Kiel-head pressure sensors
Stator 6 L.E. Total Temperature	10	0-700	°F	Stagnation tube C/A thermocouples

APPENDIX B
COMPRESSOR INSTRUMENTATION

1. COMPRESSOR AERODYNAMIC INSTRUMENTATION SUMMARY (Continued)

Stator 6 L.E. Static Pressure	3	0-100	PSIA	Wall taps
Stator 6 T.E. Static Pressure	4	0-100	PSIA	Wall taps
Station 2 Total Pressure at 12.3% span	8	0-150	PSIA	Kiel-head Pressure rakes
Station 2 Total Pressure at 34.1% span	8	0-150	PSIA	Kiel-head Pressure rakes
Station 2 Total Pressure at 54.5% span	8	0-150	PSIA	Kiel-head Pressure rakes
Station 2 Total Pressure at 73.6% span	8	0-150	PSIA	Kiel-head Pressure rakes
Station 2 Total Pressure at 91.4% span	8	0-150	PSIA	Kiel-head Pressure rakes
Station 2 Total Temperature at 12.3% span	8	0-700	°F	C/A thermocouple rakes
Station 2 Total Temperature at 34.1% span	8	0-700	°F	C/A thermocouple rakes
Station 2 Total Temperature at 54.5% span	8	0-700	°F	C/A thermocouple rakes
Station 2 Total Temperature at 73.6% span	8	0-700	°F	C/A thermocouple rakes
Station 2 Total Temperature at 91.4% span	8	0-700	°F	C/A thermocouple rakes
Station 2 OD Static Pressure	4	0-100	PSIA	Wall taps
Bleed Orifice Upstream Pressure	2	0-100	PSIA	Wall taps
Bleed Orifice Differential Pressure	2	0-25	PSID	Wall taps (delta transducer)
Bleed Orifice Total Temperature	2	0-700	°F	C/A thermo couple
Impeller Inlet Static Pressure	4	0-150	PSIA	Wall taps
Impeller Exit Rim Static Pressure	4	0-250	PSIA	Wall taps
Diff. L.E. Hub Static Pressure	4	0-250	PSIA	Wall taps
Diff. L.E. Shroud Pressure	4	0-250	PSIA	Wall taps
Diff. Throat Hub Static Pressure	4	0-250	PSIA	Wall taps
Diff. Throat Shroud Pressure	4	0-250	PSIA	Wall taps
Diff. Exit Hub Static Pressure	4	0-300	PSIA	Wall taps
Diff. Exit Shroud Static Pressure	4	0-300	PSIA	Wall taps
Diff. Dump Hub Static Pressure	4	0-300	PSIA	Wall taps

APPENDIX B
COMPRESSOR INSTRUMENTATION

1. COMPRESSOR AERODYNAMIC INSTRUMENTATION SUMMARY (Continued)

Diff. Dump Shroud Static Pressure	4	0-300	PSIA	Wall taps
Station 3 Total Pressure - 0° rakes	5	0-350	PSIA	Kiel-head
Station 3 Total Pressure - 45° rakes	5	0-350	PSIA	Kiel-head
Station 3 Total Pressure - 90° rakes	5	0-350	PSIA	Kiel-head
Station 3 Total Pressure - 135° rakes	5	0-350	PSIA	Kiel-head
Station 3 Total Temperature - 0°	5	0-900	°F	C/A thermo-couple rakes
Station 3 Total Temperature - 45°	5	0-900	°F	C/A thermo--couple rakes
Station 3 Total Temperature - 135°	5	0-900	°F	C/A thermo--couple rakes
Stator 1 L.E. Secondary Static Pressure	4	0-25	PSIA	Wall taps
Stator 2 L.E. Secondary Static Pressure	4	0-50	PSIA	Wall taps
Stator 3 L.E. Secondary Static Pressure	4	0-50	PSIA	Wall taps
Stator 4 L.E. Secondary Static Pressure	4	0-100	PSIA	Wall taps
Stator 5 L.E. Secondary Static Pressure	4	0-100	PSIA	Wall taps
Stator 6 L.E. Secondary Static Pressure	4	0-100	PSIA	Wall taps

APPENDIX B
COMPRESSOR INSTRUMENTATION

2. COMPRESSOR STRUCTURAL INSTRUMENTATION SUMMARY

a. Rotor Blades

Stage	Gage Number	Blade Number	View	Location A	B	C	D	E	F	G	H	Remarks
1	1	1	A-A	2.50	—	—	—	—	—	—	—	MRT, at fillet radius tangency
	2	7	A-A	2.50	—	—	—	—	—	—	—	MRT, at fillet radius tangency
	3	12	A-A	2.50	—	—	—	—	—	—	—	MRT, at fillet radius tangency
	4	7	A-A	—	1.91	—	—	—	—	—	—	On fillet radius, above tangency
	5	7	B-B	—	—	0.50	—	—	—	—	—	On fillet radius, above tangency
	6	1	B-B	—	2.75	—	1.38	—	—	—	—	—
	7	12	B-B	1.38	—	—	—	—	—	—	—	At trailing edge
2	8	2	C-C	1.50	—	—	—	—	—	—	—	MRT, at fillet radius tangency
	9	2	D-D	—	0.75	1.27	0.90	—	—	—	—	—
	10	8	C-C	1.50	—	—	—	—	—	—	—	MRT, at fillet radius tangency
	11	8	D-D	—	0.75	1.27	0.90	—	—	—	—	—
	12	15	D-D	—	—	—	—	—	—	—	—	At leading edge, above tangency
	13	15	D-D	1.50	—	—	—	0.28	—	—	—	—
3	14	5	C-C	1.83	—	—	—	—	—	—	—	MRT, at fillet radius tangency
	15	15	C-C	1.83	—	—	—	—	—	—	—	MRT, at fillet radius tangency
	16	22	C-C	1.83	—	—	—	—	—	—	—	MRT, at fillet radius tangency
	17	5	D-D	—	0.50	1.30	1.30	—	—	—	—	—
	18	15	E-E	0.92	0.98	2.52	—	—	—	—	—	—
4	19	2	C-C	1.50	—	—	—	—	—	—	—	MRT, at fillet radius tangency
	20	10	C-C	1.50	—	—	—	—	—	—	—	MRT, at fillet radius tangency
	21	19	C-C	1.50	—	—	—	—	—	—	—	MRT, at fillet radius tangency
	22	2	F-F	—	0.22	0.88	1.10	—	—	—	—	—
	23	10	D-D	—	—	—	—	—	—	—	—	At leading edge, above tangency
5	24	6	G-G	0.84	—	—	—	—	—	—	—	MRT, at fillet radius tangency
	25	16	G-G	0.84								MRT, at fillet radius tangency
	26	6	H-H	—	—	1.08	—	0.70	0.90	—	—	—
	27	16	H-H	—	—	0.50	—	—	—	1.40	0.38	—
	28	24	H-H	1.00	—	—	—	—	—	—	—	At trailing edge
6	29	2	G-G	1.00	—	—	—	—	—	—	—	Above fillet radius tangency
	30	9	G-G	1.00	—	—	—	—	—	—	—	Above fillet radius tangency
	31	17	G-G	1.00	—	—	—	—	—	—	—	Above fillet radius tangency
	32	2	G-G	—	0.75	—	—	—	—	—	—	Above fillet radius tangency
	33	9	H-H	—	—	0.0	—	—	—	1.38	0.56	—
	34	17	H-H	—	0.13	1.03	0.88	—	—	—	—	—

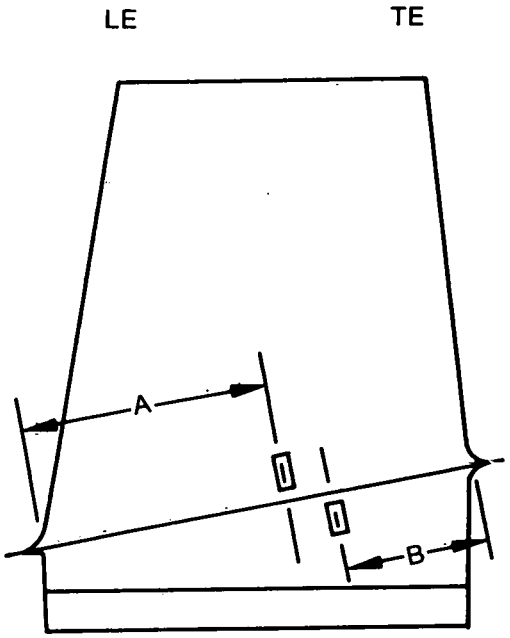

View A-A
First Stage - Convex

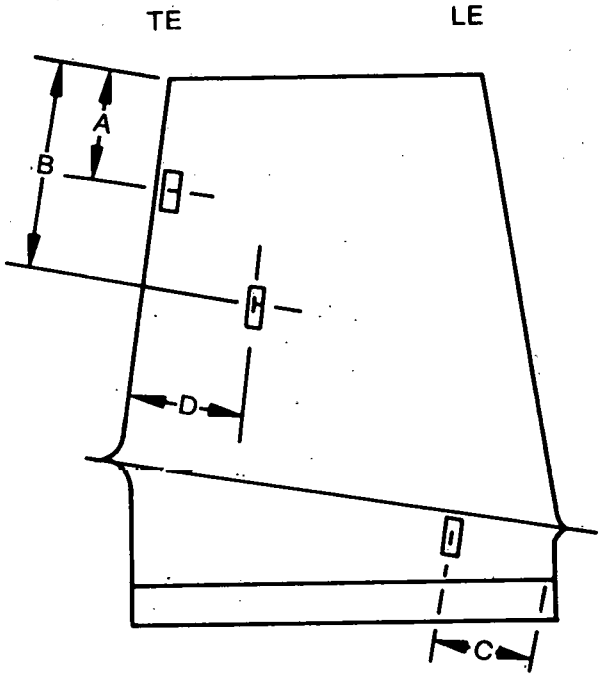

View B-B
First Stage -Concave

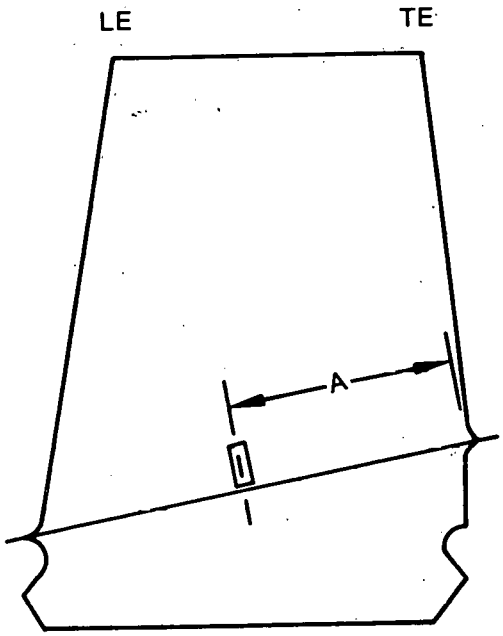

View C-C
Typical Blade
Second - Fourth Stage

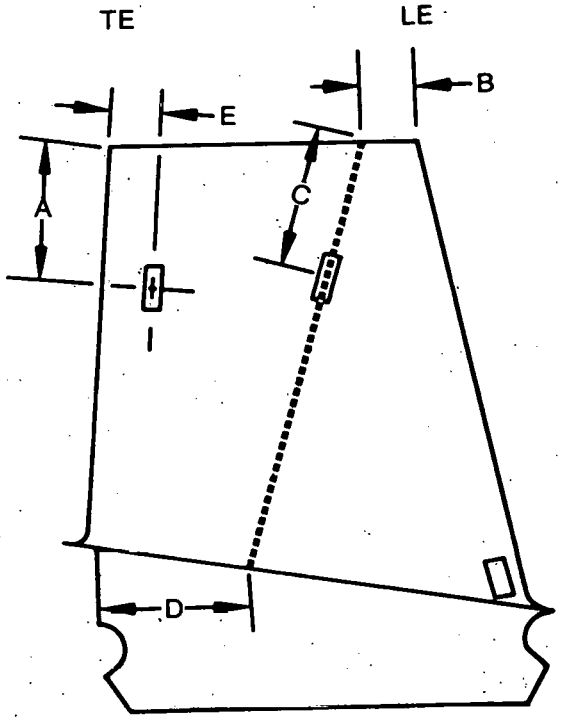

View D-D
Typical Blade
Second - Fourth Stage
Concave

FD 212908

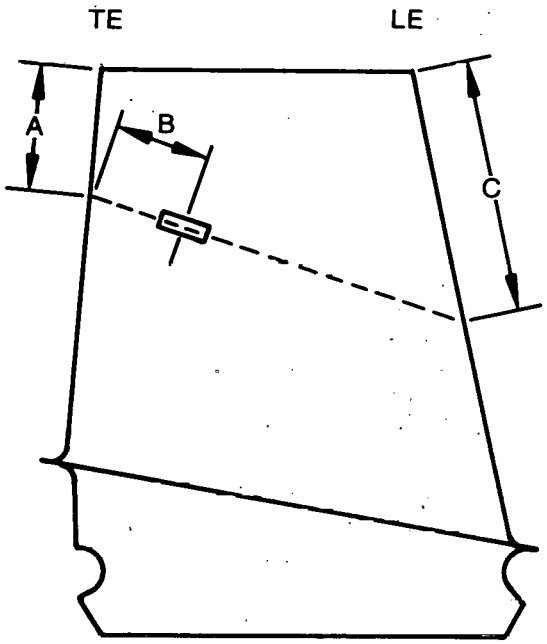

View E-E
Typical Blade
Second - Fourth Stage
Concave

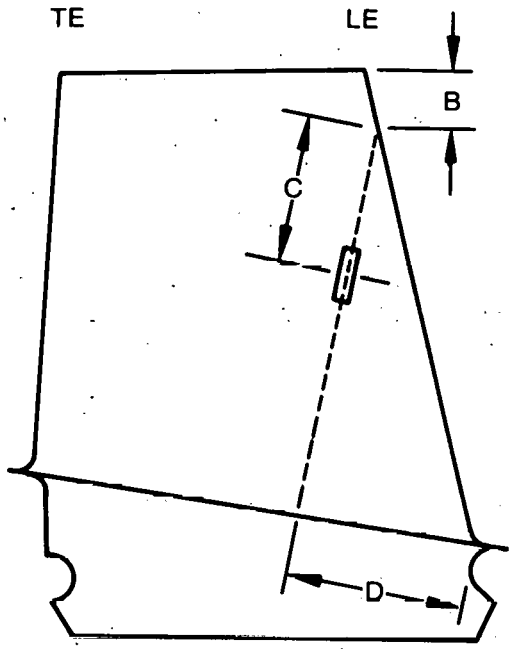

View F-F
Typical Blade
Second - Fourth Stage
Concave

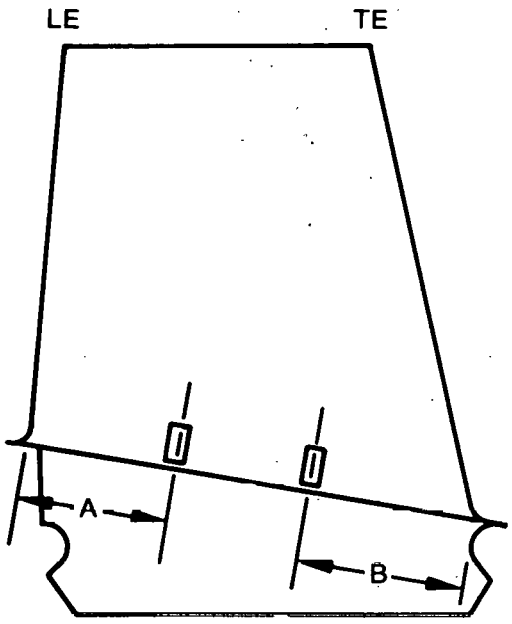

View G-G
Typical Blade
Fifth - Sixth Blade
Convex

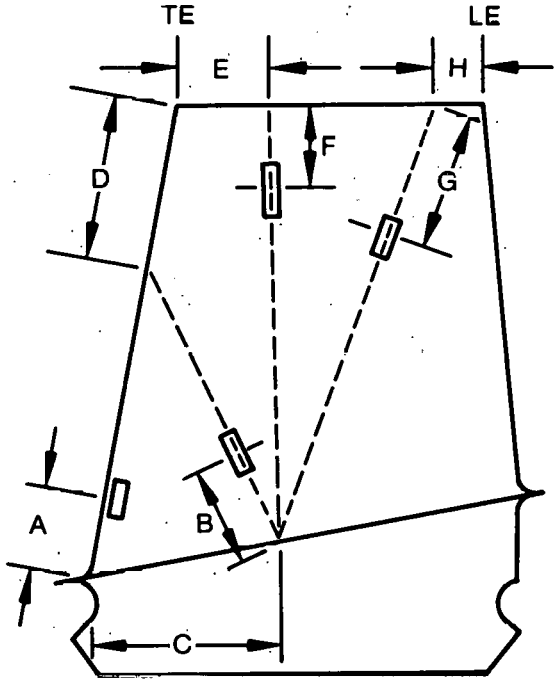

View H-H
Typical Blade
Fifth - Sixth Blade
Concave

FD 212910

APPENDIX B
COMPRESSOR INSTRUMENTATION

2. COMPRESSOR STRUCTURAL INSTRUMENTATION SUMMARY (Continued)

b. Stator Vanes

Stage	Gage Number	Blade Number	View	Location A	B	C	D	E	F	Remarks
1	1	8	A-A	1.95	0.90	—	—	—	—	Above fillet radius tangency
	2	18	A-A	1.95	0.90	—	—	—	—	Above fillet radius tangency
	3	8	B-B	—	2.55	1.00	—	—	—	Above fillet radius tangency
	4	18	B-B	—	—	—	0.0	—	—	At leading edge, above fillet radius tangency
	5	8	B-B	1.70	—	—	—	—	—	At trailing edge
2	6	9	A-A	1.50	0.70	—	—	—	—	Above fillet radius tangency
	7	20	B-B	—	2.20	0.35	—	—	—	Above fillet radius tangency
	8	20	C-C	—	—	0.65	—	1.30	—	Above fillet radius tangency
	9	20	C-C	1.03	0.68	—	1.23	—	—	—
3	10	10	A-A	1.25	1.00	—	—	—	—	Above fillet radius tangency
	11	22	A-A	1.25	1.00	—	—	—	—	Above fillet radius tangency
	12	10	C-C	0.80	0.80	—	0.80	—	—	—
	13	22	B-B	1.35	—	—	—	—	—	At trailing edge
	14	10	C-C	—	—	0.55	—	1.60	—	Above fillet radius tangency
4	15	10	A-A	1.10	0.70	—	—	—	—	Above fillet radius tangency
	16	23	C-C	—	—	0.65	—	1.30	—	Above fillet radius tangency
	17	23	C-C	—	—	—	—	0.55	0.55	Above fillet radius tangency
	18	23	B-B	—	—	—	0.33	—	—	At leading edge
5	19	10	A-A	1.00	0.80	—	—	—	—	Above fillet radius tangency
	20	23	C-C	—	—	0.50	—	1.20	—	Above fillet radius tangency
	21	23	B-B	—	—	—	0.15	—	—	At leading edge
6	22	8	A-A	1.35	1.10	—	—	—	—	Above fillet radius tangency
	23	18	C-C	—	—	0.90	—	0.95	—	Above fillet radius tangency
	24	8	A-A	—	—	1.25	1.30	—	1.10	—
	25	18	B-B	0.45	1.55	—	—	0.95	—	—
	26	18	B-B	—	—	—	0.19	—	—	At trailing edge

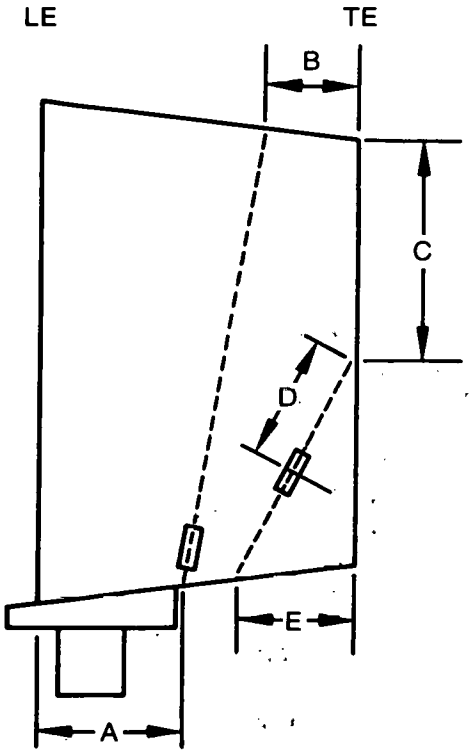

View A-A
Typical Vane
Convex

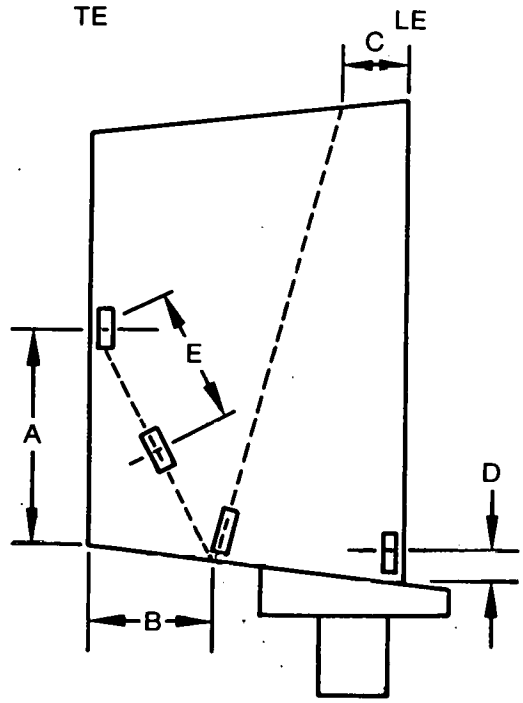

View B-B
Typical Vane
Concave

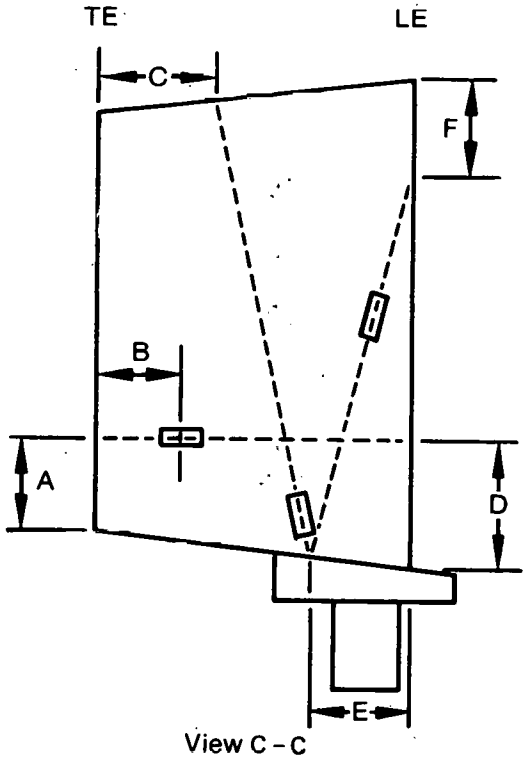

View C - C
Typical Vane
Concave

FD 212909

APPENDIX B
COMPRESSOR INSTRUMENTATION (Continued)

3. COMPRESSOR OPERATIONAL SUPPORT INSTRUMENTATION

Title	*No.*	*Range*	*Units*	*Type*
No. 1 Compartment Pressure	2	0-25	PSIA	
No. 1 Compartment Temperature	2	0-250	°F	
No. 1 Seal Pressure	2	0-25	PSIA	Wall taps
IGV T.E. ID Cavity Pressure	2	0-25	PSIA	Wall taps
No. 1 Compartment Delta Pressure	1	0-15	PSID	Wall taps (delta transducer)
No. 1 Seal Delta Pressure	1	0-15	PSID	Wall taps (delta transducer)
Front Bearing Outer Race Temperature	3	0-400	°F	C/A thermo-couples
Front Bearing Vibrations Horizontal/Vertical	2	0-3	Mils	Accelerometer
Rig Speed	1	0-17000	RPM	Electromagnetic speed pickup
IGV Vane Angle	3	0-90	deg.	Potentiometer, dial indicator
Stator 1 Vane Angle	3	0-90	deg.	Potentiometer dial indicator
Stator 2 Vane Angle	3	0-90	deg.	Potentiometer dial indicator
Stator 3 Vane Angle	1	0-90	deg.	Dial indicator
Stator 4 Vane Angle	1	0-90	deg.	Dial indicator
Stator 5 Vane Angle	1	0-90	deg.	Dial indicator
Stator 6 Vane Angle	1	0-90	deg.	Dial indicator
Inlet High Response Static Pressure	1		PSIA	Wall tap
Exit High Response Static Pressure	1		PSIA	Wall tap
High Response Temperature	1	0-900	°F	QRTC
Impeller Shroud Metal Temperature	2	0-900	°F	C/A thermo-couple
Diffuser Metal Temperature	2	0-900	°F	C/A thermo-couple
Backface Housing Metal Temperature	6	0-1300	°F	C/A thermo-couple
Impeller Tip Clearance	1	0-60	Mils	Laser clearance probe
No. 1 Brg. Lube Oil Pressure	1	0-100	PSIG	
No. 1 Brg. Lube Oil In. Temperature	1	0-600	°F	
No. 1 Brg. Lube Oil Exit Temperature	1	0-600	°F	
No. 2 Brg. Lube Oil Pressure	1	0-100	PSIG	
No. 2 Brg. Lube Oil Inlet Temperature	1	0-600	°F	
No. 2 Brg. Lube Oil Exit Temperature	1	0-600	°F	
No. 2 Brg. Oil Damper Pressure	1	0-100	PSIG	

APPENDIX B
COMPRESSOR INSTRUMENTATION (Continued)

3. COMPRESSOR OPERATIONAL SUPPORT INSTRUMENTATION (Continued)

Frt. Seal Shop Air Supply Pressure	1	0-100	PSIG	
Slipring Coolant Supply Pressure	1	0-50	PSIG	
Slipring Coolant Flow	1	0-50	GPH	
Slipring Coolant Inlet Temperature	1	0-200	°F	
Slipring Coolant Exit Temperature	1	0-200	°F	
Rotor Axial Thrust Load	3	0-3000	lbs	
Collector Static Pressure	4	0-250	PSIA	Wall taps
Collector Total Temperature	4	0-900	°F	Aspirated C/A thermocouples
Backface Cavity Tip Pressure	2	0-250	PSIA	Wall taps
Backface Cavity Tip Temperature	2	0-1300	°F	C/A thermo couples
Backface Cavity Seal Pressure	2	0-250	PSIA	Wall taps
Backface Cavity Seal Temperature	2	0-1300	°F	C/A thermo couples
Buffer Seal Cavity Pressure	2	0-250	PSIA	Wall taps
Buffer Seal Cavity Delta Pressure	1	±5	PSID	Wall taps (delta transducer)
Thrust Balance Cavity Pressure	2	0-100	PSIA	Wall taps
Thrust Balance Cavity Temperature	2	0-600	°F	C/A thermo-couples
Rear Bearing Buffer Cavity Pressure	2	0-50	PSIA	Wall taps
Rear Bearing Buffer Cavity Temperature	2	0-400	°F	C/A thermo-couples
No. 2 Compartment Pressure	2	0-25	PSIA	Wall taps
No. 2 Compartment Temperature	2	0-400	°F	C/A thermo-couples
Rear (Roller) Brg. Outer Race Temp.	3	0-400	°F	C/A thermo-couples
Rear (Ball) Brg. Outer Race Temp.	3	0-400	°F	C/A thermo-couple
Rear Bearing Vibrations (Horizontal/Vertical)	2	0-3	Mils	Accelerometer

★U.S. GOVERNMENT PRINTING OFFICE: 1981-740-145/2041